

DATE ISSUED

AUG 13 1979

ORNL-5497

Distribution and Transport of Tritium in the Peach Bottom HTGR

R. P. Wichner
F. F. Dyer

OAK RIDGE NATIONAL LABORATORY
OPERATED BY UNION CARBIDE CORPORATION · FOR THE DEPARTMENT OF ENERGY

Printed in the United States of America. Available from
National Technical Information Service
U.S. Department of Commerce
5285 Port Royal Road, Springfield, Virginia 22161
Price: Printed Copy \$8.00; Microfiche \$3.00

This report was prepared as an account of work sponsored by an agency of the United States Government. Neither the United States Government nor any agency thereof, nor any of their employees, contractors, subcontractors, or their employees, makes any warranty, express or implied, nor assumes any legal liability or responsibility for any third party's use or the results of such use of any information, apparatus, product or process disclosed in this report, nor represents that its use by such third party would not infringe privately owned rights.

ORNL-5497
Dist. Category UC-77

Contract No. W-7405-eng-26

CHEMICAL TECHNOLOGY DIVISION

HTGR BASE TECHNOLOGY PROGRAM
HTGR Chemistry Studies (189a 01329)

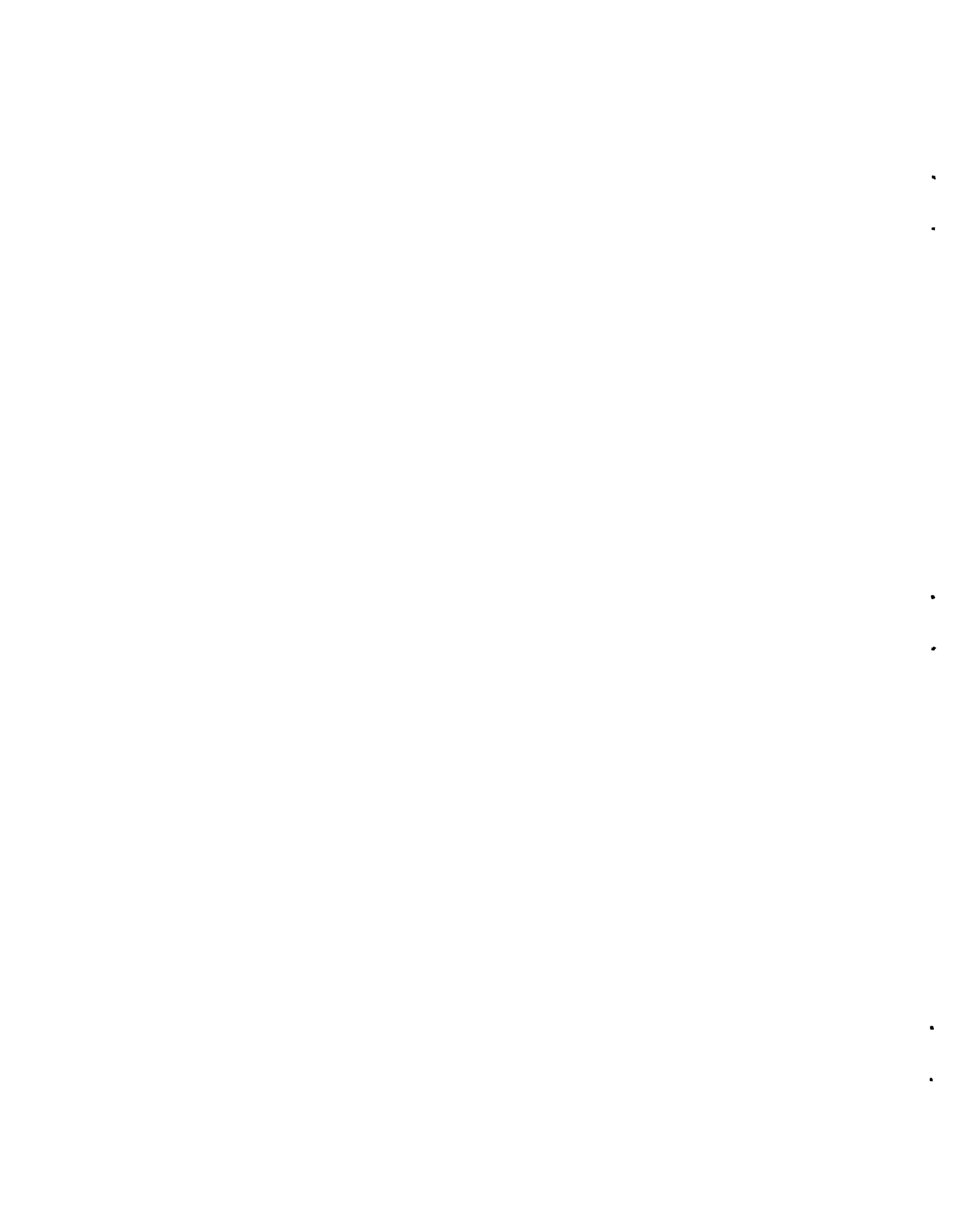
DISTRIBUTION AND TRANSPORT OF TRITIUM IN THE PEACH BOTTOM HTGR

R. P. Wichner
F. F. Dyer*

* Analytical Chemistry Division.

Date Published: August 1979

OAK RIDGE NATIONAL LABORATORY
Oak Ridge, Tennessee 37830
operated by
UNION CARBIDE CORPORATION
for the
DEPARTMENT OF ENERGY



CONTENTS

	<u>Page</u>
ABSTRACT	1
1. INTRODUCTION	2
1.1 Objective and Scope	2
1.2 Regulatory Constraints on Tritium Discharges	4
1.3 Summary of Relevant Descriptive Literature	6
1.4 Brief Description of the Peach Bottom HTGR	8
1.5 Acknowledgments	16
2. SOURCES AND PATHWAYS OF TRITIUM IN PEACH BOTTOM	17
2.1 Sources	17
2.2 Tritium Transport Paths	19
2.3 Liquid Waste Removal System	25
2.4 Gaseous Waste Removal System	27
2.5 Contaminated Solid Wastes	28
2.6 Summary of Pathways	28
3. MATERIAL PROPERTIES	28
3.1 Tritium Sorption on Graphite and Charcoal	28
3.2 Fuel Particle Failure Fractions	33
3.3 Lithium Impurity in Graphite and Fuel	36
3.4 BET Surface Areas of Graphite and Charcoal	37
4. ONSITE SURVEILLANCE OF TRITIUM AND HYDROGEN	38
4.1 Tritium in the Primary and Secondary Coolants	38
4.2 Special Tritium Survey	42
4.3 Effects of Hydrazine in Secondary Coolant on Hydrogen Levels in Primary Coolant	48
4.4 Releases of Tritium in Liquid and Gaseous Wastes	48
4.5 Levels of Hydrogen and Water in the Primary Coolant	50
5. MEASURED TRITIUM LEVELS IN FUEL ELEMENTS AND A REFLECTOR ELEMENT	51
5.1 Radial Distributions in Sleeves and Spines	52
5.2 Axial Distributions in the Sleeves and Spine	78
5.3 Levels in the Upper Reflector Assembly, Fission Product Trap, and Bottom Connector	79
5.4 Concentrations in the Fuel	86
5.5 Distribution in Radial Reflector Element A18-08	94

	<u>Page</u>
6. ESTIMATED SOURCE LEVELS, INVENTORIES, AND LOSSES	98
6.1 Source Estimation	98
6.1.1 Production of tritium in fuel	98
6.1.2 Production from ^3He in the coolant	99
6.1.3 Production from lithium in graphite	108
6.1.4 Production from ^{10}B in control rods and poisoned spines	112
6.1.5 Summary of tritium sources	118
6.2 Estimated Tritium Inventories in Core 2 Components Based on Measured Concentrations	118
6.2.1 Fuel inventory	118
6.2.2 Sleeve and spine inventories	122
6.2.3 Removable radial reflector inventory	124
6.2.4 Inventories in the upper and lower axial reflector regions of the driver fuel elements	124
6.2.5 Summary of inventories derived from observed specific activities	126
6.3 Estimated Tritium Losses from the Primary System	127
6.3.1 Transport to the fission product trapping system	127
6.3.2 Transport to the chemical cleanup system (and disposal as solid waste)	130
6.3.3 Leakage through the steam-generator tubing	131
6.3.4 Loss due to containment leakage	135
6.3.5 Discharge with gaseous waste flow	135
6.3.6 Discharge with liquid wastes	136
6.3.7 Summary of leakage rates	137
7. CONCLUSIONS AND RECOMMENDATIONS	137
7.1 Conclusions	137
7.2 Recommendations	144
8. REFERENCES	144

DISTRIBUTION AND TRANSPORT OF TRITIUM IN THE PEACH BOTTOM HTGR

R. P. Wichner
F. F. Dyer*

ABSTRACT

This report completes the first phase of a two-phase effort to describe and understand tritium production and movement in an operating high-temperature gas-cooled reactor (HTGR) system. The principal objective of phase 1 is to report the findings on tritium concentrations in core components acquired during the Peach Bottom Surveillance Program, which dealt with fission product migration in general, and a follow-on task devoted specifically to tritium. Administrative procedures are being developed for the second phase of the work to be performed in the Federal Republic of Germany under the auspices of the international "umbrella agreement" on gas-cooled reactor (GCR) development. In this effort, computer model predictions of tritium transport in the reactor system will be compared with observed concentration levels.

The types of data on tritium concentration in core components acquired include (1) radial distribution of tritium in the graphite parts of six fuel elements, (2) axial concentration profiles in five fuel elements, (3) concentration levels in the fuel, (4) concentration profiles in the fission product traps of four fuel elements, and (5) concentration measurements in a graphite reflector element. Also reported are fuel particle failure fractions, graphite BET surface areas, and lithium impurity level determinations in graphite to assist data interpretation. To augment the data resulting from our measurements, information is included from the operations reports of the Philadelphia Electric Company, which summarize on-site tritium measurements of the coolant and effluent streams, and the results of a special tritium survey conducted by General Atomic Company (GAC) in 1971.

We have gone beyond the principal objective of describing concentration levels in an attempt to obtain a preliminary understanding of the sources and fate of tritium born in the Peach Bottom core. Of the approximately 2200 Ci born during core 2 operation, 55% is estimated to be from ternary fission, 3.3% from neutron reactions with lithium impurity in the graphite, 1.9% from neutron reactions with ^3He in the coolant,

* Analytical Chemistry Division.

and an unexpectedly large share (40%) from ^{10}B , primarily in the control rods and to a lesser extent in the burnable poison elements.

Concentration profile data indicate that the tritium from ^{10}B in the poisoned fuel elements remained in place, and thus we feel (with no direct evidence) that the tritium born in the control rods was also immobile. However, tritium from the other sources migrated significantly. About 60% of the tritium due to fission migrated from the fuel and deposited in nearby graphite or passed with the fuel element purge flow to the fission product trapping system. Although there are insufficient data to firmly fix the fate of the tritium carried with the purge flow, the major portion (~90%) probably passed freely through the trapping system to rejoin the primary coolant.

Our estimate for the amount of tritium that permeated through the steam-generator tubing (1.1 Ci) is about a factor of 4 less than a previous estimate by GAC personnel. Discharges via the liquid waste and off-gas systems were estimated from concentrations reported in the operations reports. It is surprising that tritium discharge as solid waste (tritiated water adsorbed on clay) exceeded liquid and gaseous discharges. The quantity of tritium in the solid wastes was determined from the estimated transport to the chemical purification system via the steam-generator purge flow. Leakage estimates through the containment vessel were insignificant compared with gaseous discharge through the stack.

In general, a fairly good tritium mass balance was achieved. Of the portion believed to have been mobile (1325 Ci), about 83% is accounted for as measured inventory in core components and estimated discharge flows. The remainder probably resided as unmeasured inventory in unsampled reactor components, principally in the permanent radial reflector and ex-core fission product traps.

1. INTRODUCTION

1.1 Objective and Scope

The principal objective of this work is to gain a complete understanding of tritium production, distribution, and leakage in a recently operated high-temperature gas-cooled reactor (HTGR). This objective has been subdivided into two phases: (1) presentation of observed tritium levels in the fuel, coolant, and effluent streams of the Peach Bottom HTGR, along with tritium distributions observed in the core and reflector

graphite; and (2) mathematical modeling of tritium production and distribution in the Peach Bottom reactor, including a critical comparison of model predictions with observations. This report completes phase 1 of the overall objective; phase 2 is to be performed in the Federal Republic of Germany under the auspices of the international cooperative agreement on the development of gas-cooled reactor (GCR) technology, pending approval of administrative procedures which are currently in process.

In addition to the main objective of this report, results are presented and discussed regarding tritium transport paths in the reactor, and a tentative overall tritium mass balance for the four years of core 2 operation has been developed. However, it should be emphasized that without a comprehensive model for tritium movement from the core to the primary and secondary coolant and containment, these results must be considered preliminary. Nevertheless, we have provided this additional information in an attempt to further the goal of full understanding of tritium behavior in the reactor. The major tritium repositories at the end of life (EOL) of core 2 are identified as are the principal pathways for tritium movement from its various sources to the final locations. In addition, the principal gaps in the data which could hinder the full modeling effort are noted. Thus, at least a qualitative understanding of tritium behavior has been attained and the groundwork laid for a more comprehensive modeling effort.

Much of the data presented here was developed in the course of the Peach Bottom Surveillance Program conducted at Oak Ridge National Laboratory (ORNL) from 1972 through 1977. The purpose of this program within the larger effort, the Peach Bottom End-of-Life Program coordinated by General Atomic Company (GAC), was to provide data for validating the design codes used to predict fission product and temperature distributions within HTGR fuel elements and the level of primary circuit activity. The data developed during this program and included in this report are the following:

1. radial distributions of tritium concentrations in the sleeve and spine graphite at approximately four locations in six fuel elements,
2. axial distribution of tritium concentration in the graphite portion of five fuel elements,

3. data on tritium levels in individual pairs of fuel particles from one fuel element,
4. axial distribution of tritium concentrations in the fission product trap of one fuel element,
5. determinations of fuel particle failure fractions.

The above information was extracted from the series of fuel element examination reports published in the course of the Peach Bottom Surveillance Program¹⁻⁶ and a related paper.⁷ These data were subsequently augmented specifically to enhance the overall picture of tritium behavior in the reactor. The following information was obtained in this follow-on study:

1. tritium concentrations in a series of six fuel compacts taken from two fuel elements,
2. lithium impurity levels in samples of sleeve and spine graphite taken from fuel element E06-01 and from a radial reflector block,
3. BET surface area measurements on sleeve graphite and samples of charcoal from a fission product trap,
4. tritium concentrations throughout one radial reflector block,
5. axial tritium concentration profiles in the charcoal traps of three fuel elements.

The above data sets relate to the behavior of tritium in the Peach Bottom reactor core. Tritium concentrations observed in the primary and secondary coolant and in both the gaseous and liquid waste streams were extracted from ref. 8 and from the series of semiannual Peach Bottom operations reports published by the Philadelphia Electric Company. References 9 through 14 list these reports for the period of core 2 operation.

1.2 Regulatory Constraints on Tritium Discharges

Regulatory guides on maximum permitted radioactive discharges from nuclear reactors are set forth in the revised 10 CFR 50 Appendix I.¹⁵ Although these guides are specifically for light-water reactors (LWRs),

they have been applied to the Fort St. Vrain HTGR and hence, until augmented, may be assumed to apply to HTGRs. In a recent review, Gainey¹⁶ summarized the portions of these regulations pertaining to tritium releases and compared them with international practice.

The revised Appendix I of 10 CFR 50 places no specific limits on tritium concentrations in liquid or gaseous effluents from reactors or on total annual release (in curies) of tritium or other radionuclides. Instead, releases of all radionuclides from a reactor are limited by their annual dose or dose commitment to any individual in a nonrestricted area. Since the biological half-life of tritium is short (10 days), the annual dose and dose commitment to an individual are virtually identical.

Doses from liquid releases are limited to 3 millirems to the whole body and 10 millirems to any organ per year per reactor. Dose estimation must include all pathways of exposure. Tritium is not explicitly mentioned, but is simply one of the numerous nuclides that contribute to the total dose. However, it appears to be a major contributor to the annual dose; for example, Gainey reports¹⁶ that the maximum annual dose to an average adult resulting from the operation of a 1000-MW(e) HTGR equipped with a cooling tower would be 0.38 millirem/year, or more than 12% of the total annual dose allowed under Appendix I.

Gaseous discharges are limited by the revised Appendix I to yield a maximum dose of 5 millirems/year to the whole body and 15 millirems/year to the skin per reactor for any individual in an unrestricted area.

Guidelines for implementation of control technology are given in Appendix I in terms of the cost of control measures per unit of reduced annual population dose within 50 miles of the reactor. Control measures must be installed when an annual cost of \$1000 (capital plus operating) will effect a 1 man-rem dose reduction per year in a 50-mile radial zone.

Since the executive reorganization act of 1970, the Environmental Protection Agency (EPA) has played an increasing role in the regulation of radioactive releases and, evidently, will set the regulations to be enforced by the Nuclear Regulatory Commission (NRC). The necessary

modeling work required in the interpretation of the standards will be performed by the EPA.

Environmental radiation standards have recently been set forth by the EPA in 40 CFR 190.¹⁷ The main points in the standards appear to be the following:

1. The maximum annual dose to a member of the public is set at 25 millirems to the whole body, 75 millirems to the thyroid, and 25 millirems to any other organ as a result of releases from all uranium fuel cycle activities (i.e., releases from the entire fuel cycle industry in the United States).

2. Specific limits (in curies) are set for emissions of ^{85}Kr , ^{129}I , and alpha-emitting transuranics from the total uranium fuel cycle activities per gigawatt-year of electric power produced.

It should be noted that as in 10 CFR 50, tritium is not specifically mentioned in the EPA regulations. Furthermore, there is no EPA rule-making procedure in process that relates specifically to tritium releases.* Thus tritium release is not an HTGR regulatory problem at this time, but this situation could change in view of the significant portion of the maximum-allowable dose per reactor caused by tritium release from currently designed HTGRs.

1.3 Summary of Relevant Descriptive Literature

The basic descriptive document on the Peach Bottom HTGR is the final hazards summary report (FHSR)¹⁸ plus the additions relative to the major changes that were instituted following core 1 operation.¹⁹ Information on the configuration and composition of the various types of fuel elements is provided in the earlier fuel examination reports of the surveillance program,¹⁻³ and the ~25 fuel test elements (out of 804 total) are described in a report by Turner et al.²⁰ An introduction to the operation of the fission product purification and chemical cleanup systems is provided by Burnette et al.²¹ Valuable descriptive information, particularly with reference to neutron flux distributions, is provided by Wallroth et al.²²⁻²⁴

* However, a ^{14}C rule-making procedure is in process.

in their reports concerning the postirradiation examination of fuel test elements 18, 4, and 6, respectively.

More specifically with respect to tritium behavior in HTGRs, the following reports are most helpful. The recent review by Gainey¹⁶ summarizes much of the tritium literature pertaining to HTGRs, and Forsyth provides an analysis of tritium production, migration, and removal from the Dragon reactor²⁵ as well as an analysis of tritium behavior in a hypothetical 1500-MW(t) HTGR.²⁶ The bibliographies in these three reviews contain most of the pertinent literature; however, numerous references are made therein to internal documents and personal communications. An earlier work by Compere et al.²⁷ discusses tritium sources and pathways in HTGRs for use in constructing an analytical model describing distribution and release. The model, TRITGO, specifically dealt with Fort St. Vrain parameters. In addition, a number of tritium modeling studies have been performed by a group in the Jülich Institute for Reactor Development. The results of some of these studies are summarized in a paper by Rohrig et al.²⁸

The literature regarding tritium and hydrogen permeation through various metals and alloys is quite extensive. Fortunately, an excellent review by Strehlow and Savage²⁹ ties together many of the apparent inconsistencies in previous investigations. Yang et al.³⁰ specifically measured tritium permeation through the Peach Bottom steam-generator tubes and estimated leakage rates through the steam generator.

Studies regarding the retention of tritium in HTGR fuel particles are given in ref. 31 and by Walter^{32,33} for both Triso- and Biso-coated particles. These studies and others on this subject have been carefully reviewed by Gainey.¹⁶ A recent treatise by Causey³⁴ provides values for the diffusion coefficient of tritium in pyrolytic graphite and some interpretation of the factors that affect the diffusion rate.

Adsorption and desorption kinetics of hydrogen and tritium from HTGR core graphite and fuel matrix material was studied by Fischer.³⁵ Some of the specimens studied were partially oxidized, and it was found that 1.5 to 2.0% oxidation approximately doubled the equilibrium loading of tritium

on graphite. In addition, the desorption experiments were conducted in a fashion that allowed calculation of effective diffusion coefficients.

1.4 Brief Description of the Peach Bottom HTGR

The Peach Bottom primary loop is shown schematically in Fig. 1.1. The primary circuit consisted of two loops, each of which contained a helium compressor and a steam generator. The total helium flow of 210,000 kg/hr (463,000 lb_m/hr) was divided equally between the two loops, which had a combined volume of approximately 232 m³ (8200 ft³). All the large duct, pressure-containing material of both primary loops was carbon steel. Details regarding valves, compressors, reactor internal flow configuration, and steam-generator tubing geometry are provided in Sect. II-D of ref. 18.

The coolant temperatures at the core inlet and outlet of the reactor vessel were 345 and 714°C, respectively, and the primary loop pressure was nominally 32.8 atm. The coolant exited from the reactor in the inner pipe of a concentric duct arrangement consisting of an outer 42-in.-OD pipe and an inner 30-in.-OD pipe. The thermal barrier inside the inner pipe, fabricated from laminated 304 stainless steel, maintained the inner wall temperature below 371°C.

The Peach Bottom steam generators and the concentric duct connecting the reactor with them are described in detail in the report on the metallurgical examination³⁶ conducted by GAC as a part of the Peach Bottom End-of-Life Program. Feedwater entered an economizer bundle, which consisted of low-carbon steel tubes, and was discharged to the steam drum. Condensate from the drum was conducted to the evaporator section of the steam generator, composed of silicon-low-carbon steel tubing, and back to the steam drum. Vapor from the steam drum passed into an Incoloy 800 superheater section and on to the turbine. Tubing materials and tube sizes used in the steam generator are summarized in Table 1.1. The cold duct, which extended from the steam-generator outlet to the compressor and on to the entry region of the concentric pipe, consisted of 28-in.-OD carbon steel pipe.

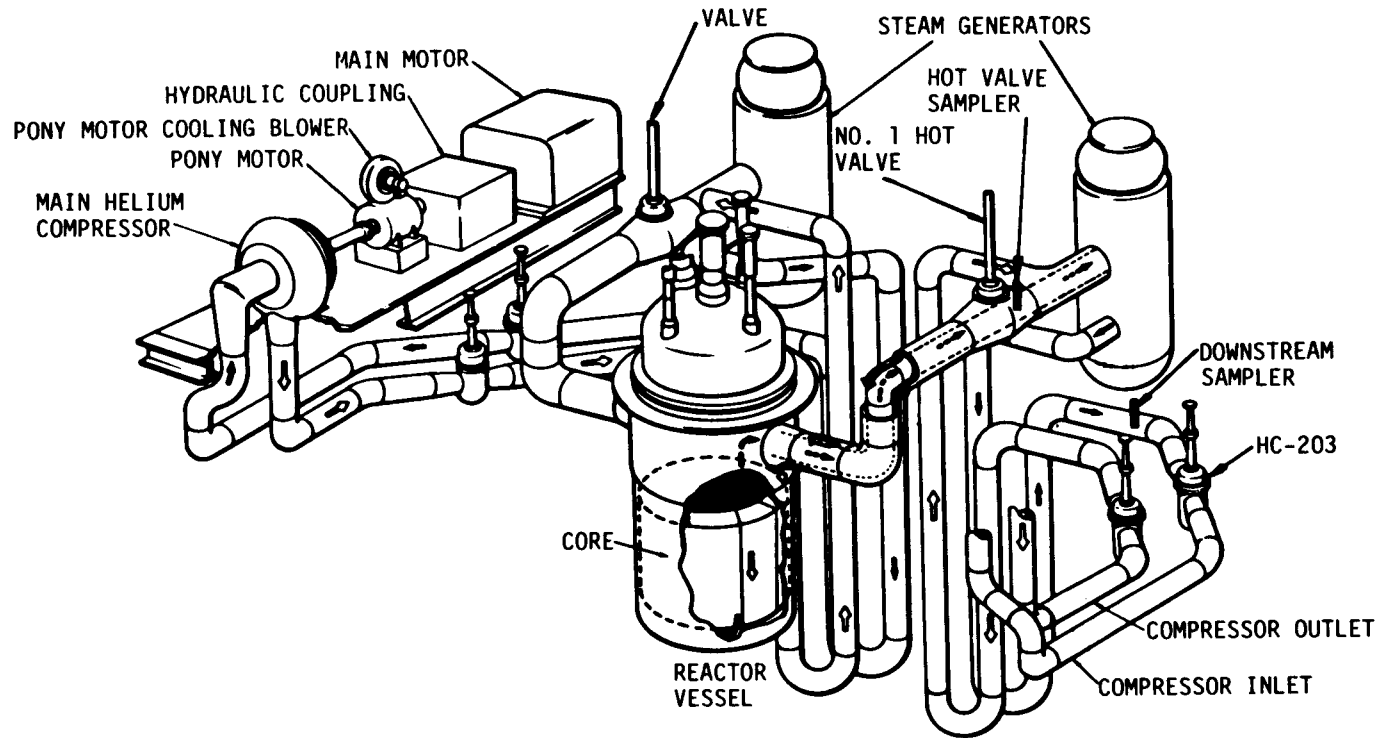


Fig. 1.1. Primary loop schematic for the Peach Bottom HTGR.

Table 1.1. Materials, surface area, and temperature range of tubing in the Peach Bottom steam generators³⁰

Section	Material	Surface area ^a (m ²)	Outside diameter (cm)	Inside diameter (cm)	Average metal temperature range (K)
Economizer	Low-carbon steel	212	1.270	0.955	513-593
Evaporator	Silicon-low-carbon steel	474	1.905	1.461	593-618
Superheater	Incoloy 800	275	1.905	1.270	693-853

^aFor two steam generators.

A diagram of the Peach Bottom fuel element is provided in Fig. 1.2. The helium coolant flow is upward, external to the 8.89-cm-diam (3.5-in.) graphite sleeve. A small portion of this flow (about 0.45 kg/hr per fuel element) was drawn into the purge hole in the top of the element and proceeded downward in the element in the gaps between the sleeve and fuel and between the fuel and graphite spine. These gaps are illustrated in Fig. 1.3. The purge gas proceeded through the active portion of the element, passed through the charcoal filters, and entered the fission product cleanup system described in Sect. 2.2.

The fuel particles were Biso-coated kernels of $(\text{Th,U})\text{C}_2$ with an initial thorium:uranium ratio of either 5.5:1 or 18.5:1. There were two separate production runs of fuel particles producing somewhat differently sized particles. No documentation exists on how many of each type of fuel particle were used or how they were deployed throughout the core, except that each fuel compact consisted of one type of fuel particle. The smaller low-thorium fuel particles had kernels with average diameters of 300 μm , compared with 400- μm kernel diameter and 135- μm coating thickness for the large particles. Fuel particle specifications for core 2 are summarized in the facility change amendment to the FHSR.¹⁹ The various types of fuel compacts and graphites used in the core are summarized in Chap. 2 of refs. 1 and 2.

According to the revised FHSR,¹⁹ the low-thorium fuel particles in core 2 experienced a maximum burnup of 13% fissions per initial metal atom (FIMA), a maximum fast fluence of 4.8×10^{21} neutrons/cm², and a maximum fuel temperature of 1510°C. The high-thorium fuel experienced less severe conditions: 5% FIMA, 2.7×10^{21} neutrons/cm², and 1200°C. Design calculations predicted that no fuel reached these maximum temperatures until 700 full-power irradiation days had been attained, after which less than 1% of the fuel was subjected to the stated temperature extremes.

Temperatures within the six fuel elements examined in the Peach Bottom Surveillance Program were estimated in a thermal analysis effort performed at GAC.³⁷ Since these elements were carefully selected to be representative of particular fuel element types and locations, the study

ORNL-DWG 78-4994

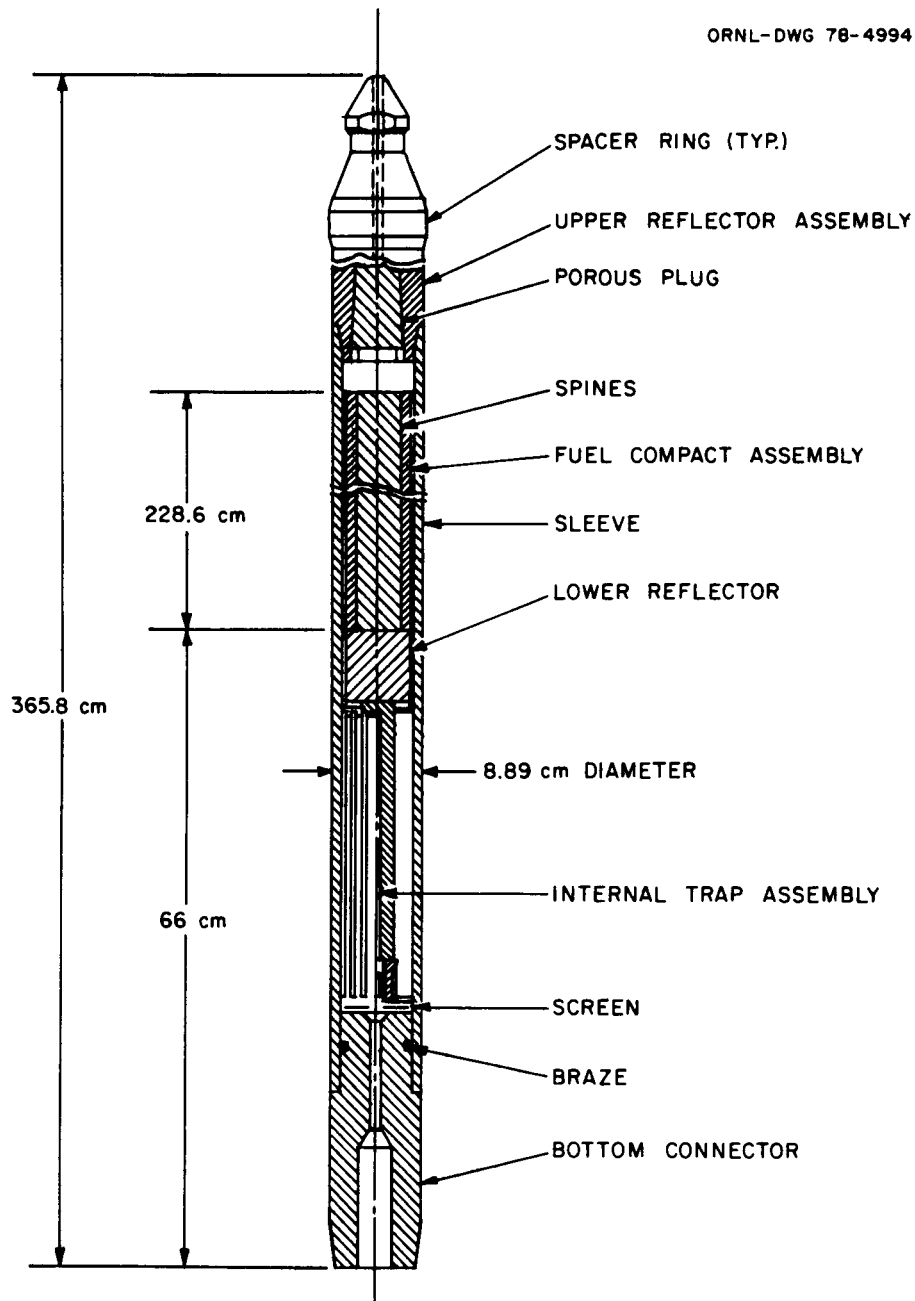


Fig. 1.2. Fuel element for the Peach Bottom HTGR.

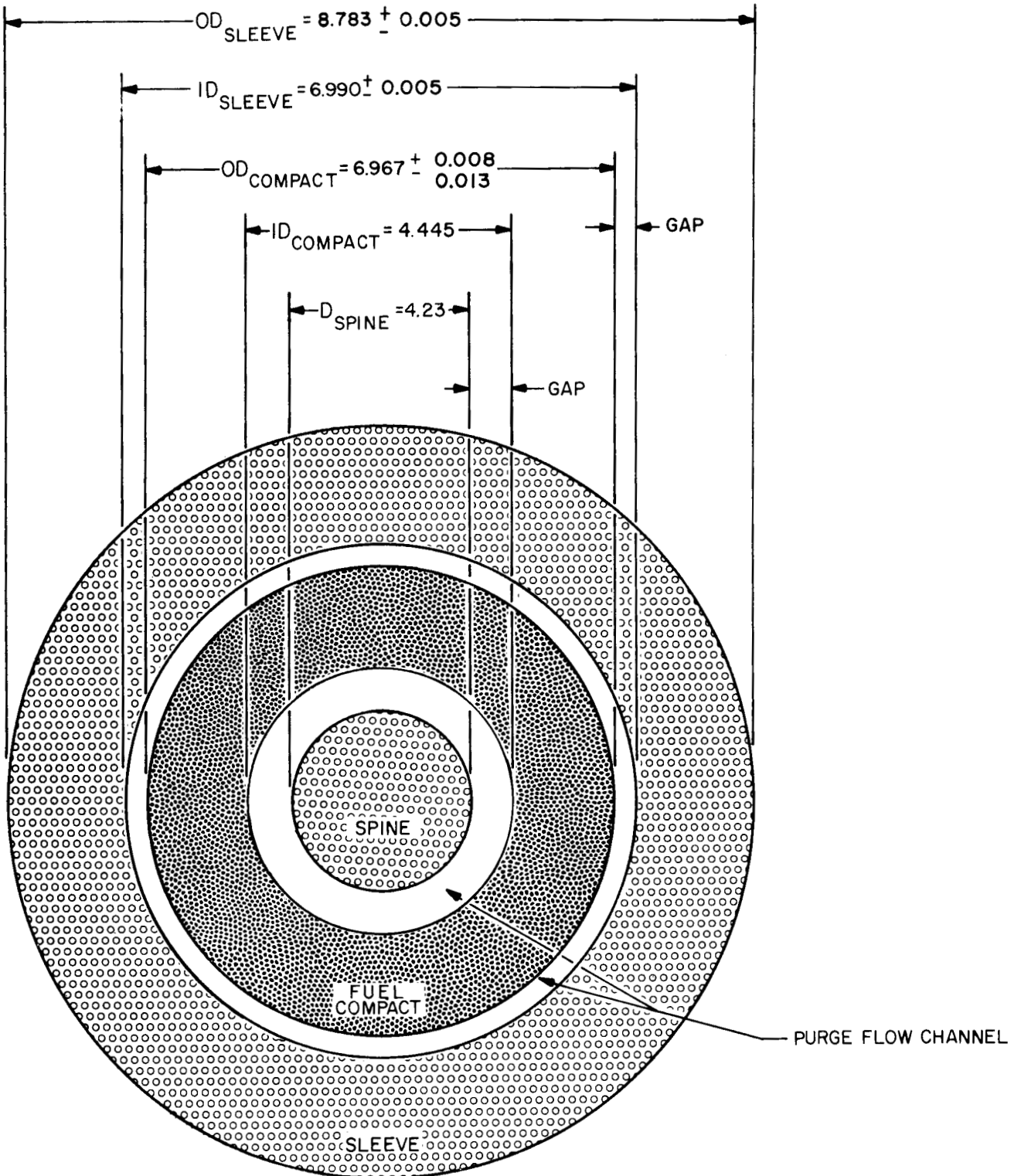


Fig. 1.3. Cross section of the Peach Bottom fuel element showing nominal preirradiation dimensions. (All dimensions in cm.)

provides a reasonably detailed temperature distribution and history within the core.

An ideal core cross section is shown in Fig. 1.4. The active core was a 277.4-cm-diam (109.2-in.) right cylinder with a 228.6-cm (90-in.) height. The radial reflector consisted of a 27-cm-thick (10.5-in.) replaceable zone and a 33-cm-thick (13-in.) permanent zone. The upper and lower reflector zones had a combined length of 137.2 cm (54 in.). Table 1.2 lists the estimated masses of graphite in each of these zones computed from the nominal fuel element and core dimension and using the following graphite densities: 1.9 g/cm³ for the sleeve, 1.85 g/cm³ for the spine, 1.8 g/cm³ for the reflector graphites, and 1.71 g/cm³ for fuel matrix material, again as given in the FHSR.¹⁹ The volume of matrix material in the core was approximated from the total volume of the fuel compacts and a 0.86 estimated volume fraction for the matrix determined from photomicrographs shown in ref. 3. The FHSR gives the density of the matrix material as 1.71 g/cm³.

In addition to 804 fuel element locations, the core contained 35 control rods and 19 emergency shutdown guide tubes. The graphite sleeve material for the control rods and emergency tubes was identical to that of the fuel element sleeves and is included in the total sleeve mass given in Table 1.2.

The reactor contained a permanent inventory of 1.1 kg of natural boron as zirconium boride distributed within the hollowed spines of 60 fuel elements. In addition, the control rods contained a variable inventory of boron as boron carbide. Each control rod was purged internally with helium that was drawn from the primary coolant in the vicinity of the inlet plenum and rejoined the primary coolant at the core exit. Hence, tritium born in the control rods, in principle at least, had available a direct pathway to the primary coolant. The boron in the poisoned spine was encased in graphite tubes (hollowed spines) and thus shielded from the fuel element purge flow that passed through each element. Section 5.3 (associated with Table 5.47) shows that tritium born in the poisoned spines did not escape to the purge gas flow (and hence the primary coolant).

ORNL-DWG 78-18294

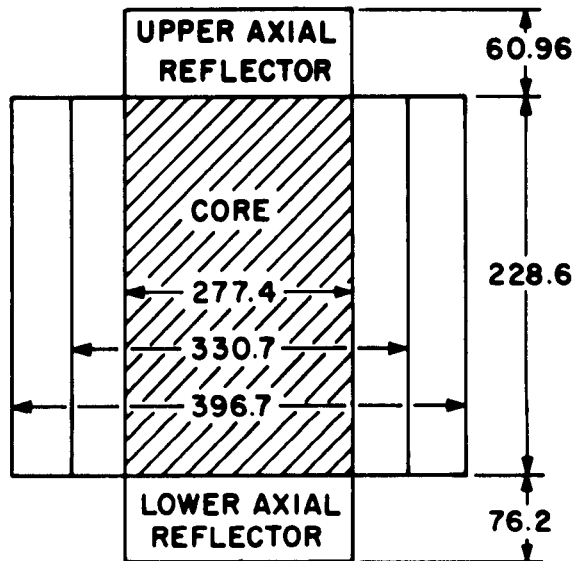
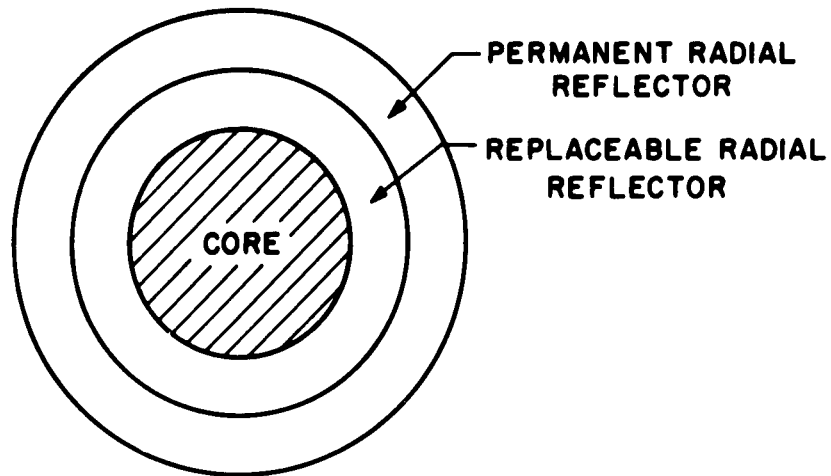


Fig. 1.4. Nominal core dimensions (cm).

Table 1.2. Graphite densities and masses in the core

	Density (g/cm ³)	Mass (g)
Graphite mass		
Sleeve	1.9	8.64 x 10 ⁶
Spine	1.85	4.48 x 10 ⁶
Axial reflector	1.8	8.33 x 10 ⁶
Removable radial reflector	1.8	9.26 x 10 ⁶
Permanent radial reflector	1.8	1.37 x 10 ⁷
Fuel matrix material	1.71	5.75 x 10 ⁶

1.5 Acknowledgments

The efforts of many persons, which were indispensable in the course of this study, are gratefully acknowledged. In particular, W. J. Martin and L. L. Fairchild were instrumental for the logistics involved in the dissections and preparation of the large numbers of samples from both the fuel and reflector elements. The efforts of Mr. Fairchild were expanded considerably in 1978 when Mr. Martin retired. L. D. Bible and W. F. Rogers (Analytical Chemistry Division) skillfully sectioned fuel element graphite with a remotely operated lathe facility designed and installed by L. C. Bate, and Mr. Bate was very instrumental in establishing procedures for remotely burning highly radioactive graphite and collecting the HTO therefrom. R. F. Apple did much of the graphite combustion work required for tritium analysis and adapted the procedures to the determination of tritium in fuel. The expertise of Hugh Parker in beta counting of tritium is particularly recognized. We also appreciate the helpful comments provided by E. L. Compere and M. J. Haire in their technical review. Finally, we express thanks to Betty Drake for the efficient and accurate preparation of this report.

2. SOURCES AND PATHWAYS OF TRITIUM IN PEACH BOTTOM

2.1 Sources

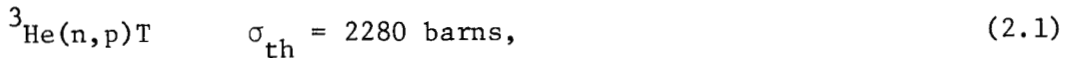
The literature regarding the production rates of tritium in nuclear reactors has been summarized by Gainey.¹⁶ This review also compares the calculations of Compere et al.,²⁷ Forsyth,²⁶ and an internal GAC document on tritium production rates in a 3000-MW(t) HTGR, so that the major tritium sources in the Peach Bottom HTGR are fairly clear.

The largest tritium source was due to ternary fission of ^{235}U , and since ^{233}U accounted for about 25% of the total fissile inventory at the end of core life, ternary fission of ^{233}U was also a significant contributor. Some experimental values of tritium yields from ^{233}U and ^{235}U fission are listed in Table 2.1, taken from Gainey.¹⁶ Note that the yield for ^{235}U increases with neutron energy, a trend anticipated also for ^{233}U . Thus, the simplification used by Compere et al.,²⁷ who employed a tritium yield of 1.0×10^{-4} atom/fission for fissions in an HTGR flux spectrum irrespective of fissile parent, seems to be reasonable.

Table 2.1. Some reported literature values for tritium yields from ^{235}U and ^{233}U fission (Gainey¹⁶)

Tritium yield [atoms/fission ($\times 10^4$)]		
^{233}U	^{235}U	
1.1	0.85 ± 0.09	Thermal neutrons
0.88 ± 0.07	0.75 ± 0.08	Thermal neutrons
	0.95 ± 0.08	Thermal neutrons
	0.8 ± 0.01	Thermal neutrons
	2.0 - 2.2	Fast neutrons

According to Compere²⁷ and Forsyth,²⁶ following ternary fission in importance, tritium is produced via the following two reactions at approximately equal rates in HTGRs:



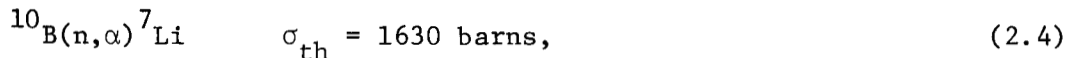
The effective thermal cross sections given for these reactions in Table 2.1 are those reported by Compere et al.²⁷ averaged for the neutron energy range 0 to 2.39 eV. Since neutronics calculations performed at GAC on the Peach Bottom HTGR employed four neutron energy groupings of which the lowest, or "thermal," group was the 0- to 2.38-eV range, effective thermal cross sections employed here should be averaged over this energy range in order to utilize flux level information generated by GAC.

In large HTGRs, where as much as 5% of the helium inventory resides in the core, it is stated that (ref. 16) the ${}^3\text{He}$ concentration equilibrates in about 40 days provided the helium leakage rate exceeds 0.2%/day. (Actually, design calculations usually assume a primary system leakage of 0.01%/day; hence equilibration times for ${}^3\text{He}$ are far longer than 40 days in large HTGRs.) In the Peach Bottom HTGR, a far smaller portion of the helium inventory was in the core, so the ${}^3\text{He}$ burnout rate was not significant. However, the helium leakage (hence makeup) rate was much higher, about 0.8%/day, establishing a ${}^3\text{He}$ concentration equilibrium in about 125 days.

Tritium may also be produced from ${}^{10}\text{B}$ in natural boron either directly via



or via the chain



As for the thermal-neutron reactions (2.1) and (2.2), the value of the cross section for reaction (2.4) given in Table 2.1 is the effective value averaged over the thermal group energy range as reported in ref. 27. The cross sections for the fast-neutron reactions [(2.3) and (2.5)] are

shown in Fig. 2.1 as a function of incident neutron energy.* Although the reaction $^{10}\text{B}(n,2\alpha)\text{T}$ is usually categorized as a fast-neutron reaction, the $1/v$ section extending to about 10 keV appears to have some significance. Nevertheless, in the estimates of tritium production rates given in Sect. 6.1.4, we will assume the effective fast cross-section value given by Gainey¹⁶ of 0.050 barn, averaged over neutron energies greater than 0.18 MeV. Presumably, this effective cross section takes the lower energy range into account.

The cross section for the fast reaction $^7\text{Li}(n,n'\alpha)\text{T}$ is also displayed in Fig. 2.1 as a function of neutron energy. This appears to be truly a fast reaction with a threshold energy of 2.281 MeV. As above, we will employ the average fast cross-section value of 0.153 barn for this reaction effective over the neutron energy range in excess of 0.18 MeV. Table 2.2 summarizes the significant neutron reactions producing tritium and the assumed effective cross sections used in Sect. 6.1 for tritium production rate estimates.

The relative values of tritium production rates from these four sources are illustrated in Table 2.3, which lists results of three reported calculations for similar, large HTGRs. In these studies, 60 to 69% of the tritium source was from ternary fission, 12 to 23% from ^3He , 8 to 24% from ^6Li , and the balance from ^{10}B . Our estimates for the Peach Bottom HTGR developed in Sect. 6.1 are in accord as to the relative importance of ternary fission, but we calculate a significantly higher relative importance of the ^{10}B source, principally from reactions in the control rods. Concurrently, our estimates of the importance of the ^6Li and ^3He sources, which are based on actual impurity level measurements, are much lower than indicated by the three studies shown in Table 2.3.

2.2 Tritium Transport Paths

The simplified flowsheet of the reactor primary circuit and cleanup systems shown in Fig. 2.2 illustrates the principal source locations and pathways for tritium in the Peach Bottom reactor. The major sources are

*Courtesy of R. M. Westfall, Neutron Physics Division.

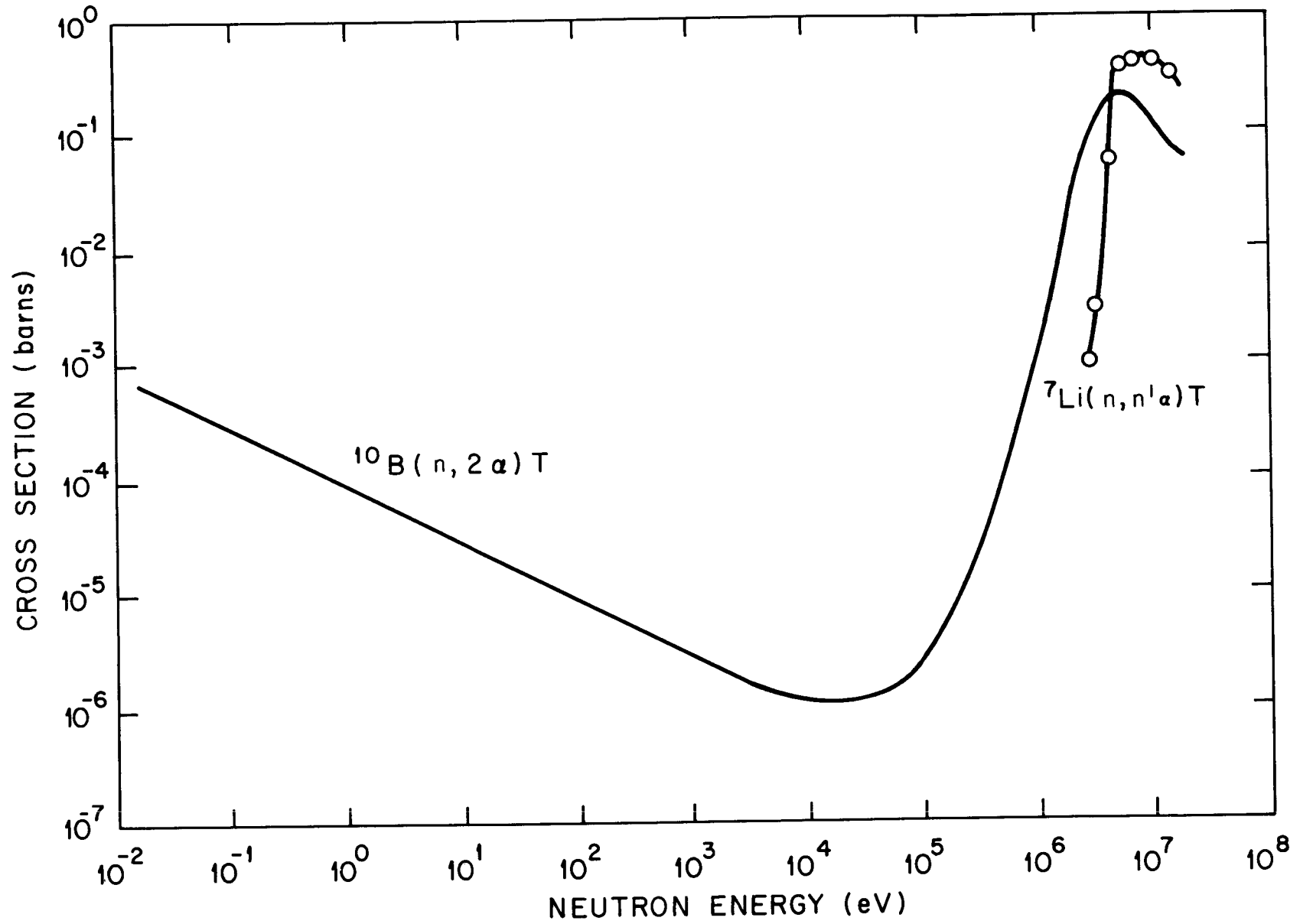


Fig. 2.1. Cross section for reactions $^{10}\text{B}(n, 2\alpha)\text{T}$ and $^7\text{Li}(n, n'\alpha)\text{T}$ from ENDF/B-IV.

Table 2.2. Effective cross sections for significant neutron reactions producing tritium

Reaction	Symbol	Cross section (barns)	Energy range (eV)	Source
$^3\text{He}(n,p)\text{T}$	σ_3	2280	0-2.38	27
$^6\text{Li}(n,\alpha)\text{T}$	σ_6	408	0-2.38	27
$^{10}\text{B}(n,2\alpha)\text{T}$	σ_{10}'	0.050	$>0.18 \times 10^6$	16
$^{10}\text{B}(n,\alpha)^7\text{Li}$	σ_{10}	1630	0-2.38	27
$^7\text{Li}(n,n'\alpha)\text{T}$	σ_7'	0.153	$>0.18 \times 10^6$	16

Table 2.3. Comparison of calculated tritium production rates in a 3000-MW(t) HTGR¹⁶

Reference	Production rate (Ci/year)					Total
	Ternary fission	^3He	^6Li	^{10}B		
				Path (2.4)	Path (2.5)	
27	9,213	1771	3843	410	376	15,614
26	19,866	6716	2376	Neglected		28,958
Internal GAC	11,000	3680	2813	919		18,412

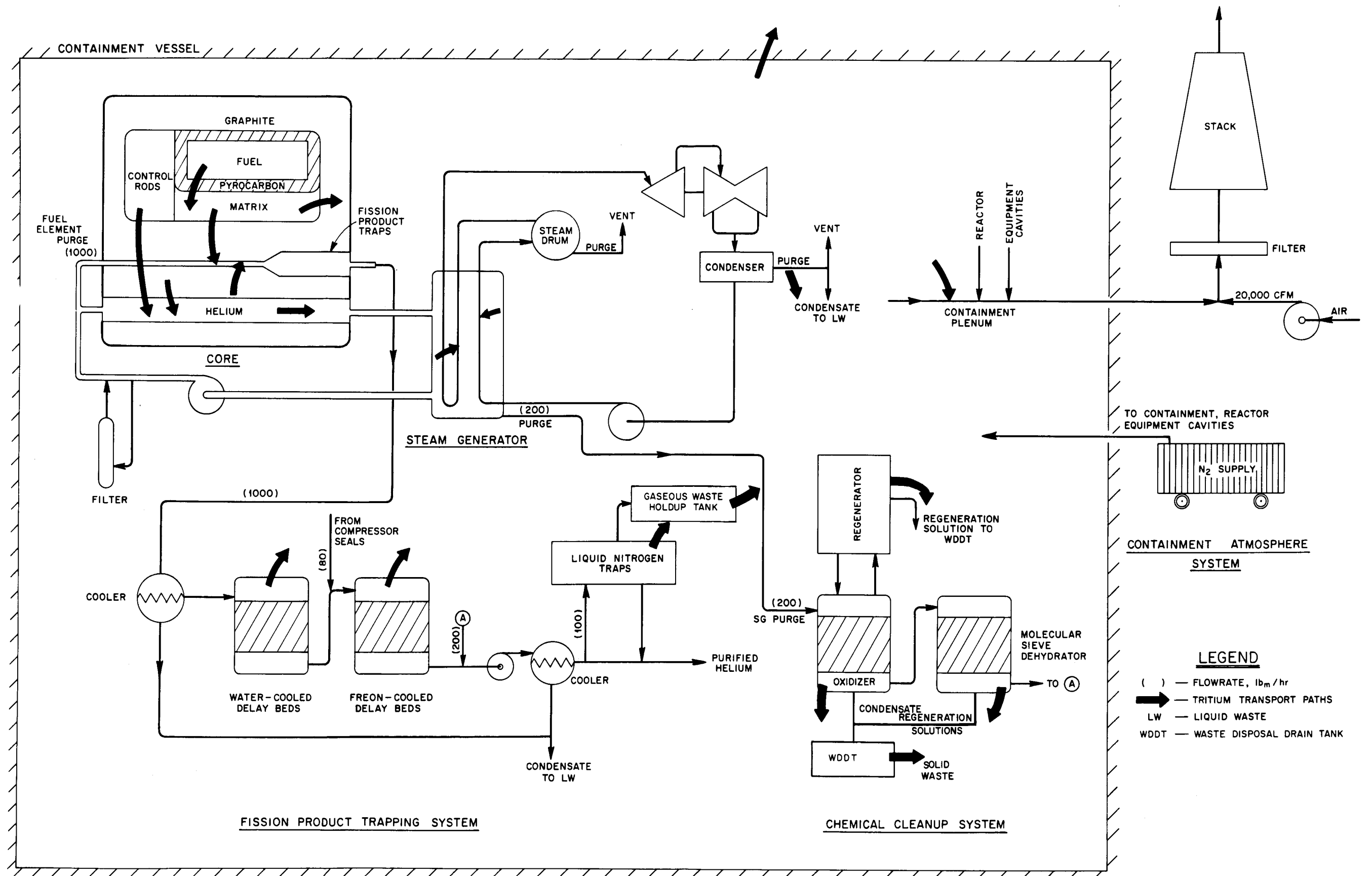


Fig. 2.2. Simplified flowsheet of Peach Bottom HTGR illustrating tritium transport paths.

ternary fission in the fuel and neutron reactions with ^{10}B in the control rods and poisoned spines. In close physical association with the fission source is the tritium produced in the matrix material from both tramp fuel and lithium contaminant. The two other principal tritium sources are the core graphite (from lithium contamination) and the helium coolant in the core (from the ^3He contaminant).

Pathways for tritium migration in the core and steam generator are indicated by the bold arrows in Fig. 2.2. Tritium may migrate from the fuel through the pyrocarbon coating and matrix material directly into the helium purge gas flow. Alternatively, some of the tritium formed in the fuel may pass into the sleeve graphite, either directly at points of contact with the fuel compact or through the purge flow gap, where it may pass into the helium coolant along with the tritium born in the sleeve graphite.

In addition, the tritium born in the control rods due to neutron reaction with boron and that formed in the radial reflector due to lithium impurity content could pass directly into the helium coolant. The control rods are purged with a small flow of purified helium ($100 \text{ lb}_m/\text{hr}$ for all rods) which joins the main coolant in the vicinity of the upper plenum. This purge flow, in principle, could be a vehicle for transporting a portion of the control rod tritium to the main coolant. In addition, the radial reflector blocks and removable reflector elements were cooled by a small fraction of the main coolant flows and therefore could have picked up a portion of the tritium born within the block or element.

A small portion of the tritium picked up by the fuel element purge flow was permanently retained in the fission product trap located within the base of each fuel element, but the major portion left the core in the purge stream and entered the fission product trapping system.

If the dew point of the fuel element purge gas was sufficiently high, some water containing HTO would condense in the cooler upstream from the first charcoal delay bed. This condensate, together with that from the cooler downstream of the compressor in the Freon-cooled bed, was conducted to the liquid waste system.

It was estimated that HT, which is the principal chemical form for tritium in the reactor coolant, would be delayed for only a few hours by the water- and Freon-cooled delay beds.²¹ Only a small degree of permanent chemisorption on charcoal would occur at these intermediate temperatures (see Sect. 6.3.1). Periodically (approximately yearly during reactor shutdowns), the delay beds were regenerated by allowing them to warm up; during this process any adsorbed HT in the bed desorbed, along with other gases, and entered the containment volume. Ultimately, after dilution and monitoring, the gases released during regeneration of the delay beds left the reactor as gaseous effluent. However, any tritium entering the beds as HTO, which was a small portion of the total tritium at this point, would probably have been permanently retained in the bed.

Therefore, it appears that the water- and Freon-cooled delay beds did not play a significant role in the disposition of tritium in the reactor or significantly affect the quantity released. This is seemingly ironic since the charcoal traps in the fuel elements contained significant quantities of permanently trapped tritium. Data presented in Sect. 5 show that the fuel element trap contained an average of about 400 $\mu\text{Ci/g}$ of tritium at EOL, which means that only 450 kg of charcoal would have been needed to permanently trap the estimated 350 Ci that entered the purge gas flow in four years of operation.* The cold delay beds contained far more than this amount of charcoal.†

About 10% of the purified helium leaving the Freon-cooled bed was diverted to liquid-nitrogen-cooled charcoal beds. This system was originally intended to capture argon and krypton (as well as methane, nitrogen, and HT) for bottling and shipment to a disposal area. However, as operated, the off-gas from the frequent regeneration of the liquid-nitrogen-cooled

* Estimated in Sect. 6.3.1.

† The reason for the relative ineffectiveness of the water- and Freon-cooled delay beds for tritium retention is demonstrated by Fig. 6.3. Adsorption of tritium on charcoal is near the minimum at these temperatures — too low for chemisorption but too high for physical adsorption. On the other hand, a significant portion of the fuel element charcoal trap was at a sufficiently high temperature for chemisorption to be effective.

beds was collected in a holdup tank for assay and subsequently discharged to the containment volume. Operational reports⁹⁻¹⁴ indicate that more than 99% of the tritium activity in the stack off-gas flow originated from the regeneration of the liquid-nitrogen-cooled beds. This was confirmed by discussions with operating personnel.

A smaller helium purge flow (~ 200 vs ~ 1000 $\frac{\text{lb}_m}{\text{hr}}$ for the fuel element purge) was drawn from the steam generator to the chemical cleanup system, which consisted of an oxidizer unit and a molecular-sieve dehydrator (Fig. 2.2). Gaseous HT was converted to HTO in the oxidizer and drawn off to the waste disposal drain tank (WDDT) from the condenser downstream from the unit. Additional HTO was removed by the molecular-sieve dehydrator downstream from the oxidizer. At frequent intervals, the molecular sieve was regenerated, releasing the trapped water which was also conducted into the WDDT. A vent on WDDT contributed to the presence of tritiated humidity in the containment atmosphere. After the contents of the WDDT were assayed, the liquids were adsorbed on clay and shipped off-site as solid wastes.

Some of the tritium that entered the primary coolant circuit, primarily as HT, diffused through the steam-generator tubing and entered the secondary coolant, where it is expected to have exchanged rapidly with hydrogen in water. Since water molecules predominated in the secondary system, isotopic exchange would render HTO the dominant tritium species. Thus the tritium that diffused through the steam generator tubing was ultimately drawn into the containment sump (via condensate from the condenser purge or condenser blowdown), which served as a collection point for liquid wastes.

2.3 Liquid Waste Removal System

The Peach Bottom FHSR¹⁸ identifies four classes of liquid wastes.

Class A, normally radioactive liquids, includes the caustic solution and water from the regeneration of the oxidizer in the chemical cleanup system, water condensed from the oxidizer in the chemical cleanup system, water condensed from the regeneration of the molecular sieve dehydrater,

and oil drained from control drive and compressor lubrication systems. Although not explicitly mentioned, the condensate from the steam drum and condenser purge are also in this category.

Class B, potentially radioactive liquids, includes various reactor and laboratory floor drains and cooling water from various helium and equipment coolers.

Classes C and D are nonradioactive liquids and sanitary sewage, respectively.

Class A and B liquids (except the condensate from the chemical cleanup system) were directed to a reservoir in the containment vessel termed the containment or radwaste sump and then transferred to the waste receiver tanks located outside the containment. The wastes were then sent to the radwaste system or, if radioactivity levels were found to be sufficiently low, directly to the waste monitor tanks for discharge to the main cooling water effluent at a controlled rate. A more complete description of the liquid waste system is provided in Fig. V1-1 and Table V1-1 of ref. 18.

Following initial reactor operation, an additional collection tank was installed for condensate from the oxidizer and dehydrator units in the chemical cleanup system and for the scrubber solutions used for regenerating the oxidizer. The motivation for the placement of this additional vessel, WDDT, was to isolate the highly caustic regeneration solution from the liquid waste system and thereby prevent corrosion. However, since these liquids contained the highest levels of tritiated water of all liquid wastes, the WDDT also provided a means for significantly reducing the quantity of tritium discharged with the liquid waste flow. Operation of the WDDT is not described in the FHSR because of its late installation; however, surveillance personnel reported that it was vented to the containment and thereby contributed to the observed tritium levels in the containment atmosphere. Operations personnel report that the liquid contents of the WDDT were adsorbed on a clay-type sorbent, packaged, and shipped offsite as solid wastes. At no time were the liquids in the WDDT allowed to pass into the liquid waste system for disposal to Conowingo Pond.

2.4 Gaseous Waste Removal System

The primary route for removal of radioactive gaseous wastes from the reactor was via the liquid-nitrogen-cooled delay beds in the fission product cleanup system (see Fig. 2.2). Approximately monthly, these beds were allowed to warm for regeneration, at which time the desorbed gases, principally argon and krypton with some nitrogen and methane, were collected in the gaseous waste isolation tank, inventoried, and released to the containment volume for disposal via the stack. The removal route for all other gaseous wastes as well was by entry into the containment atmosphere and, after filtration and dilution with about 20,000 scfm of air, dispersal through the off-gas stack.

Under normal operation, several pieces of equipment were vented to the containment volume. The most important discharges were the noncondensables from condenser purge lines (see Fig. 2.2). In addition, the waste disposal drain tank, which collected HTO-containing liquids from the cleanup system, contributed tritiated humidity to the containment.

During reactor operation, the estimated containment volume of 720,000 ft³ was pressurized to 8 psig with nitrogen obtained from tank cars. Evidently, the small but unspecified flow of nitrogen provided to maintain containment pressure during reactor operation also served to sweep vented gases to the containment exhaust plenum and then to the stack. Technical specifications restricted leakage from the containment to the outside air to 0.2%/day at the 8-psig pressure, and containment leakage tests performed in 1972 indicated that the actual leakage rate was less than the specified amount.¹⁰ In three consecutive tests, an average leakage rate of 0.1%/day was observed at the full containment pressure. The principal leakage points were identified as the main personnel air lock and one of several electrical penetrations.

During periods of reactor shutdown when access to the containment was necessary, the inert-nitrogen containment atmosphere was replaced with air to allow maintenance work. The tritium inventory in the containment was thereby periodically disposed of at these times via dispersal through the stack.

2.5 Contaminated Solid Wastes

As noted above, the liquid contents of the WDDT were adsorbed on clay and disposed of as solid wastes. Other contaminated solid wastes (equipment, clothing, etc.) contained insignificant amounts of tritium.

2.6 Summary of Pathways

The various tritium pathways in the Peach Bottom reactor are presented in Sects. 2.2 to 2.5 and in Fig. 2.2. Detailed modeling of tritium behavior in this reactor may require descriptive information that is not available in the operation reports, the FHSR, and the various GAC documents. Further descriptions may be needed in the following areas:

1. Information is needed on the behavior of the three sets of charcoal delay beds in the fission product trapping system with respect to tritium. Tritium as HT was not considered in the design of these beds; nevertheless, there was some HT holdup in these beds and therefore some HT release during bed regeneration.

2. Data regarding the purge rate of the main condenser and boiler blowdown rate are required to model this tritium pathway from the secondary coolant to the liquid waste system.

3. Tritium inventory determinations on the contents of the WDDT, which may be available in the archive of the operation records, would be helpful in more firmly establishing the quantity of tritium disposed of as solid waste. (An indirect determination of this amount is presented in Sect. 6.3.2.)

3. MATERIAL PROPERTIES

3.1 Tritium Sorption on Graphite and Charcoal

It is generally agreed that the sorptive capacity of graphite for HT acts as a buffer and strongly influences the quantity of tritium that enters the coolant. Early in core life, tritium levels in the coolant should remain low while the fresh graphite is being loaded with tritium.³⁸ In

addition to the adsorptive behavior on graphite, tritium model development requires data on the retention and desorption of both HT and HTO from charcoal. The charcoal-filled fission product traps in the fuel elements, which are unique to the Peach Bottom design, were found to permanently retain significant quantities of tritium. However, much of the tritium evidently passed through the traps to the charcoal delay beds in the chemical cleanup system. These beds, although not designed for tritium retention, may have significantly affected the general level of tritium in the containment atmosphere [i.e., reactivation of these beds by allowing them to warm allowed release of adsorbed HT (but not HTO) to the containment atmosphere].

Some conventional wisdom regarding the adsorption of hydrogen on carbon is given by Trapnell³⁹ based on experiments conducted by Barrer and Rideal in the thirties. According to Trapnell, hydrogen is physically adsorbed on charcoal in increasing amounts with decreasing temperature for levels below about -70°C . Above -70°C and up to about 300°C , little adsorption occurs; however, above 300°C the capacity again rises as chemisorption rates increase. Indications are that sorptive capacity again falls as temperatures in the 1400 to 1600°C range are approached.

These features are borne out in the brief review of this subject by Gainey.¹⁶ Figure 3.1, taken from Gainey and based on data presented by Redmond and Walker,⁴⁰ presents data on TSP nuclear graphite for temperatures between 900 and 1500°C . Note that for low tritium pressures the equilibrium loading in graphite increases up to $\sim 1100^{\circ}\text{C}$ and subsequently falls at higher temperatures.

The degree of low-temperature sorption of H_2 on activated charcoal, taken from Dushman,⁴¹ is indicated in Table 3.1. The quantity adsorbed per unit pressure of H_2 increases with decreasing temperature from 0 to -183°C , and only a small variation of loading per unit applied partial pressure is observed in the charcoal data. Equilibrium hydrogen loadings on charcoal at low temperature and on TSP graphite at high temperature are compared in Table 3.1. Contrary to the data for charcoal, adsorption on graphite per unit H_2 partial pressure falls significantly with

ORNL-DWG 78-18293R

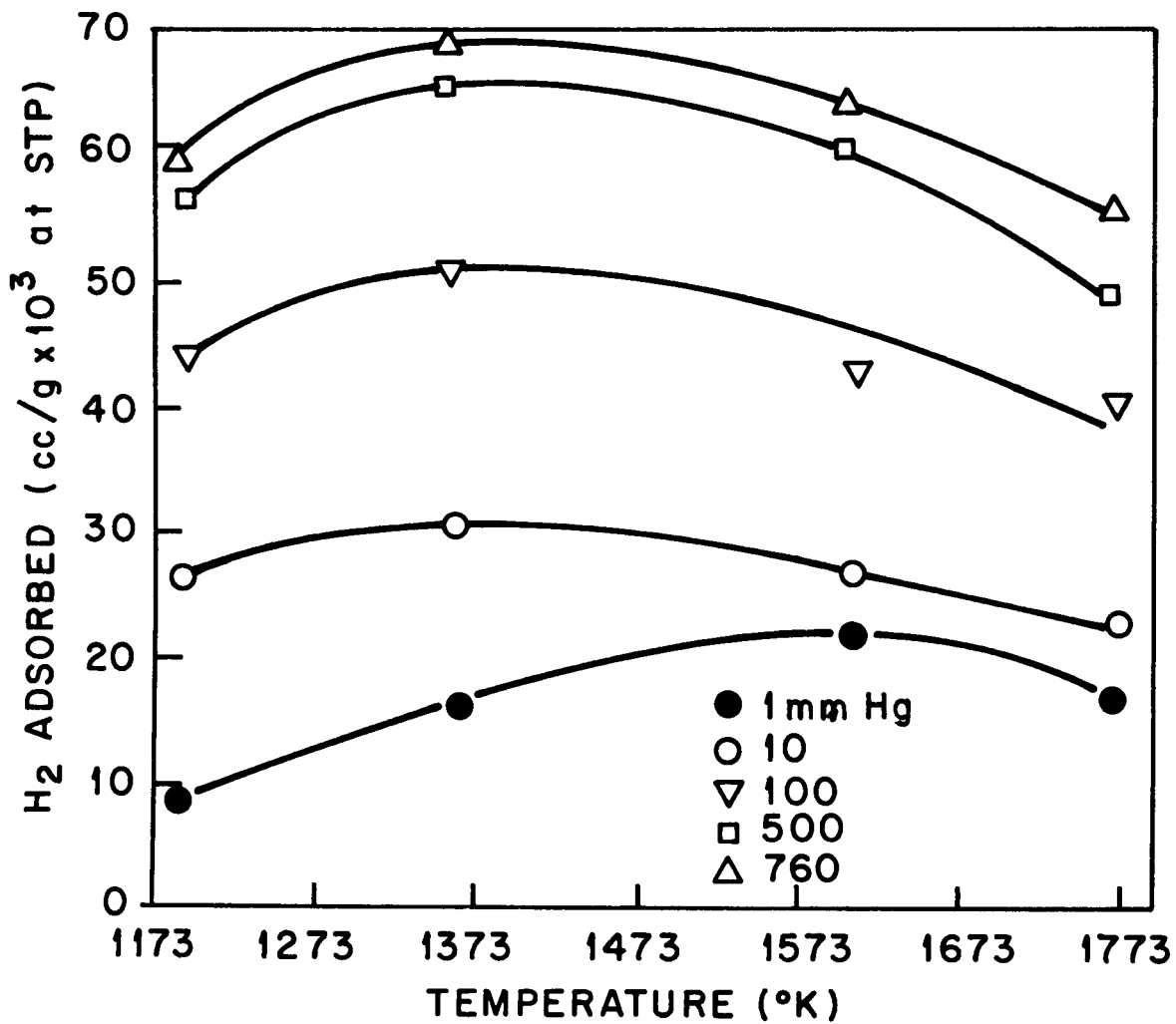


Fig. 3.1. Sorption of hydrogen on TSP nuclear graphite between 1100 and 1700 K for a range of tritium partial pressures.³⁶

Table 3.1. Equilibrium H₂ and T₂ loadings on charcoal and graphite

Temperature (°C)	T ₂ or H ₂ partial pressure (mm Hg)	H ₂ or T ₂ adsorbed per unit pressure (cc STP/g·mm Hg)	Material	Source		
-183	7 x 10 ⁻⁴ 0.023	6.8 11.1	H ₂ on activated charcoal	Dushman ⁴¹		
-78	7.9 67.5 722.0	7.4 x 10 ⁻³ 7.8 x 10 ⁻³ 7.6 x 10 ⁻³				
0	17.4 744.0	2.2 x 10 ⁻³ 2.1 x 10 ⁻³				
900	1 100 760	9 x 10 ⁻³ 4.4 x 10 ⁻⁴ 7.8 x 10 ⁻⁵			H ₂ on TSP nuclear graphite	Redmond and Walker ⁴⁰
1100	1 100 760	0.016 5 x 10 ⁻⁴ 9.1 x 10 ⁻⁵				
1500	1 100 760	0.018 4 x 10 ⁻⁴ 2.4 x 10 ⁻⁵				
900	0.85	0.03	T ₂ on matrix graphite	Fischer ³⁵		
	0.85	0.069	T ₂ on matrix graphite (1.9% oxidized)			
	0.85	4.3 x 10 ⁻³	T ₂ on AL2-500 graphite			
	0.85	8.3 x 10 ⁻³	T ₂ on AL2-500 graphite (1.5% oxidized)			

increasing pressure, at least in the range 1 to 760 mm Hg. [For reference, 10 ppmv (parts per million by volume) H_2 at 50 atm operating pressure corresponds to 0.38 mm Hg.] However, it is perhaps surprising to note that loadings on graphite at low partial pressure at temperatures from 1100 to 1500°C exceed those reported for activated charcoal down to -78°C.

Table 3.1 also lists data presented by Fischer³⁵ on matrix graphite and on a coal-based nuclear graphite designated AL2-500. Nuclear graphite types AL2-500 and TSP show very similar equilibrium loadings for T_2 and H_2 for comparable temperatures and partial pressures. The TSP graphite adsorbed 9×10^{-3} cc STP/g at 900°C and 1 mm partial pressure, which is only about a factor of 2 different from that reported by Fischer for unoxidized AL2-500 at the same temperature with 0.85 mm Hg tritium partial pressure. (However, Fischer's tabulated values represent concentrations averaged over the entire sample volume. Localized concentrations adjacent to the tritium source were about a factor of 5 higher.) Fischer's data also show that adsorption on matrix graphite exceeds that of moderator or structural quality nuclear graphite by a factor of 7 and that oxidation of from 1.5 to 1.9% increases adsorption by about a factor of 2. The high sorptivity of matrix graphite as well as the increase of sorption with degree of oxidation are both undoubtedly related to surface area effects. Therefore, whenever possible, it would be helpful to present tritium sorption data in terms of internal surface area rather than per unit mass of graphite or charcoal.

Nevertheless, Fig. 3.1 and Table 3.1 illustrate reasonably well the anticipated behavior of both the Peach Bottom core graphite and the low-temperature delay beds with respect to equilibrium capacity of H_2 or HT. However, the sorptive behavior of tritium on the fuel element charcoal operating at intermediate temperatures of $\sim 300^\circ\text{C}$ is not covered by these data.

Additional data reported by Dushman⁴¹ indicate that the retentivity of charcoal for H_2O at about room temperature greatly exceeds the capacity for H_2 when compared on a molar basis. The difference at room temperature is about a factor of 1600 in terms of moles adsorbed per gram per unit applied partial pressure. Further, Dushman observes that charcoals tend

to retain from 2.3 to 10 mg/g of moisture on desorption under even harsh conditions. In view of this, the tritium that arrived at the delayed beds as HTO (the smaller portion of the total tritium) was probably completely adsorbed in the delay beds and did not desorb while the beds were being regenerated.

3.2 Fuel Particle Failure Fractions

Fuel particle failure fractions in eight compacts taken from two irradiated Peach Bottom fuel elements were determined by a hot-chlorine leaching procedure. In this method, the mass of thorium and uranium removed by chlorination is used as a measure of the degree of particle failure. The existing procedure had to be modified because the Peach Bottom fuel compact was too large for the available chlorination apparatus. A method was therefore devised for cutting a sample (~ 10 g) from the compact and electrolytically cleaning the cut surfaces in a hot cell.* The cleaning operation removed fuel particles damaged by cutting to keep them from being counted as normally failed particles. A clean surface was obtained by a controlled, electrolytic deconsolidation of the surface zone at room temperature employing a movable anode placed adjacent to the damaged surface of the specimen.

The method was initially tested in a cold laboratory using samples from an unirradiated archive compact, with results shown in Table 3.2. Each sample contained $\sim 14,000$ to $\sim 17,000$ fuel particles. Columns 4 to 7 indicate the amounts of uranium and thorium leached and the leach time and temperature. The two leach conditions tested showed similar failure fractions. The measured thorium/uranium ratio in the leachate corresponded closely to the expected ratio of 5.5, thereby lending confidence to the procedure. The last two columns in the table indicate the calculated particle failure fraction based on a mean particle mass of $198 \mu\text{g}$ observed for the archive compact and values of $81.3 \mu\text{g}$ of thorium and $15.0 \mu\text{g}$ of uranium per kernel based on the observed mean kernel size and the theoretical density of $(\text{Th,U})\text{C}_2$. Both thorium and uranium leach masses

*Method developed by J. L. Botts, Analytical Chemistry Division, who also carried out the related measurements.

Table 3.2. Particle failure fractions for Peach Bottom archive compact

Sample mass (g)	Particles		Chlorination conditions		Metal recovered		Th/U weight ratio	Failure rate (%) based on ^b :	
	Mass (g)	Number ^a	Time (hr)	Temp. (°C)	Th (mg)	U (µg)		Th	U
8.6586	2.8585	14,400	46	1000	3.47	635	5.46	0.296	0.294
8.4610	2.8573	14,400	46	1000	3.31	581	5.70	0.283	0.269
9.9006	3.3384	16,900	6	1500	3.25	619	5.25	0.236	0.244
9.3094	3.4566	17,500	6	1500	4.36	800	5.45	0.306	0.305
							Av	0.28	0.28

^a198 µg per particle.

^b81.3 µg of thorium and 15 µg of uranium per particle.

yielded an average failure fraction of 0.28% for the four archive compact samples.

It was subsequently determined (by total deconsolidation and analyses of electrolyte, matrix, and residue) that about 0.18% of this archive failure fraction was due to heavy-metal contamination of the matrix. Thus, the observed failure rate of the archive sample was actually 0.10%, with the balance (0.18%) due to matrix contamination.

Particle failure fraction results are shown in Table 3.3 for eight fuel compacts contained in two fuel elements. Element E11-07 received 700 equivalent full-power days (EFPDs) of irradiation, and F03-01 was an end-of-life (EOL) element, receiving 900 EFPDs of irradiation. As shown in the table, the measured thorium/uranium ratio in the leached heavy metal (column 4) is usually less than that predicted from neutronics considerations (column 3). This was possibly caused by the greater difficulty in completely capturing ThCl_4 due to its low vapor pressure relative to UCl_4 . Consequently, the failure fraction determinations based on leached uranium, which are higher, are probably more reliable.

Table 3.3. Particle failure fraction in irradiated
Peach Bottom HTGR fuel

Element No.	Compact No.	Th/U weight ratio		Percent of failed particles based on:	
		Calc.	Meas.	Th	U
E11-07	2	7.11	7.64	0.68	0.64
	13	7.82	4.83	0.25	0.41
	16	7.78	9.58	0.22	0.18
	28	6.94	3.68	0.33	0.63
F03-01	2	6.51	3.54	0.17	0.31
	13	8.17	6.80	1.55	1.87
	19	7.86	3.43	0.35	0.79
	28	6.46	5.43	0.27	0.33
Archive (av of 4)		5.50	5.47	0.28	0.28 ^a

^a0.18% due to matrix contamination.

From these limited uranium-based data, we can nevertheless conclude that (1) the percentage of failed particles at 700 EFPDs (element E11-07) was only slightly higher than the background value of 0.28% obtained for the archive; (2) the failed particle fraction for the 900-EFPD case (F03-01) averaged 0.55% above background, compared with 0.19% for 700 EFPDs, and since the two elements were irradiated at approximately equal temperatures, a slight irradiation service effect on failure fraction is observed; and (3) the fuel particle failure fraction at EOL was probably <1%, about one-fourth of which was background (i.e., due to manufactured failures and matrix contamination).

3.3 Lithium Impurity in Graphite and Fuel

Table 3.4 gives the concentrations of lithium measured in selected samples of Peach Bottom graphite and fuel. Components analyzed included two archive specimens of fuel element sleeves, a specimen of spine and sleeve taken from element E06-01, samples of the radial reflector element A18-08, and a specimen of fuel taken from one archive fuel compact. Each component was sampled at only one axial location; the samples on which lithium impurity determinations were made are given in the table.

Table 3.4. Concentration of lithium in graphite and fuel of the Peach Bottom HTGR

Sample description	Samples analyzed	Li concentration (ppb)
Archive sleeve QA 3290	3	≤ 3
Archive sleeve QA 1010	3	8 ± 4
E06-01 sleeve ^a	3	9
Overall sleeve average	9	7 ± 1
E06-01 spine ^a	3	≤ 1
Reflector element ^b A18-08	7	7 ± 4
Archive fuel compact	5	10
Charcoal trap of element F05-05	2	15

^aSamples cut from section adjacent to compact.

^bSamples cut from cross-sectional specimen located axially 2 ft from bottom of element.

All analyses were performed by spark-source mass spectrometry, whereby a specimen is exposed to sparks generated by a 20-kV alternating current forming singly charged ions that are analyzed in a mass spectrometer. Samples used in this study were formed by core drilling graphite rods about 3 mm in diameter by 10 mm long. Two of the rods were used as the positive and negative electrodes in the mass spectrometer. The more abundant ^7Li isotope was measured principally because the doubly charged carbon ions interfere with the detection of singly charged ^6Li ions.

3.4 BET Surface Areas of Graphite and Charcoal

The BET surface areas of Peach Bottom HTGR graphite samples and charcoal from the fission product trap of a fuel element are given in Table 3.5. The measurements were carried out using argon as the adsorbing gas. The graphite specimens tested, including samples from the archive sleeve, the sleeve and spine of fuel element E06-01, and radial reflector element A18-18, were prepared by core drilling small cylinders (~ 5 mm diam by 10 mm length) from bulk material. Several such specimens, sufficient for a combined weight of 5 to 6 g, were employed for the analysis.

Table 3.5. BET surface areas of graphite and charcoal
from Peach Bottom HTGR

Specimen description	Surface area (m^2/g)
Archive sleeve QA 3240	<0.1
E06-01 sleeve	0.2
E06-01 spine	1.06
A18-08 radial reflector	0.36
Charcoal from F03-01 fission product trap	1190

4. ONSITE SURVEILLANCE OF TRITIUM AND HYDROGEN

This section summarizes the results of onsite routine and special survey measurements of tritium and hydrogen that were carried out by the Philadelphia Electric Company and the General Atomic Company (GAC). These measurements consisted mainly of values for the concentrations of hydrogen and tritium in the primary coolant (present as H_2 , HT, H_2O , and HTO) and the concentration of HTO in the secondary coolant. The results reported here were taken principally from ref. 8. Also summarized are the liquid and gaseous releases of tritium that were tabulated in the monthly and semiannual operations reports submitted by the Philadelphia Electric Company to the U.S. Atomic Energy Commission.⁹⁻¹⁴

4.1 Tritium in the Primary and Secondary Coolants

Figures 4.1 to 4.3 show the concentrations of tritium that were measured in the primary and secondary coolants in 1971, 1973, and 1974, respectively. These data were taken from ref. 8, which reported that sampling difficulties invalidated measurements in 1972. From late 1972 until final shutdown in 1974, tritium in both the primary and secondary coolants was monitored on numerous occasions each year. The measurements of 3H in the primary coolant involved oxidizing the HT to HTO so that the measured activity represented the sum of the HT and HTO originally in the coolant. In 1974, a Cary ionization chamber was used to continuously monitor the HT concentration in the primary coolant. This measurement involved routing a small sample flow of primary coolant through a liquid-nitrogen-cooled trap to delay all activities except HT. The tritium present as HTO was thus removed, and that present as HT was measured by passing the coolant through an ionization chamber. The results are plotted in Fig. 4.3, along with the sum of the HT and HTO levels in the primary coolant and HTO concentrations in the secondary coolant that were measured independently. As shown in the figure, the sum of the HT and HTO concentrations, compared with the separately measured HT level, indicates that most of the tritium in the primary coolant was in the HT form. Although no values for the concentrations of HTO in the helium are given

ORNL-DWG 78-18295

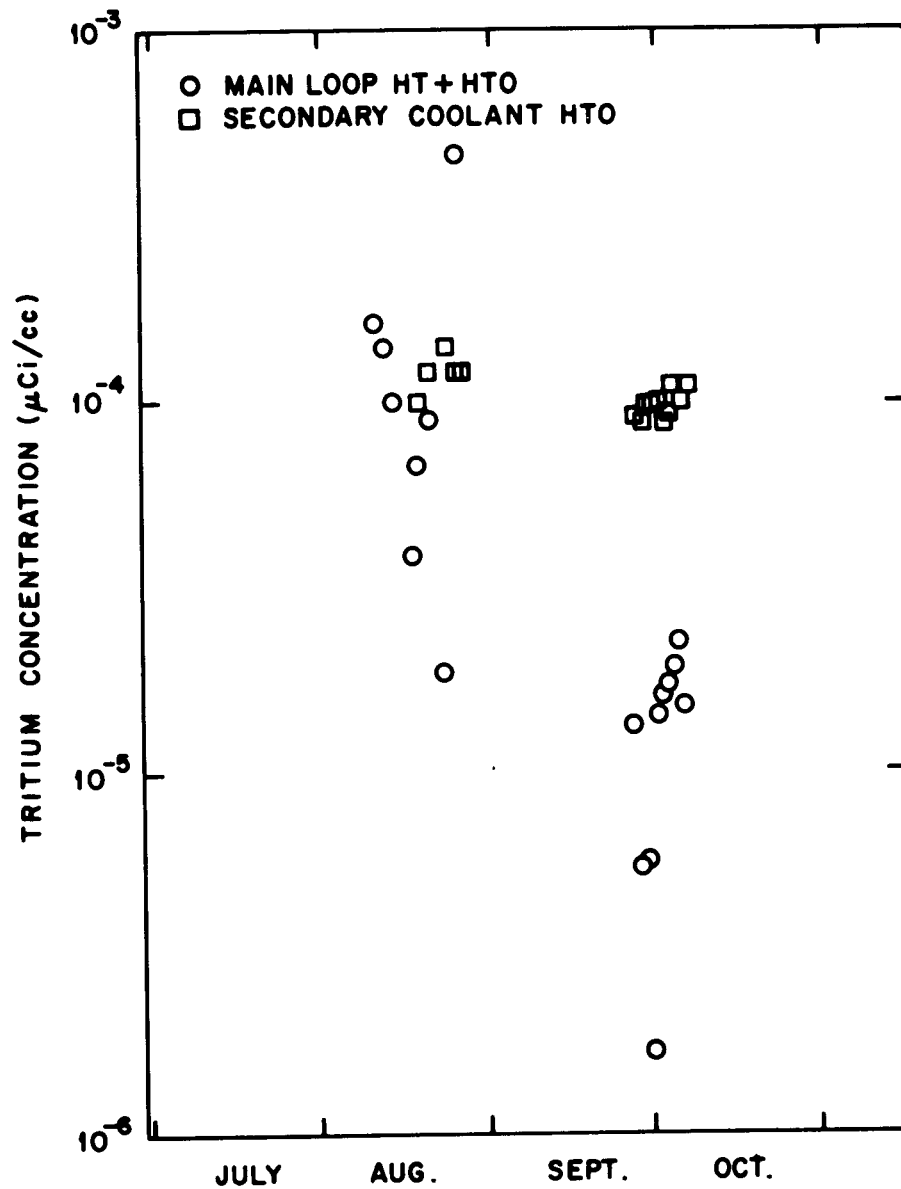


Fig. 4.1. Concentration of tritium observed in primary and secondary coolants in 1971 (reprinted from ref. 8).

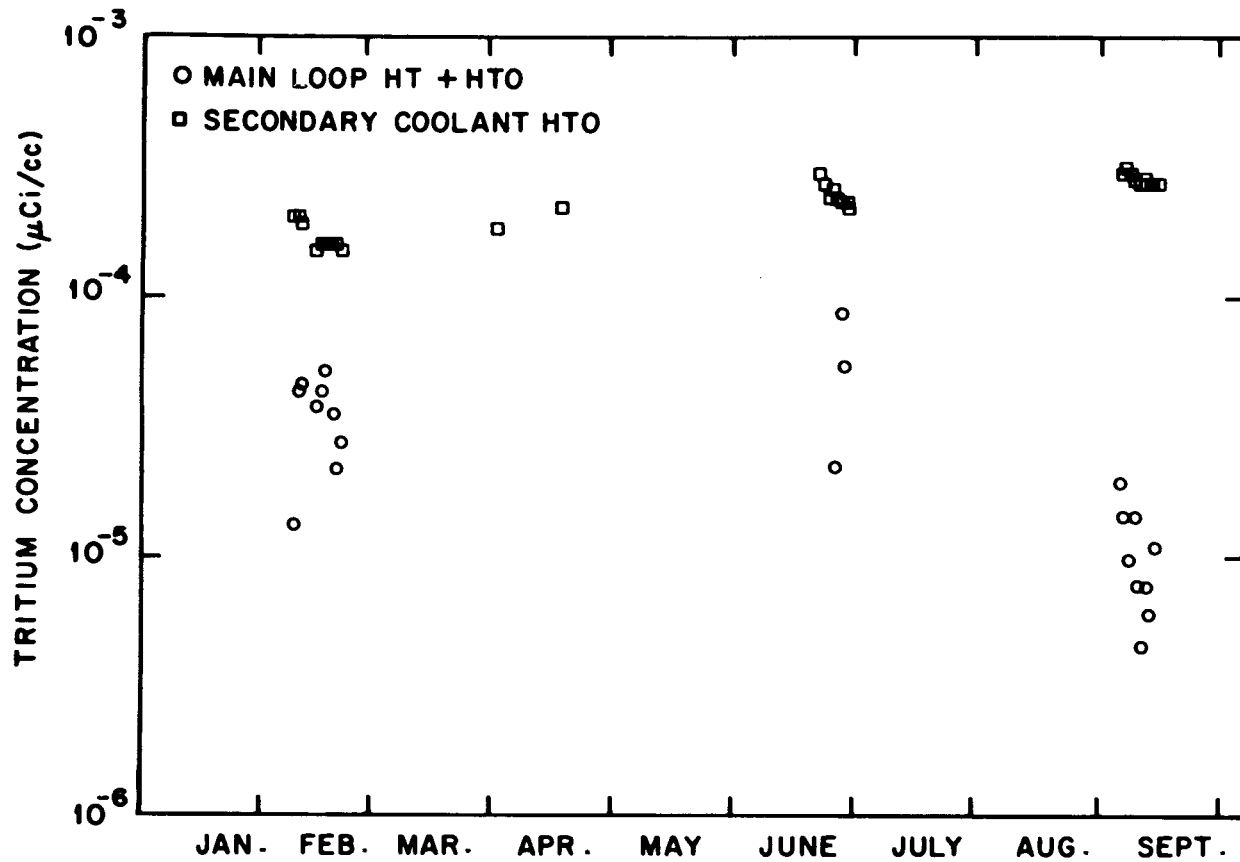


Fig. 4.2. Concentration of tritium observed in primary and secondary coolants in 1973 (reprinted from ref. 8).

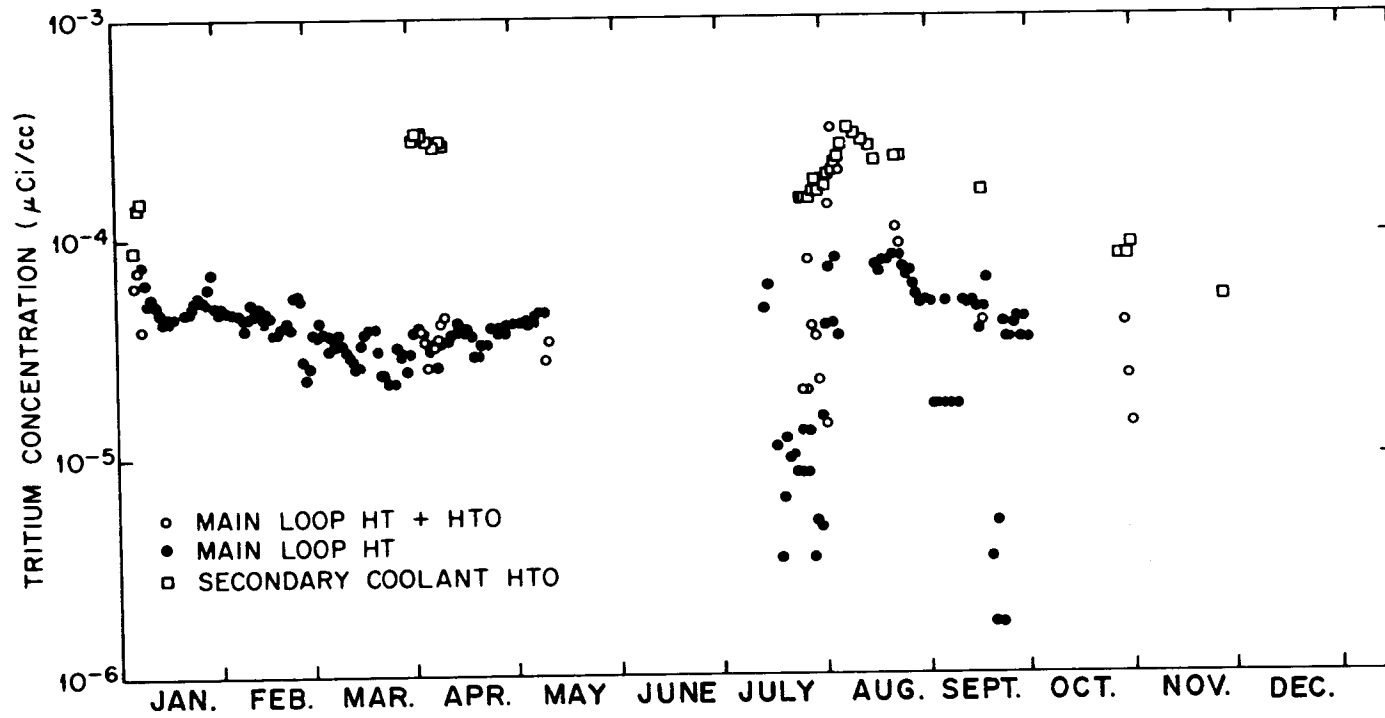


Fig. 4.3. Concentration of tritium observed in primary and secondary coolants in 1974 (reprinted from ref. 8).

in ref. 8, it was stated that the HTO was several orders of magnitude lower than HT.

As noted in Sect. 3.1, activated charcoal cooled to liquid-nitrogen temperature adsorbs a significant amount of HT. However, the fact that the sum of the HT and HTO concentrations in the coolant determined by a different procedure was observed to be equal to the HT concentration measured by the continuous monitor indicates that the liquid-nitrogen-cooled charcoal removed only a small portion of the HT in the continuous sample and that the tritium present as HTO was small compared with the amount in HT. Since the continuous tritium monitoring system was empirically calibrated with a stream of helium containing a known concentration of HT, it is possible that a constant fraction of the HT in both the coolant and calibrating gas was adsorbed and thus resulted in a correct measurement of HT in the coolant. Further evidence indicating that hydrogen (and thus HT) is adsorbed on liquid-nitrogen-cooled charcoal is provided by the data presented in Sect. 4.5. The plots of H_2 concentration in the coolant vs time in Figs. 4.4 to 4.7 show large increases of H_2 in the coolant during warmup of liquid-nitrogen-cooled charcoal traps (Fig. 4.4) and during a period when the traps were bypassed (Fig. 4.7). Therefore, the adsorption of HT and H_2 on charcoal in the liquid-nitrogen-cooled trap played a significant role in establishing the distribution of tritium in the reactor.

4.2 Special Tritium Survey

During the second half of 1971, GAC made a special survey to determine (1) a material balance for tritium in the reactor and (2) the main sources of tritium in the waste disposal system. The locations from which samples were taken and the concentrations of tritium found are given in Table 4.1. Although ref. 8 states that 3H in the stack effluent was measured, no concentrations were given.

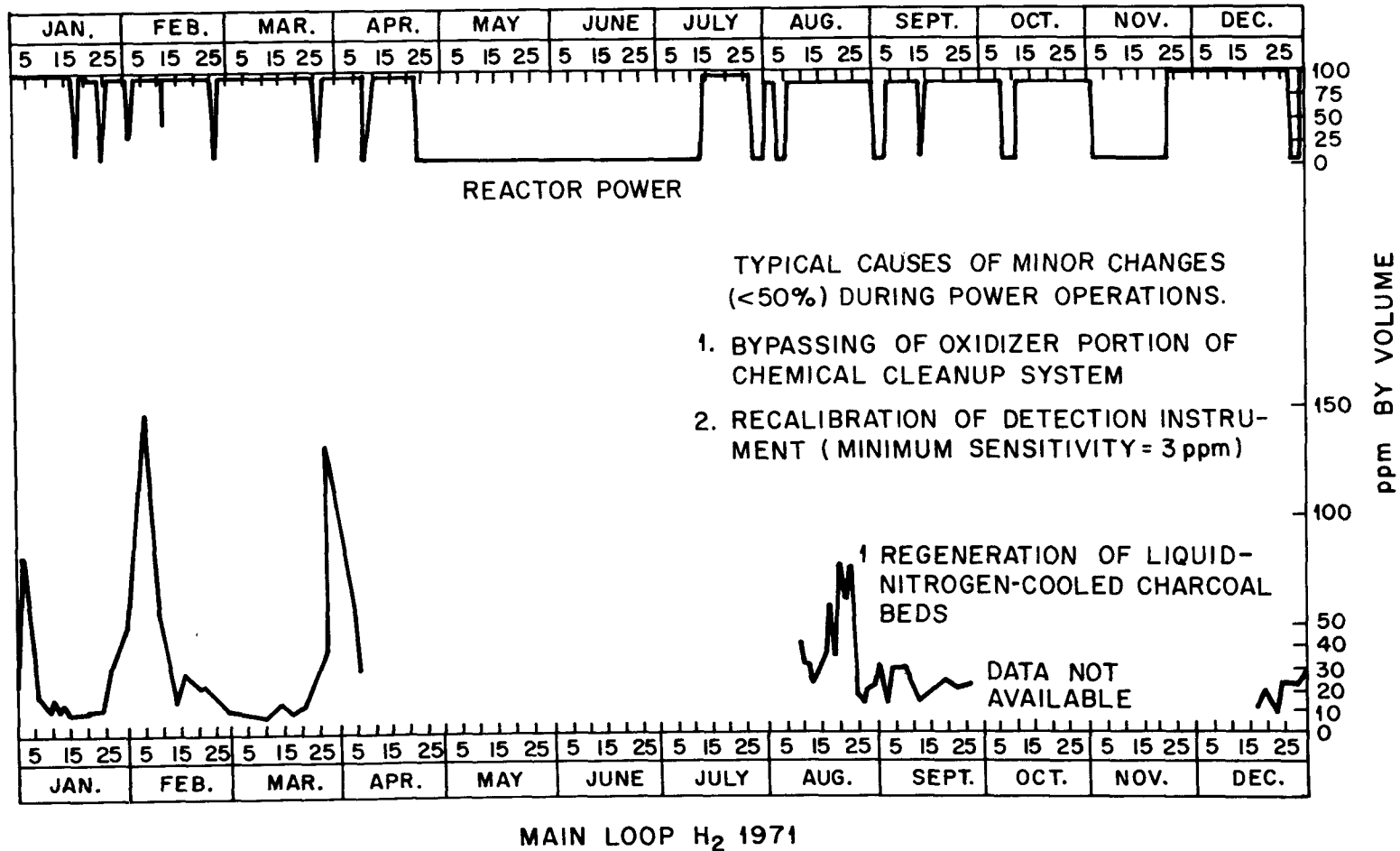


Fig. 4.4. Concentration of H₂ observed in the primary coolant in 1971 (reprinted from ref. 8).

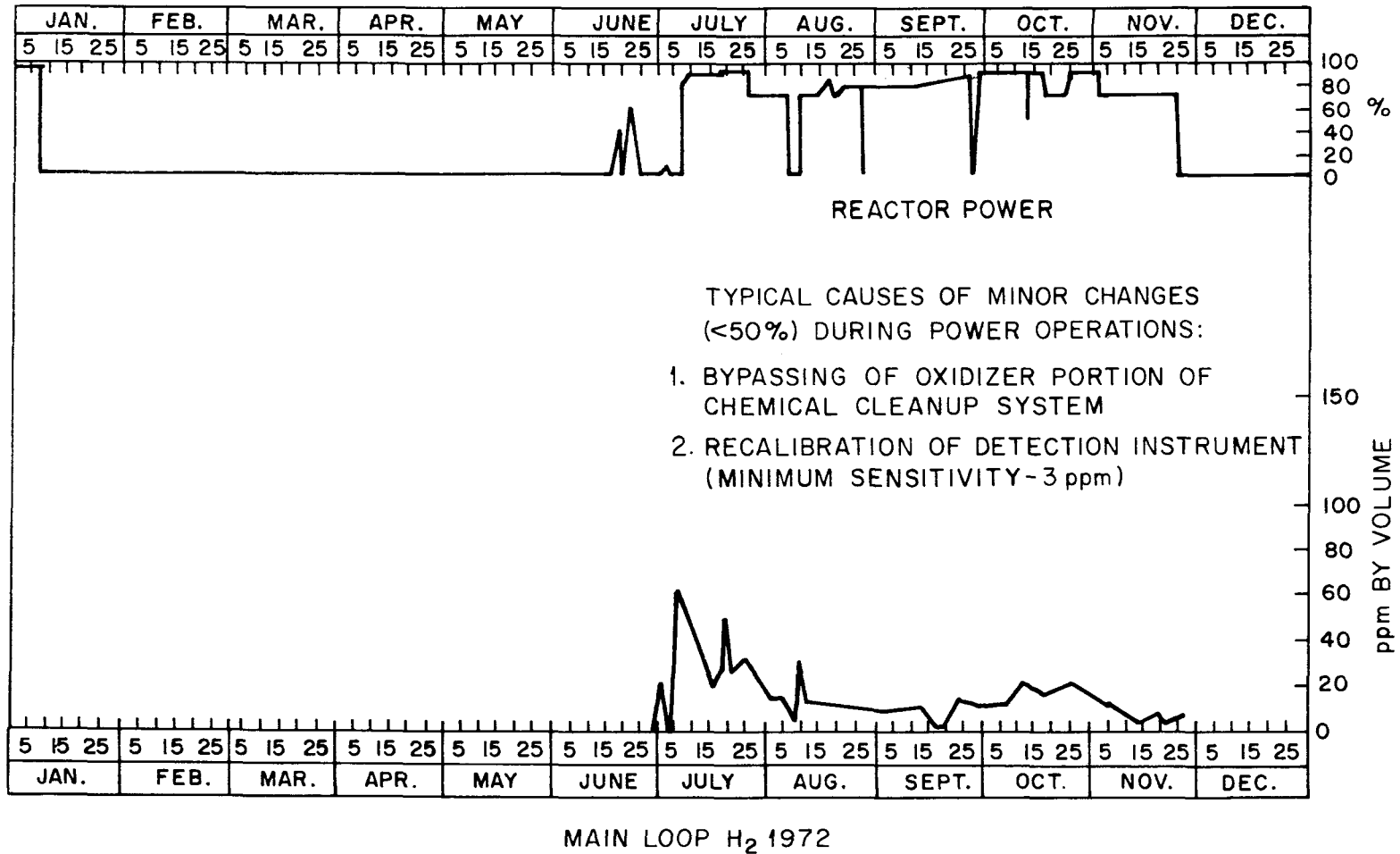
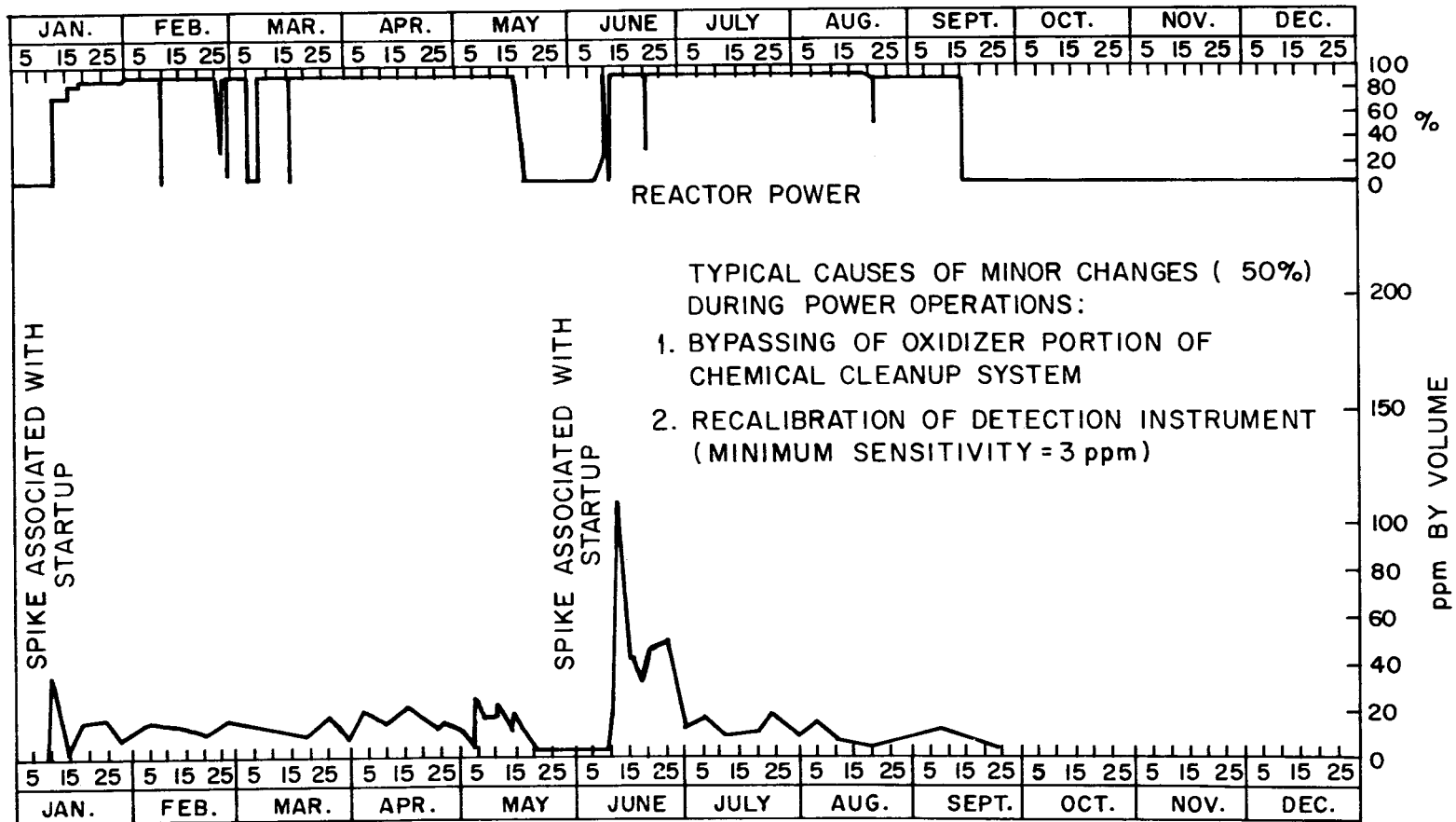


Fig. 4.5. Concentration of H₂ observed in the primary coolant in 1972 (reprinted from ref. 8).



MAIN LOOP H₂ 1973

Fig. 4.6. Concentration of H₂ observed in the primary coolant in 1973 (reprinted from ref. 8).

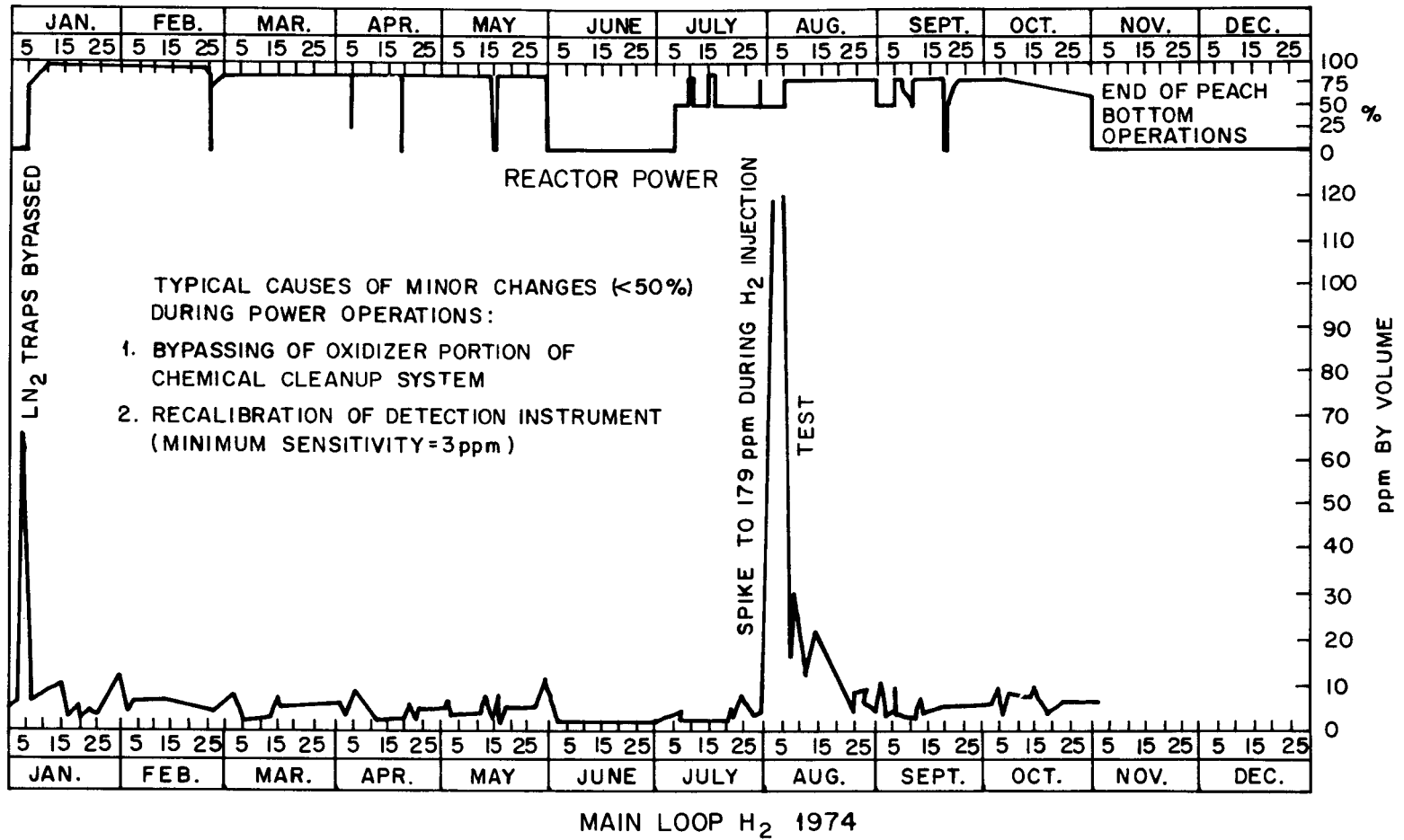


Fig. 4.7. Concentration of H₂ observed in the primary coolant in 1974 (reprinted from ref. 8).

Table 4.1. Typical levels of tritium found during tritium surveys at Peach Bottom^a

Sample location	HT + HTO ^b ($\mu\text{Ci}/\text{cm}^3$)	HTO ($\mu\text{Ci}/\text{ml}$)
Fuel element purge	5×10^{-5}	
Containment atmosphere	5×10^{-7}	
Air room atmosphere	ND ^c	
Outside air	ND	
⁸⁵ Kr holdup tanks	1×10^{-2}	
N ₂ -Ar holdup tanks	6×10^{-3}	
Deaerator		2×10^{-4}
Condensate		2×10^{-4}
Steam drum 1		2×10^{-4}
Steam drum 2		2×10^{-4}
Air ejector	2×10^{-7}	
Waste disposal drain tank		400
Main coolant loop 1	2×10^{-5}	
Main coolant loop 2	2×10^{-5}	

^aReproduced from ref. 8.

^bConcentrations refer to nominal reactor conditions of temperature and pressure.

^cND = nondetected; levels were at or below background for the instrumentation.

4.3 Effects of Hydrazine in Secondary Coolant on Hydrogen Levels in Primary Coolant

Hydrazine was added to the secondary coolant water to scavenge occluded oxygen and thereby reduce the corrosion rate. The decomposition of hydrazine in the secondary coolant was initially considered a possible source of the higher-than-expected steady-state levels of hydrogen in the primary coolant. To test this hypothesis, a special study was carried out over a period of several days during which the level of hydrazine was dropped from 150 to 15 ppm and maintained for about seven days. Levels of tritium and hydrogen in the primary coolant were monitored prior to, during, and following level reduction. The results of this study, taken from ref. 8, are presented in Fig. 4.8.

Although it is not evident from the results plotted in Fig. 4.8, ref. 8 stated that the tritium and hydrogen levels in the primary coolant dropped about 20% following reduction of the hydrazine level. Such a slight reduction showed that hydrazine in the secondary coolant did not significantly influence the observed tritium and hydrogen levels in the primary coolant. During the period of testing with reduced hydrazine levels, an unscheduled reduction in reactor power also occurred, resulting in marked reductions of the tritium and hydrogen levels in the primary coolant. These periods of reduced power, along with the observed variations of the hydrogen and tritium levels, are indicated in Fig. 4.8. After the power returned to normal, the levels of tritium and hydrogen rose to their previous values. Figure 4.8 shows that the level of tritium in the secondary coolant was not significantly influenced by the hydrazine test or the power reduction.

4.4 Releases of Tritium in Liquid and Gaseous Wastes

Table 4.2 lists the tritium activities that were reported⁹⁻¹⁴ to have been released via liquid and gaseous wastes. The activity of tritium in waste effluents prior to the second half of 1971 was not discussed in the operations reports (with the exception of May 1971). The sources of the liquid and gaseous wastes were briefly described in Sects. 2.3 and 2.4 of this report.

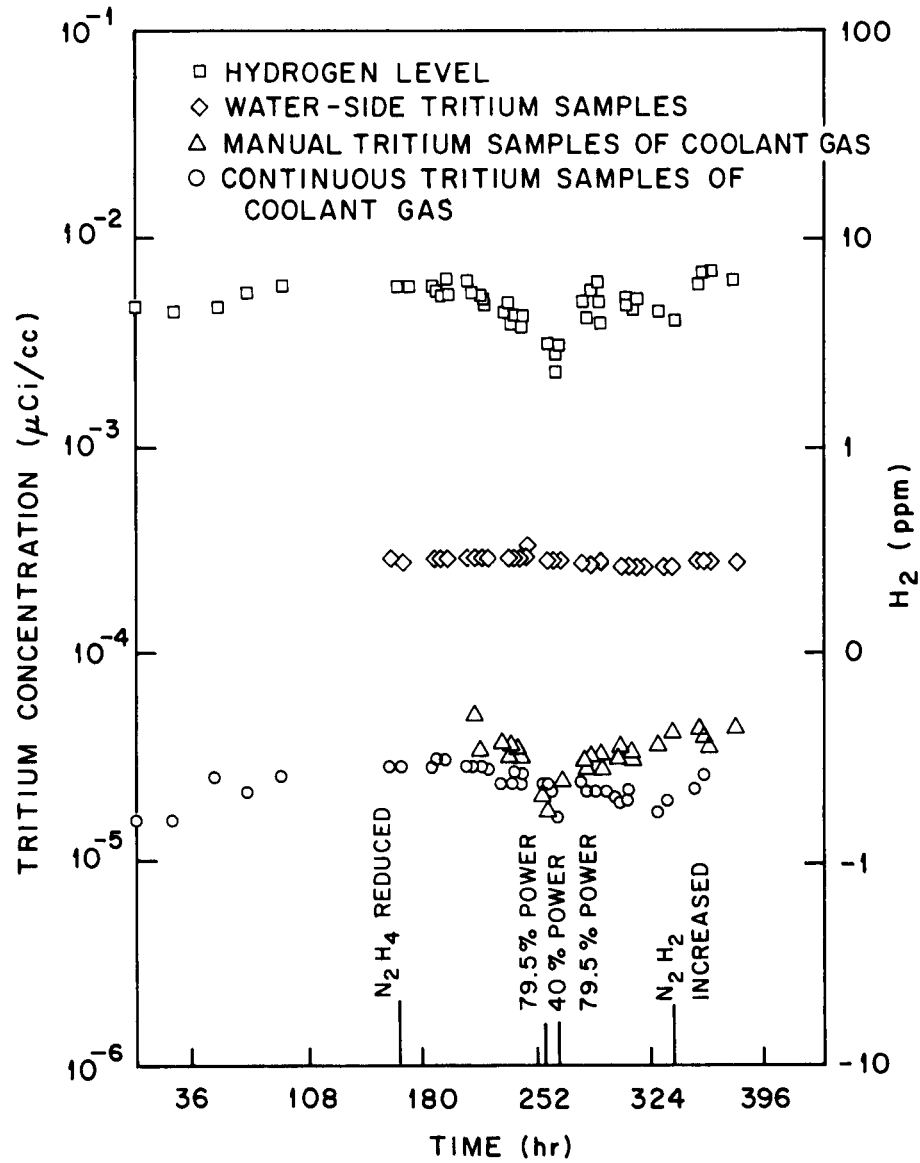


Fig. 4.8. Tritium and hydrogen levels before, during, and after reduction of N_2H_4 levels in the secondary coolant of the Peach Bottom reactor during 1971 tests. (Reprinted from ref. 8.)

Table 4.2. Tritium released in liquid and gaseous waste
from the Peach Bottom HTGR^a

Year	Tritium activity (Ci)	
	In liquid waste	In gaseous waste
1970 ^b		
1971	2.0	3.5
1972	1.7	0.9
1973	5.0	6.2
1974	<u>2.7</u>	<u>24.3</u>
Total	9.4	31.4

^aData taken from semiannual operations reports.⁹⁻¹⁴

^bRecords not available.

4.5 Levels of Hydrogen and Water in the Primary Coolant

Plots of the hydrogen concentrations in the primary coolant for the years 1971 through 1974, given in ref. 8, are reproduced as Figs. 4.4 through 4.7. Generally, the hydrogen level ranged between 5 and 20 ppmv except for an occasional "spike" when the hydrogen concentration increased to 110 ppmv. The hydrogen in the spikes, which usually occurred during reactor startup, was thought to be principally from the oil that leaked into the primary system from the helium cleanup plant. (See ref. 8 for a discussion of oil ingress into the primary coolant system.)

Although moisture monitors were incorporated in the primary circuit, little information was published concerning moisture levels in the coolant, perhaps because the level was frequently too low to be detected. A concentration value of 0.006 ppmv was reported for May 1974. The moisture monitors, which contained a hydrated form of phosphorus pentoxide ($P_2O_5 \cdot 1.5 H_2O$) in an electrolytic cell, were found to have a short functional lifetime. It was postulated that the extremely dry helium caused the P_2O_5 to dehydrate, thus causing the cells to malfunction.

5. MEASURED TRITIUM LEVELS IN FUEL ELEMENTS
AND A REFLECTOR ELEMENT

This section gives the results of tritium measurements on six Peach Bottom HTGR fuel elements and one removable reflector element. The fuel elements studied included E06-01, which was irradiated 384 EFPDs; E11-07, a 701-EFPD element; and elements E14-01, F03-01, E01-01, and F05-05, which were irradiated 898 EFPDs. The last four elements were operated the entire life of core 2 and were removed after the reactor was shut down for decommissioning on October 31, 1974. Pre- and postirradiation dimensions and desorptions, core locations, and other detailed descriptive material regarding these elements are provided in published examination reports.¹⁻⁶ Element E14-01 was unique in this series in that it was one of the 60 elements that contained a poisoned spine.

The tritium levels in these fuel elements were first studied as part of a broader program concerned with fission product surveillance in this reactor. In this early phase of the study, measurements of tritium levels were restricted mainly to the radial distributions of tritium (along with ^{14}C and ^{90}Sr) in the sleeves and spines of the elements. A much more limited part of the study included the determination of tritium in the upper reflector assembly, in the bottom connector, and in a few fuel particles. These data, which have been abstracted from the published examination reports,¹⁻⁶ are more extensive than the data used in the present study. They are included here to provide a record of all tritium-related measurements performed in the surveillance work. More comprehensive tritium transport analyses, which may be conducted at some future time, would likely make further use of this body of information. (For example, the tritium radial profiles provide information on tritium diffusion in graphite; tritium concentrations in the purge hole portion of fuel element may be used as a measure of tritium levels in the primary coolant if equilibrium sorption data are provided; similarly, the axial concentration profiles in fuel element charcoal traps may be used to determine tritium concentration in the purge gas.)

In a later study directed specifically toward an understanding of the behavior of tritium, additional measurements of tritium were made on the previously studied fuel elements, and the distribution of tritium in a Peach Bottom reflector block was determined. Other properties related to the levels of tritium (e.g., the concentrations of ^6Li in graphite components) were also studied and results are reported in Sect. 3.4. The measurements made under the programmatic studies are summarized in Sect. 1.1.

One objective of the expanded experimental studies was to determine the effects of operating temperatures on the release of tritium from Peach Bottom fuel. In this portion of the work, tritium was measured in bulk fuel specimens, weighing several grams and containing several thousand particles, taken from six fuel compacts that had operated over a wide temperature range.

In addition, the data regarding tritium levels in the fuel element charcoal traps were augmented during this period of time. The charcoal traps were not only a significant repository for tritium in core, but perhaps more importantly, tritium levels in the fuel element purge flow could possibly be inferred from the measured levels in the trap. It was hoped that, in turn, this could be used as a measure of tritium leakage from the core to the ex-core fission product trapping system.

5.1 Radial Distributions in Sleeves and Spines

Tables 5.1 through 5.41 summarize the measured radial distributions of tritium in the sleeves and spines of the six Peach Bottom HTGR fuel elements cited above. The data are tabulated as microcuries of tritium per gram of graphite at the given radial distance from the surface adjacent to the fuel. As indicated in Sect. 1.1, these results were abstracted from the series of reports describing the examinations of the fuel elements.¹⁻⁶

The mean tritium activity values given in the radial distribution tables were derived by numerical integration of the radial distributions and are used in Sect. 5.2 to define the axial distributions of tritium in

Table 5.1. Radial distribution of tritium found in E06-01
spine at compact 7
(corrected to January 6, 1972)

Sample	Thickness of cut ^a (mm)	Distance to center of cut from OD (mm)	Tritium activity ($\mu\text{Ci/g}$)
1	1.59	1.02	3.06E+00
2	2.54	3.08	1.63E+00
3	3.18	5.94	1.07E+00
4	3.18	9.11	1.07E+00
5	3.18	12.29	1.06E+00
6	7.27	17.51	9.00E-01
			Mean 1.52E+00

^aThickness of sample milled from spine.

Table 5.2. Radial distribution of tritium found in E06-01
sleeve at compact 7
(corrected to January 6, 1972)

Sample	Thickness of cut ^a (mm)	Distance to center of cut from ID (mm)	Tritium activity ($\mu\text{Ci/g}$)
1	0.92	0.44	4.56E+01
2	1.02	1.41	2.87E+01
3	1.02	2.42	1.05E+01
4	1.02	3.44	5.04E+00
5	1.02	4.45	6.68E+00
6	1.02	5.47	6.84E+00
7	1.02	6.49	6.72E+00
8	1.02	7.50	6.44E+00
9	0.64	8.33	8.32E+00
10	0.64	8.96	1.00E+01
			Mean 1.28E+01

^aThickness of sample milled from sleeve.

Table 5.3. Radial distribution of tritium found in E06-01
spine at compact 16
(corrected to January 7, 1972)

Sample	Thickness of cut ^a (mm)	Distance to center of cut from OD (mm)	Tritium activity (μ Ci/g)
1	1.59	0.98	2.91E+00
2	2.54	3.04	1.80E+00
3	3.18	5.90	1.44E+00
4	3.18	9.08	1.16E+00
5	3.18	12.25	8.70E-01
6	3.18	15.43	1.11E+00
7	4.14	19.08	1.17E+00
		Mean	1.61E+00

^aThickness of sample milled from spine.

Table 5.4. Radial distribution of tritium found in E06-01
sleeve at compact 16
(corrected to January 7, 1972)

Sample	Thickness of cut ^a (mm)	Distance to center of cut from ID (mm)	Tritium activity (μ Ci/g)
1	1.96	0.96	1.13E+01
2	1.02	2.45	1.03E+01
3	1.02	3.47	1.57E+01
4	1.02	4.48	1.69E+01
5	1.02	5.50	1.55E+01
6	1.02	6.51	1.72E+01
7	1.02	7.53	1.95E+01
8	0.64	8.35	2.50E+01
9	0.64	8.99	2.85E+01
		Mean	1.67E+01

^aThickness of sample milled from sleeve.

Table 5.5. Radial distribution of tritium found in E06-01
spine at compact 26
(corrected to January 7, 1972)

Sample	Thickness of cut ^a (mm)	Distance to center of cut from OD (mm)	Tritium activity ($\mu\text{Ci/g}$)
1	2.35	1.85	1.44E+00
2	1.78	3.85	1.00E+00
3	3.18	6.25	7.00E-01
4	3.18	9.45	6.30E-01
5	3.18	12.64	5.10E-01
6	6.92	17.69	4.20E-01
			Mean 8.69E-01

^aThickness of sample milled from spine.

Table 5.6. Radial distribution of tritium found in E06-01
sleeve at compact 26
(corrected to January 7, 1972)

Sample	Thickness of cut ^a (mm)	Distance to center of cut from ID (mm)	Tritium activity ($\mu\text{Ci/g}$)
1	0.92	0.45	6.02E+00
2	1.02	1.42	4.41E+00
3	1.02	2.43	4.31E+00
4	1.02	3.45	3.89E+00
5	1.02	4.47	3.52E+00
6	1.02	5.48	4.16E+00
7	1.02	6.50	5.65E+00
8	1.02	7.51	5.71E+00
9	0.64	8.34	7.72E+00
10	0.64	8.97	9.48E+00
			Mean 5.29E+00

^aThickness of sample milled from sleeve.

Table 5.7. Radial distribution of tritium found in E11-07
spine at compact 5
(corrected to September 14, 1973)

Sample	Thickness of cut ^a (mm)	Distance to center of cut from OD (mm)	Tritium activity ($\mu\text{Ci/g}$)
1	0.13	0.06	4.19E+00
2	0.38	0.32	5.14E+00
3	0.38	0.70	3.88E+00
4	0.76	1.27	4.66E+00
5	0.76	2.03	5.01E+00
6	0.76	3.56	4.65E+00
7	0.76	5.08	4.40E+00
8	0.76	6.60	3.50E+00
9	1.52	9.27	3.48E+00
10	1.59	17.20	2.79E+00
11	3.18	19.60	2.50E+00
			Mean 3.89E+00

^aThickness of sample milled from spine.

Table 5.8. Radial distribution of tritium found in E11-07
sleeve at compact 5
(corrected to September 14, 1973)

Sample	Thickness of cut ^a (mm)	Distance to center of cut from ID (mm)	Tritium activity ($\mu\text{Ci/g}$)
1	0.13	0.06	1.29E+01
2	0.13	0.19	2.86E+01
3	0.13	0.32	7.13E+01
4	0.25	0.51	9.34E+01
5	0.76	1.40	2.92E+01
6	0.76	2.92	1.80E+01
7	0.76	4.46	1.14E+01
8	0.76	5.97	1.13E+01
9	0.76	7.49	9.50E+00
10	0.38	8.83	1.10E+01
11	0.20	9.50	2.16E+01
			Mean 2.05E+01

^aThickness of sample milled from sleeve.

Table 5.9. Radial distribution of tritium found in Ell-07
spine at compact 12
(corrected to September 14, 1973)

Sample	Thickness of cut ^a (mm)	Distance to center of cut from OD (mm)	Tritium activity ($\mu\text{Ci/g}$)
1	0.20	0.10	1.66E+01
2	0.38	0.39	1.11E+01
3	0.38	0.77	8.64E+00
4	0.76	1.35	7.33E+00
5	0.76	2.11	6.15E+00
6	0.76	3.63	4.66E+00
7	0.76	5.16	3.59E+00
8	0.76	6.68	2.58E+00
9	1.52	9.35	2.03E+00
10	1.59	16.99	8.60E-01
11	3.18	19.40	8.00E-01
			Mean 3.99E+00

^aThickness of sampled milled from spine.

Table 5.10. Radial distribution of tritium found in Ell-07
sleeve at compact 12
(corrected to September 14, 1973)

Sample	Thickness of cut ^a (mm)	Distance to center of cut from ID (mm)	Tritium activity ($\mu\text{Ci/g}$)
1	0.13	0.06	3.13E+01
2	0.13	0.19	2.75E+01
3	0.13	0.32	2.76E+01
4	0.25	0.51	2.34E+01
5	0.76	1.53	8.74E+01
6	0.46	2.90	5.54E+01
7	0.76	4.27	6.02E+01
8	0.76	5.79	7.17E+01
9	0.76	7.32	1.27E+01
10	0.38	8.65	1.11E+01
11	0.13	9.30	1.23E+01
			Mean 4.59E+01

^aThickness of sample milled from sleeve.

Table 5.11. Radial distribution of tritium found in E11-07
spine at compact 18
(corrected to September 14, 1973)

Sample	Thickness of cut ^a (mm)	Distance to center of cut from OD (mm)	Tritium activity ($\mu\text{Ci/g}$)
1	0.25	0.13	7.47E+00
2	0.38	0.45	5.49E+00
3	0.38	0.83	7.23E+00
4	0.76	1.40	4.93E+00
5	0.76	2.16	4.02E+00
6	0.76	3.68	3.14E+00
7	0.76	5.21	2.35E+00
8	1.52	7.11	1.90E+00
9	1.52	10.16	3.01E+00
10	1.59	17.00	1.01E+00
11	3.18	19.40	9.90E-01
		Mean	3.06E+00

^aThickness of sample milled from spine.

Table 5.12. Radial distribution of tritium found in E11-07
sleeve at compact 18
(corrected to September 14, 1973)

Sample	Thickness of cut ^a (mm)	Thickness to center of cut from ID (mm)	Tritium activity ($\mu\text{Ci/g}$)
1	0.13	0.06	3.25E+01
2	0.13	0.19	2.33E+01
3	0.13	0.32	1.32E+01
4	0.13	0.45	3.80E+00
5	0.76	1.27	4.57E+00
6	0.76	2.79	4.75E+00
7	0.76	4.32	5.70E+00
8	0.76	5.84	9.10E+00
9	1.27	7.37	1.43E+01
10	0.38	8.70	2.47E+01
11	0.23	9.40	2.84E+01
		Mean	1.16E+01

^aThickness of sample milled from sleeve.

Table 5.13. Radial distribution of tritium found in Ell-07
spine at compact 28
(corrected to September 14, 1973)

Sample	Thickness of cut ^a (mm)	Distance to center of cut from OD (mm)	Tritium activity (μ Ci/g)
1	0.20	0.10	1.36E+01
2	0.38	0.39	3.72E+00
3	0.38	0.78	2.38E+00
4	0.76	1.35	2.27E+00
5	0.76	2.11	2.09E+00
6	0.76	3.63	2.03E+00
7	0.76	5.16	1.78E+00
8	0.76	6.68	1.58E+00
9	0.71	8.18	1.61E+00
10	1.59	17.18	1.02E+00
11	3.18	19.56	1.03E+00
		Mean	2.01E+00

^aThickness of sample milled from spine.

Table 5.14. Radial distribution of tritium found in Ell-07
sleeve at compact 28
(corrected to September 14, 1973)

Sample	Thickness of cut ^a (mm)	Distance to center of cut from ID (mm)	Tritium activity (μ Ci/g)
1	0.13	0.06	3.16E+00
2	0.13	0.19	1.06E+01
3	0.13	0.32	7.71E+00
4	0.13	0.45	5.74E+00
5	0.38	0.70	3.34E+00
6	0.76	1.27	2.41E+00
7	0.76	2.79	1.96E+00
8	0.76	4.32	2.05E+00
9	0.76	5.84	2.26E+00
10	0.76	7.37	3.22E+00
11	0.38	8.70	4.38E+00
12	0.25	9.40	7.74E+00
		Mean	3.26E+00

^aThickness of sample milled from sleeve.

Table 5.15. Radial distribution of tritium found in E14-01
sleeve at compact 7
(corrected to October 31, 1974)

Sample	Thickness of cut ^a (mm)	Distance to center of cut from ID (mm)	Tritium activity ($\mu\text{Ci/g}$)
1	0.13	0.06	2.22E+01
2	0.13	0.19	5.07E+01
3	0.13	0.32	4.70E+01
4	0.25	0.51	4.30E+01
5	0.76	1.40	5.00E+01
6	0.76	2.90	4.72E+01
7	0.76	4.50	5.26E+01
8	0.76	6.00	5.17E+01
9	0.76	7.50	5.68E+01
10	0.38	8.80	4.69E+01
11	0.18	9.50	6.49E+01
		Mean	5.27E+01

^aThickness of sample milled from sleeve.

Table 5.16. Radial distribution of tritium found in E14-01
spine at compact 23
(corrected to October 31, 1974)

Sample	Thickness of cut ^a (mm)	Distance to center of cut from OD (mm)	Tritium activity ($\mu\text{Ci/g}$)
1	0.13	0.06	8.07E+00
2	0.25	0.25	4.32E+00
3	0.25	0.51	3.54E+00
4	0.38	0.83	3.44E+00
5	0.38	1.21	3.51E+00
6	0.76	2.54	3.08E+00
7	0.76	4.06	2.08E+00
8	0.76	5.59	2.12E+00
9	0.76	7.11	2.17E+00
10	0.76	8.64	2.78E+00
11	0.89	9.46	6.25E+00
		Mean	3.94E+00

^aThickness of sample milled from spine.

Table 5.17. Radial distribution of tritium found in E14-01
sleeve at compact 23
(corrected to October 31, 1974)

Sample	Thickness of cut ^a (mm)	Distance to center of cut from ID (mm)	Tritium activity (μ Ci/g)
1	0.13	0.06	3.09E+00
2	0.13	0.19	2.57E+01
3	0.13	0.32	1.74E+01
4	0.25	0.51	1.07E+01
5	0.76	1.40	9.86E+00
6	0.76	2.92	1.22E+01
7	0.76	4.45	1.43E+01
8	0.76	5.97	1.73E+01
9	0.76	7.49	2.24E+01
10	0.38	8.83	2.60E+01
11	0.15	9.47	3.84E+01
		Mean	1.80E+01

^aThickness of sample milled from sleeve.

Table 5.18. Radial distribution of tritium found in E14-01
spine at compact 28
(corrected to October 31, 1974)

Sample	Thickness of cut ^a (mm)	Distance to center of cut from OD (mm)	Tritium activity (μ Ci/g)
1	0.13	0.06	1.20E+01
2	0.25	0.25	1.17E+01
3	0.25	0.51	4.85E+00
4	0.38	0.83	4.91E+00
5	0.38	1.20	5.17E+00
6	0.76	2.54	5.24E+00
7	0.76	4.06	4.41E+00
8	0.76	5.59	3.66E+00
9	0.76	7.11	3.24E+00
10	0.76	8.64	3.41E+00
11	0.89	9.46	5.00E+00
		Mean	4.79E+00

^aThickness of sample milled from spine.

Table 5.19. Radial distribution of tritium found in E14-01
sleeve at compact 28
(corrected to October 31, 1974)

Sample	Thickness of cut ^a (mm)	Distance to center of cut from ID (mm)	Tritium activity ($\mu\text{Ci/g}$)
1	0.13	0.06	1.52E+00
2	0.13	0.19	1.91E+01
3	0.13	0.32	1.31E+01
4	0.25	0.51	7.01E+00
5	0.69	1.36	5.81E+00
6	0.76	2.85	6.30E+00
7	1.52	3.99	7.10E+00
8	1.52	5.51	7.70E+00
9	0.76	7.42	8.80E+00
10	0.38	8.75	1.01E+01
11	0.13	9.39	1.48E+01
		Mean	8.25E+00

^aThickness of sample milled from sleeve.

Table 5.20. Radial distribution of tritium found in F03-01
spine at compact 5
(corrected to October 31, 1974)

Sample	Thickness of cut ^a (mm)	Distance to center of cut from OD (mm)	Tritium activity ($\mu\text{Ci/g}$)
1	0.13	0.06	5.20E+01
2	0.38	0.32	1.92E+01
3	0.76	0.89	5.97E+00
4	0.76	1.65	3.12E+00
5	0.76	2.41	4.98E+00
6	0.76	3.94	4.62E+00
7	0.76	5.46	4.35E+00
8	0.76	6.99	3.77E+00
9	1.52	8.89	3.83E+00
10	1.59	16.20	2.31E+00
11	3.18	18.60	2.07E+00
		Mean	5.30E+00

^aThickness of sample milled from spine.

Table 5.21. Radial distribution of tritium found in F03-01
sleeve at compact 5
(corrected to October 31, 1974)

Sample	Thickness of cut ^a (mm)	Distance to center of cut from ID (mm)	Tritium activity ($\mu\text{Ci/g}$)
1	0.25	0.13	1.42E+01
2	0.25	0.38	4.19E+01
3	0.46	0.74	4.18E+01
4	0.38	1.54	1.10E+02
5	0.76	2.87	4.11E+00
6	0.76	3.63	1.47E+00
7	0.76	5.16	1.31E+00
8	0.76	7.44	1.31E+00
9	0.38	8.70	2.42E+00
10	0.25	9.40	1.25E+01
			Mean 1.77E+01

^aThickness of sample milled from sleeve.

Table 5.22. Radial distribution of tritium found in F03-01
spine at compact 12
(corrected to October 31, 1974)

Sample	Thickness of cut ^a (mm)	Distance to center of cut from OD (mm)	Tritium activity ($\mu\text{Ci/g}$)
1	0.18	0.09	1.59E+01
2	0.38	0.37	1.20E+01
3	0.76	0.94	6.31E+00
4	0.76	1.70	6.68E+00
5	0.76	2.46	6.14E+00
6	0.76	4.00	5.42E+00
7	0.76	5.51	4.76E+00
8	0.76	7.04	4.66E+00
9	1.52	8.94	3.73E+00
10	1.59	16.20	2.54E+00
11	3.18	18.60	2.48E+00
			Mean 5.06E+00

^aThickness of sample milled from spine.

Table 5.23. Radial distribution of tritium found in F03-01
sleeve at compact 12
(corrected to October 31, 1974)

Sample	Thickness of cut ^a (mm)	Distance to center of cut from ID (mm)	Tritium activity ($\mu\text{Ci/g}$)
1	0.13	0.06	4.53E+01
2	0.25	0.25	5.43E+01
3	0.25	0.76	4.56E+01
4	0.76	1.65	4.65E+01
5	0.76	3.20	6.91E+01
6	0.76	4.70	9.03E+01
7	0.76	6.20	7.99E+01
8	0.76	7.70	6.54E+01
9	0.38	9.00	5.84E+01
10	0.25	9.40	4.95E+01
			Mean 6.84E+01

^aThickness of sample milled from sleeve.

Table 5.24. Radial distribution of tritium found in F03-01
spine at compact 18
(corrected to October 31, 1974)

Sample	Thickness of cut ^a (mm)	Distance to center of cut from ID (mm)	Tritium activity ($\mu\text{Ci/g}$)
1	0.15	0.08	1.01E+01
2	0.38	0.34	6.30E+00
3	0.76	0.91	4.40E+00
4	0.76	1.68	4.16E+00
5	0.76	2.44	2.69E+00
6	0.76	3.96	3.01E+00
7	0.76	5.49	2.75E+00
8	0.76	7.01	2.83E+00
9	1.52	8.92	2.82E+00
10	1.59	17.15	2.32E+00
11	3.18	19.50	2.02E+00
			Mean 3.18E+00

^aThickness of sample milled from spine.

Table 5.25. Radial distribution of tritium found in F03-01
sleeve at compact 18
(corrected to October 31, 1974)

Sample	Thickness of cut ^a (mm)	Distance to center of cut from ID (mm)	Tritium activity ($\mu\text{Ci/g}$)
1	0.38	0.19	1.77E+01
2	0.38	0.57	1.67E+01
3	0.76	1.14	1.98E+01
4	0.76	2.70	2.11E+01
5	0.76	4.20	2.96E+01
6	0.76	5.70	4.58E+01
7	0.76	7.20	7.11E+01
8	0.38	8.60	4.18E+01
9	0.28	9.30	4.35E+01
			Mean 3.85E+01

^aThickness of sample milled from sleeve.

Table 5.26. Radial distribution of tritium found in F03-01
spine at compact 28
(corrected to October 31, 1974)

Sample	Thickness of cut ^a (mm)	Distance to center of cut from OD (mm)	Tritium activity ($\mu\text{Ci/g}$)
1	0.15	0.08	1.42E+01
2	0.38	0.34	7.03E+00
3	0.76	0.91	1.94E+00
4	0.76	1.68	1.87E+00
5	0.76	2.44	1.93E+00
6	0.76	3.96	1.46E+00
7	0.76	5.49	1.25E+00
8	0.76	7.01	1.12E+00
9	1.52	8.92	8.70E-01
10	1.59	17.00	5.20E-01
11	3.18	19.40	4.70E-01
			Mean 1.67E+00

^aThickness of sample milled from spine.

Table 5.27. Radial distribution of tritium found in F03-01
sleeve at compact 28
(corrected to October 31, 1974)

Sample	Thickness of cut ^a (mm)	Distance to center of cut from ID (mm)	Tritium activity ($\mu\text{Ci/g}$)
1	0.38	0.19	1.70E-01
2	0.38	0.57	1.60E+01
3	0.76	1.51	1.35E+01
4	0.76	3.00	1.41E+01
5	0.76	4.60	1.01E+01
6	0.76	6.10	2.26E+01
7	0.76	7.60	3.45E+01
8	0.38	8.90	4.22E+01
9	0.38	9.70	3.39E+01
			Mean 2.35E+01

^aThickness of sample milled from sleeve.

Table 5.28. Radial distribution of tritium found in E01-01
sleeve at compact 4
(corrected to October 31, 1974)

Sample	Thickness of cut ^a (mm)	Distance to center of cut from ID (mm)	Tritium activity ($\mu\text{Ci/g}$)
1	0.51	0.26	8.82E+01
2	0.51	0.66	2.23E+02
3	0.76	1.20	1.39E+02
4	0.76	2.72	1.06E+01
5	0.76	4.24	1.04E+01
6	0.76	5.76	1.06E+01
7	0.76	7.28	9.30E+00
8	0.51	8.80	1.05E+01
9	0.08	9.60	3.64E+01
			Mean 3.83E+01

^aThickness of sample milled from sleeve.

Table 5.29. Radial distribution of tritium found in E01-01
sleeve at compact 12
(corrected to October 31, 1974)

Sample	Thickness of cut ^a (mm)	Distance to center of cut from ID (mm)	Tritium activity ($\mu\text{Ci/g}$)
1	0.51	0.25	4.31E+01
2	0.25	0.64	3.84E+01
3	0.76	1.14	3.59E+01
4	0.76	2.66	4.32E+01
5	0.76	4.18	6.12E+01
6	0.76	5.70	6.87E+01
7	0.76	7.20	8.37E+01
8	0.02	8.70	1.00E+02
9	0.15	9.60	7.05E+01
			Mean 6.80E+01

^aThickness of sample milled from sleeve.

Table 5.30. Radial distribution of tritium found in E01-01
sleeve at compact 18
(corrected to October 31, 1974)

Sample	Thickness of cut ^a (mm)	Distance to center of cut from ID (mm)	Tritium activity ($\mu\text{Ci/g}$)
1	0.51	0.25	1.16E+01
2	0.25	0.64	1.85E+01
3	0.76	1.14	1.40E+01
4	0.76	2.66	1.54E+01
5	0.76	4.18	1.81E+01
6	0.76	5.70	2.40E+01
7	0.76	7.22	3.71E+01
8	0.76	8.74	7.82E+01
9	0.08	9.60	9.51E+01
			Mean 3.47E+01

^aThickness of sample milled from sleeve.

Table 5.31. Radial distribution of tritium found in E01-01
spine at compact 23
(corrected to October 31, 1974)

Sample	Thickness of cut ^a (mm)	Distance to center of cut from OD (mm)	Tritium activity (μ Ci/g)
1	0.20	0.10	3.90E+00
2	0.38	0.39	2.72E+00
3	0.76	0.97	2.54E+00
4	0.76	1.73	2.04E+00
5	0.76	2.49	2.35E+00
6	0.76	4.01	2.21E+00
7	0.76	5.54	2.03E+00
8	0.76	7.06	2.03E+00
9	1.52	8.58	1.98E+00
10	1.59	16.80	1.73E+00
11	3.18	19.20	1.77E+00
			Mean 2.11E+00

^aThickness of sample milled from spine.

Table 5.32. Radial distribution of tritium found in E01-01
spine at compact 28
(corrected to October 31, 1974)

Sample	Thickness of cut ^a (mm)	Distance to center of cut from OD (mm)	Tritium activity (μ Ci/g)
1	0.15	0.08	6.42E+00
2	0.38	0.34	2.28E+00
3	0.76	0.91	3.13E+00
4	0.76	1.67	3.29E+00
5	0.76	2.43	3.78E+00
6	0.76	3.95	3.48E+00
7	0.76	5.47	2.59E+00
8	0.76	6.99	2.39E+00
9	1.52	8.89	2.26E+00
10	1.59	17.28	1.61E+00
11	3.18	19.60	1.43E+00
			Mean 2.67E+00

^aThickness of sample milled from spine.

Table 5.33. Radial distribution of tritium found in E01-01
sleeve at compact 28
(corrected to October 31, 1974)

Sample	Thickness of cut ^a (mm)	Distance to center of cut from ID (mm)	Tritium activity ($\mu\text{Ci/g}$)
1	0.51	0.25	9.50E+00
2	0.25	0.64	1.55E+01
3	0.76	1.14	8.80E+00
4	0.76	2.66	8.20E+00
5	0.76	4.18	9.60E+00
6	0.76	5.70	1.21E+01
7	0.76	7.22	1.83E+01
8	0.76	8.74	2.69E+01
9	0.20	9.60	4.23E+01
		Mean	1.64E+01

^aThickness of sample milled from sleeve.

Table 5.34. Radial distribution of tritium found in F05-05
spine at compact 5
(corrected to October 31, 1974)

Sample	Thickness of cut ^a (mm)	Distance to center of cut from OD (mm)	Tritium activity ($\mu\text{Ci/g}$)
1	0.13	0.07	4.32E+01
2	0.38	0.32	9.50E+00
3	0.76	0.89	8.10E+00
4	0.76	1.65	6.90E+00
5	0.76	2.40	5.80E+00
6	0.76	3.90	7.90E+00
7	0.76	5.50	7.50E+00
8	0.76	7.00	6.60E+00
9	1.52	8.90	6.40E+00
10	1.59	17.20	4.00E+00
11	3.18	19.60	3.90E+00
		Mean	7.14E+00

^aThickness of sample milled from spine.

Table 5.35. Radial distribution of tritium found in F05-05
sleeve at compact 5
(corrected to October 31, 1974)

Sample	Thickness of cut ^a (mm)	Distance to center of cut from ID (mm)	Tritium activity ($\mu\text{Ci/g}$)
1	0.64	0.32	6.80E+00
2	0.25	0.77	3.71E+01
3	0.25	1.02	2.19E+01
4	0.76	2.28	8.20E+00
5	0.76	3.80	1.30E+00
6	0.76	5.30	1.00E+00
7	0.76	6.80	1.10E+00
8	0.76	8.40	1.50E+00
9	0.18	9.20	1.90E+01
		Mean	6.27E+00

^aThickness of sample milled from sleeve.

Table 5.36. Radial distribution of tritium found in F05-05
spine at compact 12
(corrected to October 31, 1974)

Sample	Thickness of cut ^a (mm)	Distance to center of cut from OD (mm)	Tritium activity ($\mu\text{Ci/g}$)
1	0.13	0.07	9.50E+00
2	0.38	0.32	9.90E+00
3	0.76	0.89	1.01E+01
4	0.76	2.40	7.70E+00
5	0.76	3.90	6.80E+00
6	0.76	5.50	6.40E+00
7	0.76	7.00	4.60E+00
8	1.52	8.90	6.00E-01
9	1.59	17.20	8.00E-01
10	3.18	19.60	2.90E+00
		Mean	4.75E+00

^aThickness of sample milled from spine.

Table 5.37. Radial distribution of tritium found in F05-05
sleeve at compact 12
(corrected to October 31, 1974)

Sample	Thickness of cut ^a (mm)	Distance to center of cut from ID (mm)	Tritium activity ($\mu\text{Ci/g}$)
1	0.38	0.19	5.97E+01
2	0.25	0.89	7.72E+01
3	0.76	2.20	8.87E+01
4	0.76	3.70	8.35E+01
5	0.76	5.20	7.05E+01
6	0.76	6.70	5.28E+01
7	0.76	8.20	4.12E+01
8	0.25	9.20	2.78E+01
			Mean 6.49E+01

^aThickness of sample milled from sleeve.

Table 5.38. Radial distribution of tritium found in F05-05
spine at compact 18
(corrected to October 31, 1974)

Sample	Thickness of cut ^a (mm)	Distance to center of cut from OD (mm)	Tritium activity ($\mu\text{Ci/g}$)
1	0.18	0.09	7.70E+00
2	0.38	0.37	5.20E+00
3	0.76	0.94	4.30E+00
4	0.76	1.70	3.90E+00
5	0.76	2.50	3.80E+00
6	0.76	4.00	3.60E+00
7	0.76	5.50	3.30E+00
8	0.76	7.00	3.00E+00
9	1.52	8.90	2.30E+00
10	1.59	17.20	1.90E+00
11	3.18	19.60	8.00E-01
			Mean 3.13E+00

^aThickness of sample milled from spine.

Table 5.39. Radial distribution of tritium found in F05-05
sleeve at compact 18
(corrected to October 31, 1974)

Sample	Thickness of cut ^a (mm)	Distance to center of cut from ID (mm)	Tritium activity ($\mu\text{Ci/g}$)
1	0.51	0.26	1.34E+01
2	0.25	1.15	1.72E+01
3	0.76	2.40	1.87E+01
4	0.76	3.93	2.33E+01
5	0.76	5.45	2.92E+01
6	0.76	6.97	4.55E+01
7	0.76	8.49	6.48E+01
8	0.13	9.30	6.61E+01
			Mean 3.43E+01

^aThickness of sample milled from sleeve.

Table 5.40. Radial distribution of tritium found in F05-05
spine at compact 28
(corrected to October 31, 1974)

Sample	Thickness of cut ^a (mm)	Distance to center of cut from OD (mm)	Tritium activity ($\mu\text{Ci/g}$)
1	0.13	0.07	2.26E+01
2	0.38	0.32	6.30E+00
3	0.76	0.89	5.00E+00
4	0.76	1.70	4.10E+00
5	0.76	2.40	4.50E+00
6	0.76	3.90	3.70E+00
7	0.76	5.50	3.10E+00
8	0.76	7.00	2.50E+00
9	1.52	8.90	2.40E+00
10	1.59	17.20	1.80E+00
11	3.18	19.60	1.70E+00
			Mean 3.50E+00

^aThickness of sample milled from spine.

Table 5.41. Radial distribution of tritium found in F05-05 sleeve at compact 28 (corrected to October 31, 1974)

Sample	Thickness of cut ^a (mm)	Distance to center of cut from ID (mm)	Tritium activity ($\mu\text{Ci/g}$)
1	0.51	0.26	2.39E+01
2	0.76	0.64	1.76E+01
3	0.76	2.16	1.48E+01
4	0.76	3.68	1.05E+01
5	0.76	5.20	1.51E+01
6	0.76	6.72	1.76E+01
7	0.76	8.24	2.19E+01
8	0.13	9.10	2.90E+01
		Mean	1.68E+01

^aThickness of sample milled from sleeve.

the sleeve and spine. The methods used to radially dissect the sleeve and spine specimens and effect radiochemical analysis of tritium were previously described² and will only be briefly reviewed. The specimens were radially dissected with a modified conventional 5-ft bed lathe that was operated remotely in a hot cell. The powdered turnings from the sleeve and spine were collected and burned in a tube furnace at 850°C in a stream of moist oxygen. Tritium as HTO was condensed in a trap cooled with a dry ice-acetone bath. A tube containing alumina was placed in the gas circuit upstream of the HTO collection trap to condense and filter out radionuclides such as ¹³⁷Cs that may have been partially vaporized in the combustion chamber. The alumina filter was held at about 125°C to prevent holdup of the tritiated water. After combustion, the H₂O and HTO in the trap were eluted with water into a volumetric flask, and tritium was measured by beta counting aliquots of the solution with a liquid scintillation counter.

Plots of the radial distribution of tritium in the sleeves and spines of elements E11-07, F03-01, and F05-05 are shown in Figs. 5.1 to 5.4.

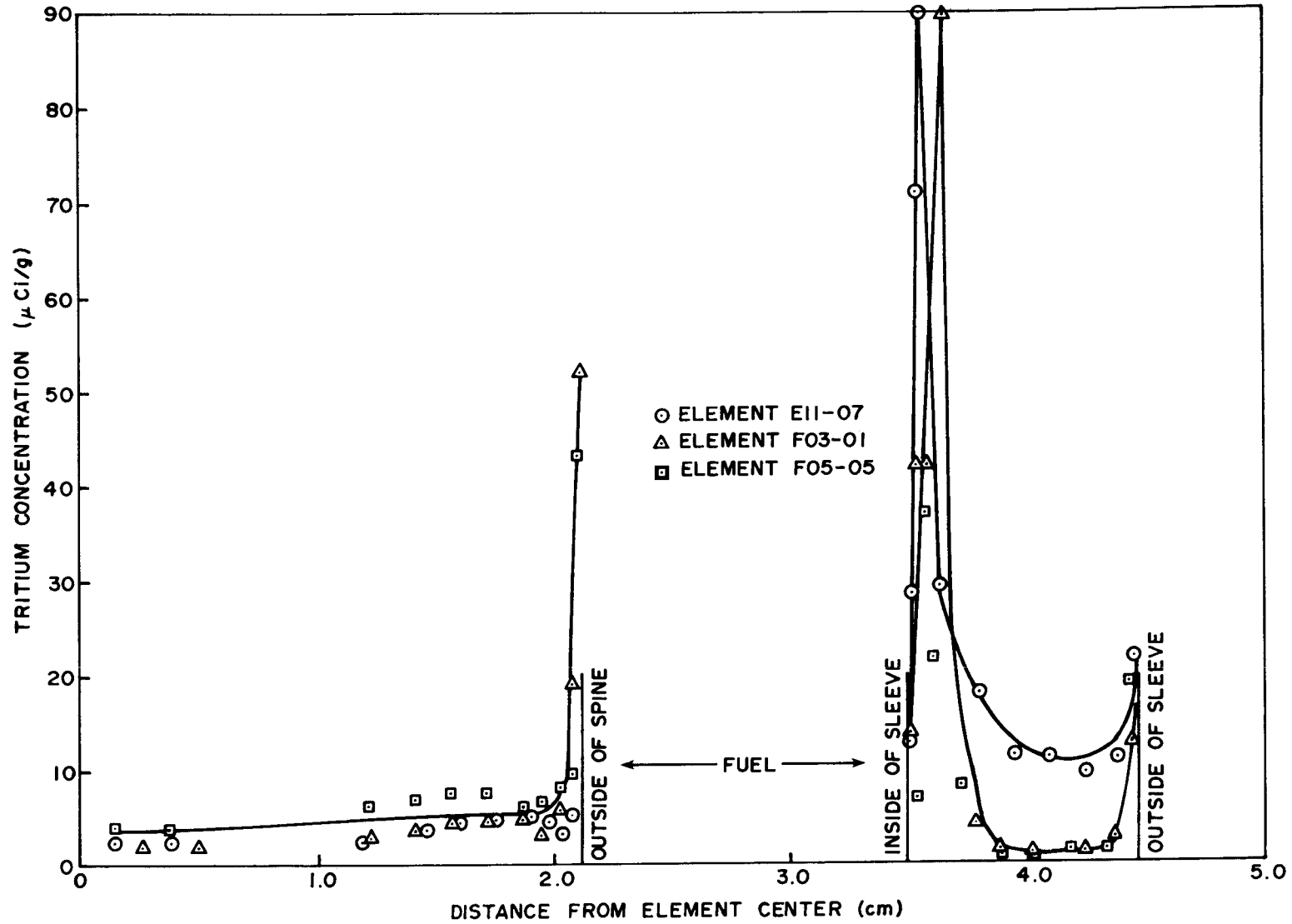


Fig. 5.1. Radial distribution of tritium in spine and sleeve of Peach Bottom HTGR fuel elements E11-07, F03-01, and F05-05 at compact 5.

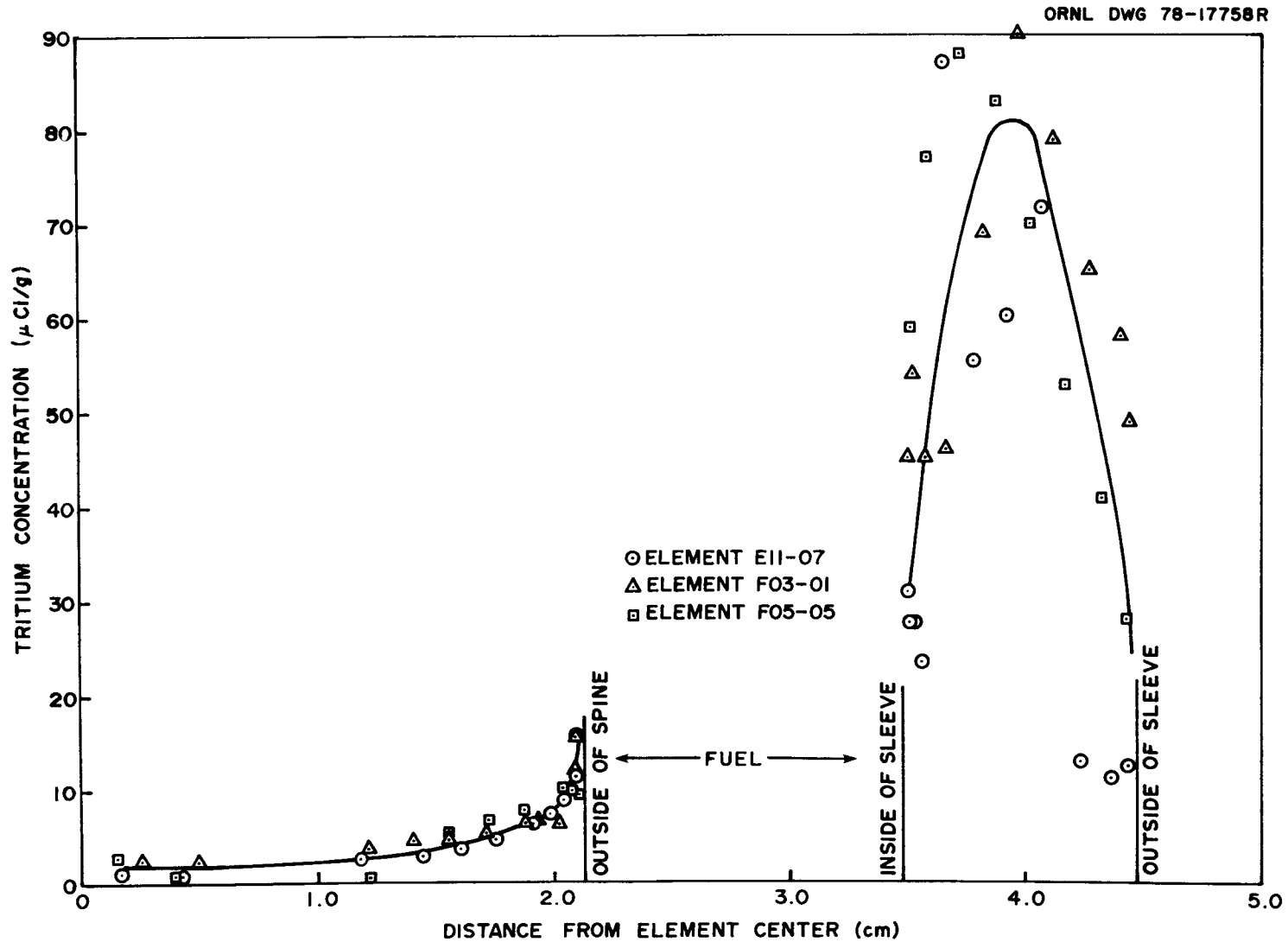


Fig. 5.2. Radial distribution of tritium in spine and sleeve of Peach Bottom HTGR fuel elements E11-07, F03-01, and F05-05 at compact 12.

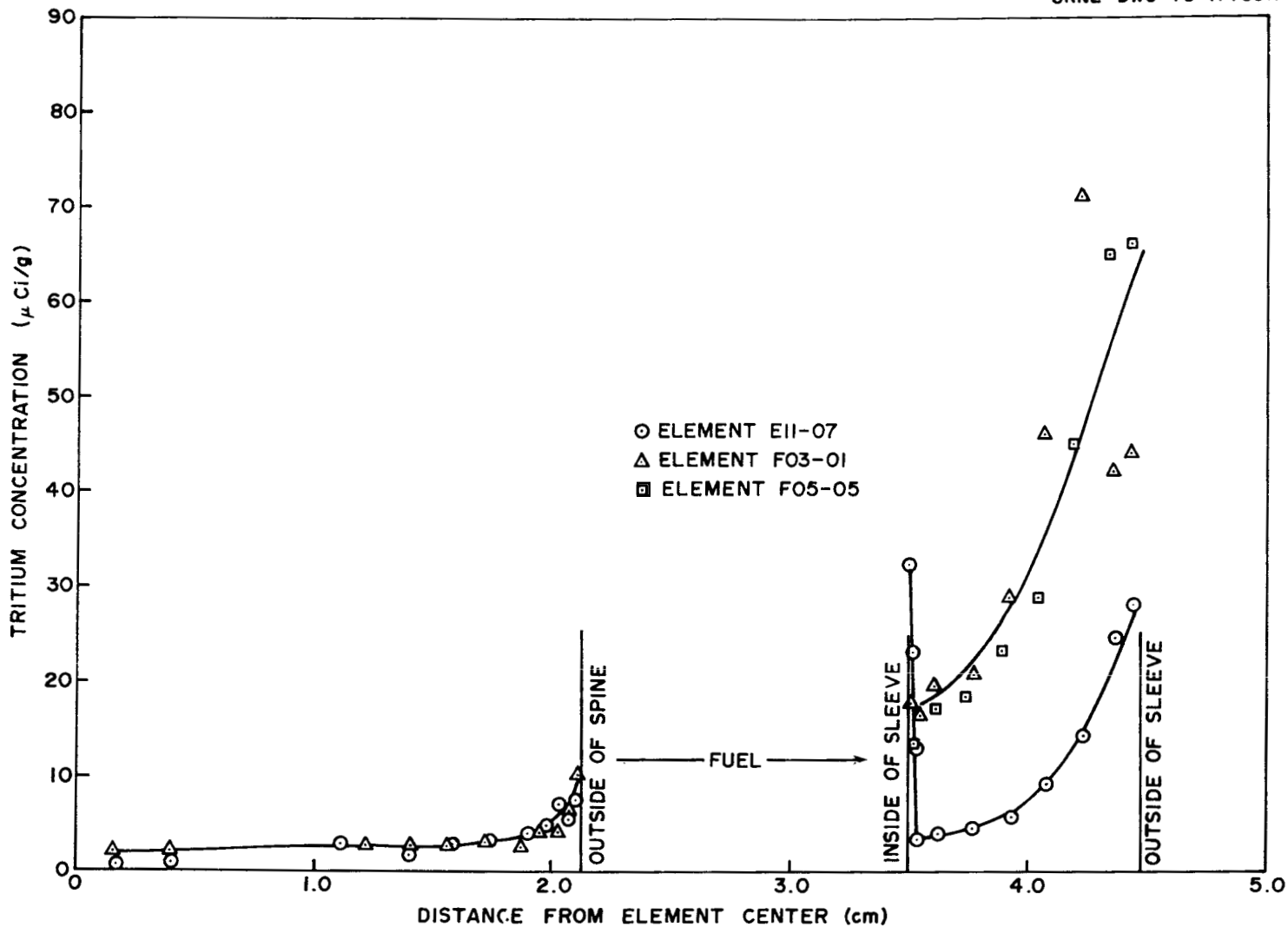


Fig. 5.3. Radial distribution of tritium in spine and sleeve of Peach Bottom HTGR fuel elements E11-07, F03-01, and F05-05 at compact 18.

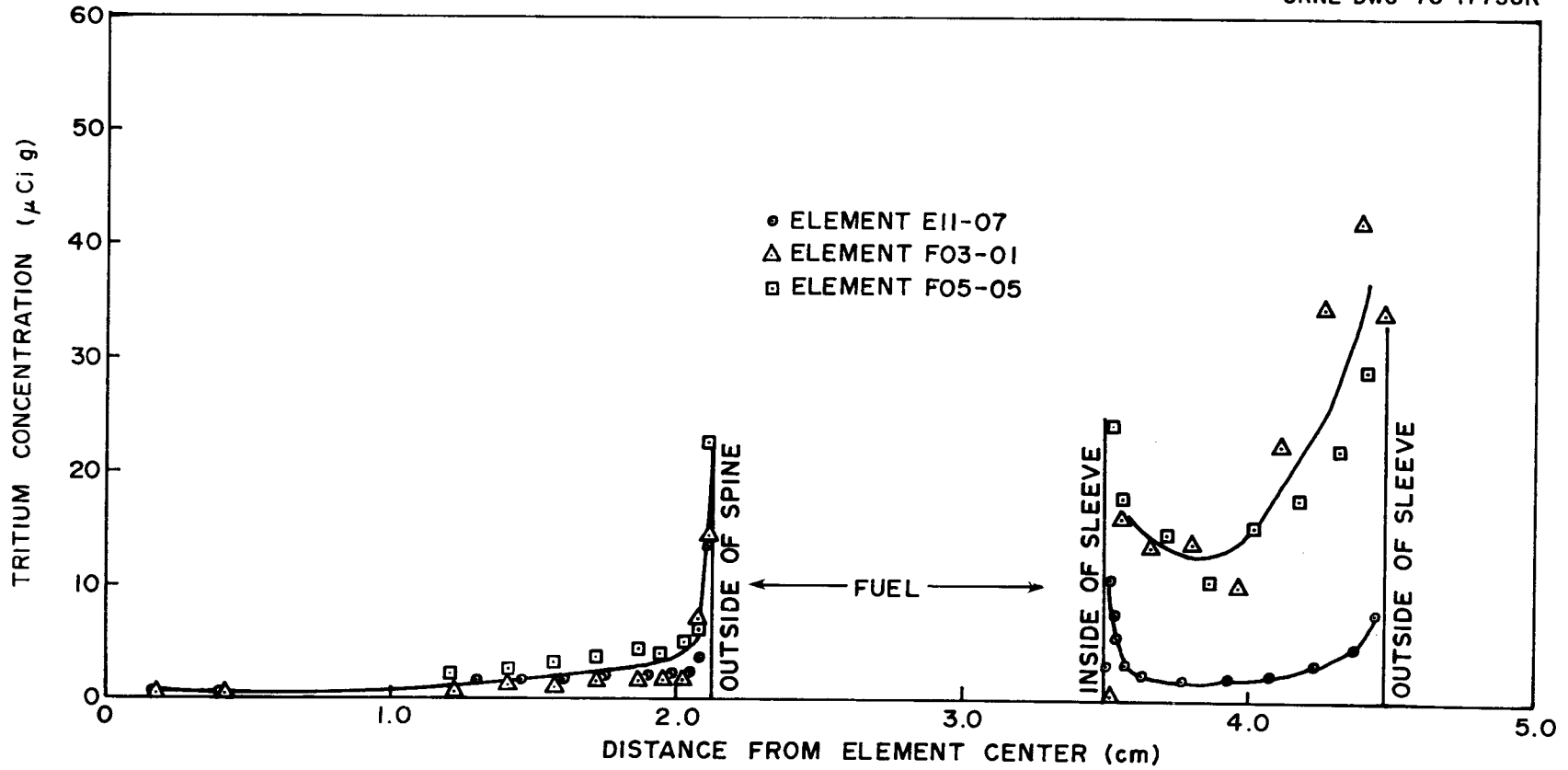


Fig. 5.4. Radial distribution of tritium in spine and sleeve of Peach Bottom HTGR fuel elements E11-07, F03-01, and F05-05 at compact 28.

Each figure represents the radial tritium distribution in the sleeves and spines of the three elements at a given axial location specified according to the number* of the compact that was adjacent to the dissected specimen. Although the data show considerable scatter, there is also much similarity among the distributions found in the sleeves and the three elements at each axial location. For example, adjacent to compact 5 (Fig. 5.1), the concentration of tritium in the sleeve rapidly reaches a relatively high maximum near the inner radius about 1 to 1.5 mm from the inside surface. The concentration then falls rapidly with increasing radial location and remains low (5 to 10 $\mu\text{Ci/g}$) until within ~ 1 mm of the exterior surface and then rises again. Opposite compact 12, Fig. 5.2, the concentration maximum occurs more toward the center of the sleeve, and the distribution seems to be nearly symmetrical around the sleeve center. Opposite compacts 18 and 28 (Figs. 5.3 and 5.4), the distributions in the sleeves are similar and reach a maximum near the sleeve exterior.

The radial distributions in the sleeves of the other three examined elements (E06-01, E14-01, and E01-01) were not measured in as many axial locations as were those for which data are plotted; however, the reader may observe from the tabular data that the levels are similar and the radial profiles roughly exhibit the axial dependence discussed above.

The concentrations of tritium in the spines were all lower than those in the sleeves, and the distributions were all similar. Little or no dependency on axial location was apparent in the radial distributions.

5.2 Axial Distributions in the Sleeves and Spine

Values representing the axial distribution of tritium in the sleeves and spines of the fuel elements, except for element E06-01, were derived from the radial distributions rather than being measured directly. The results are given as mean concentrations below each column of radial distribution data in Tables 5.1 through 5.41 and are summarized in

* There were 30 fuel compacts per element, numbered from the bottom to the top of the core; each compact was 7.62 cm (3 in.) long.

Table 5.42. The axial concentration values were derived from the radial concentration profile by summation of the product of tritium concentration and weight of graphite represented in the volumes between the radial cuts. Thereby, a mass-averaged tritium concentration was obtained for each axial location.

The results are plotted in Fig. 5.5, which shows the axial distributions of tritium in the sleeves and spines of four of the Peach Bottom fuel elements (E11-07, F03-01, E01-01, and F05-05). The plotted data for the sleeves and spines are average values for the four elements at each of the axial locations. The standard deviations, shown as error bars about the averages, reflect the element-to-element variation among the spine and sleeve samples at the given axial location. The two data points with no indicated error refer to determinations from a single fuel element. As can be seen, the concentration of ^3H is generally much larger in the sleeves than in the spines.

For comparison, Fig. 5.5 also gives the axial distribution of tritium in the reflector block A18-08 (discussed in Sect. 5.5) and typical tritium activities found in the bottom reflector graphite and in charcoal from the fission product traps (discussed in Sect. 5.3). The tritium levels in the reflector block lie between the sleeve and spine, and the average tritium concentration in all the fission product traps measured was about 300 $\mu\text{Ci/g}$, as indicated in the upper-left corner of Fig. 5.5.

5.3 Levels in the Upper Reflector Assembly, Fission Product Trap, and Bottom Connector

The external regions of the Peach Bottom fuel elements were sampled for tritium on three occasions. The upper reflector of element E06-01 was sampled at a location of 22 cm from the top of the element; those data, taken from ref. 1, are reported in Table 5.43. The bottom connectors of elements E11-07 and F03-01 were radially sampled at an axial location just below the point where they connected to the sleeves. These results, taken from ref. 4 and listed in Tables 5.44 and 5.45, show that tritium levels near the outer surface of the bottom connector are somewhat higher than those in the interior graphite. Although the three elements

Table 5.42. Axial distribution of tritium in sleeves
and spines of Peach Bottom HTGR
fuel elements

Element	Reference date	Compact	Tritium distribution ($\mu\text{Ci/g}$)	
			In sleeve ^a	In spine ^a
E06-01	1/6/72	2	(5.9)	(0.55)
		3	(6.9)	
		4		(0.61)
		7	12.8 (9.9)	1.52 (1.53)
		10	(15.9)	(1.69)
		14	(24.7)	(1.78)
		16	16.7	1.61 (1.57)
		18	(11.3)	
		22	(6.0)	(1.11)
		26	5.3 (5.6)	0.87 (1.11)
E11-07	9/14/73	5	20.5	3.9
		8		
		12	45.9	4.0
		16		
		18	11.6	3.1
		20		
		28	3.3	2.0
E14-01	10/31/74	1		(6.5)
		7	52.7	
		8		(6.9)
		16		(6.9)
		20		(5.3)
		23	18.0	3.9
		28	8.2	4.8
F03-01	10/31/74	5	17.7	5.3
		12	68.4	5.1
		18	38.5	3.2
		28	23.5	1.7
E01-01	10/31/74	4	38.3	
		12	68.0	
		18	34.7	
		23		2.1
		28	16.4	2.7
F05-05	10/31/74	5	6.3	7.1
		12	64.9	4.7
		18	34.3	3.1
		28	16.8	3.5

^aValues in parentheses were measured directly; other values were derived from radial distributions.

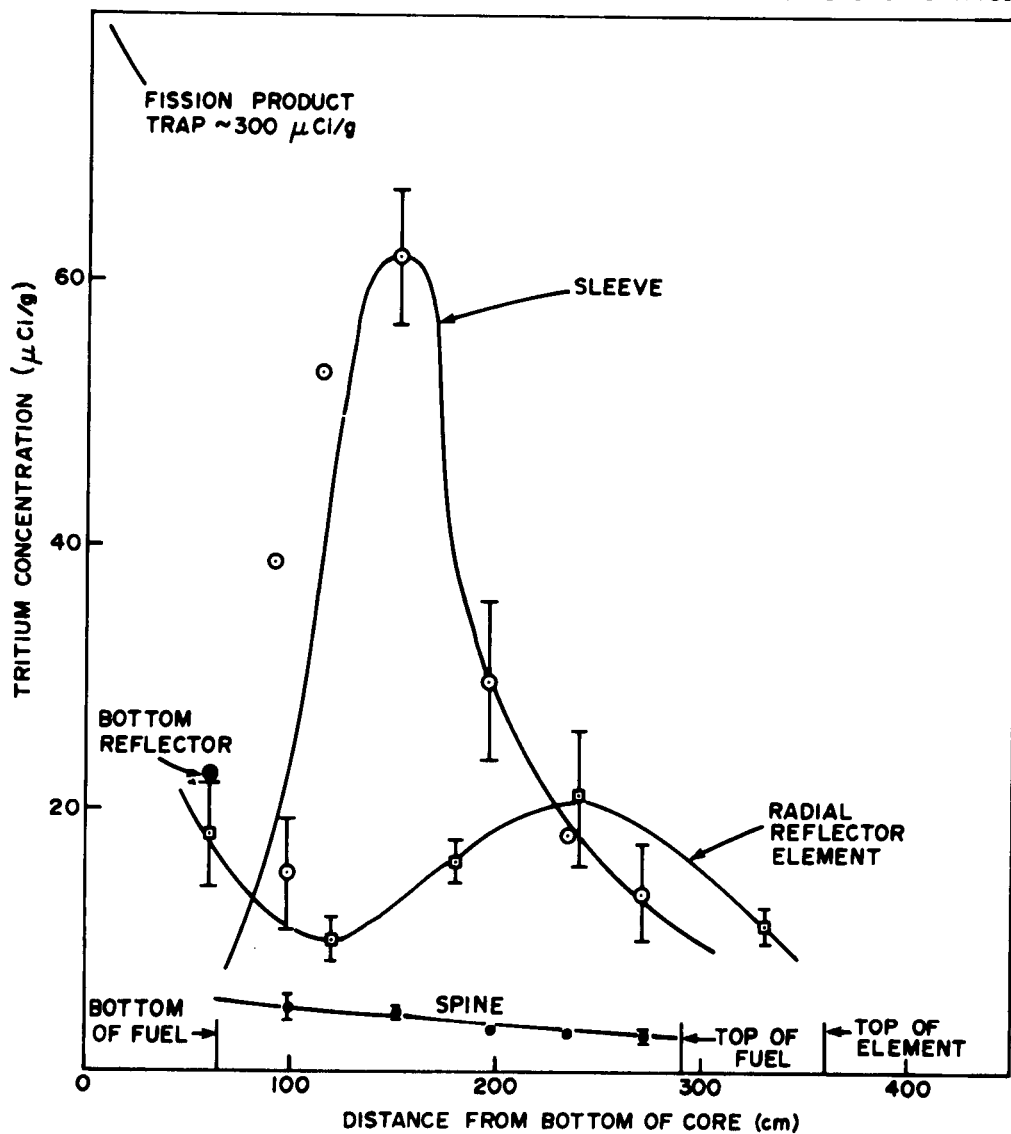


Fig. 5.5. Axial distribution of tritium in fuel element sleeve and spine (average of observed concentrations in elements E11-07, F03-01, E01-01, and F05-05) and in radial reflector element A18-08.

Table 5.43. Radial distribution of tritium in the top reflector
of element E06-01, 22 cm from the top of the element
(corrected to January 6, 1972)

Thickness of cut ^a (mm)	Distance to center of cut from OD (mm)	Tritium activity ($\mu\text{Ci/g}$)
1.02	0.51	1.3
2.03	2.03	0.2
5.08	5.59	0.7
1.02	13.21	0.4

^aRadial width of sample.

Table 5.44. Radial distribution of tritium in the bottom connector
of element E11-07 near the connector to sleeve
(corrected to September 14, 1973)

Thickness of cut ^a (mm)	Distance to center of cut from OD (mm)	Tritium activity ($\mu\text{Ci/g}$)
0.51	0.25	4.51
1.02	1.02	0.25
1.02	2.03	0.24
1.52	3.3	0.55
1.52	0.94	0.29
1.52	1.55	0.49
1.52	2.16	0.22
1.52	2.46	0.33
1.59	3.55	0.26
1.59	3.7	0.60

^aRadial width of sample.

Table 5.45. Radial distribution of tritium in bottom connector of element F03-01 near the connector to sleeve (corrected to October 31, 1974)

Thickness of cut ^a (mm)	Distance to center of cut from OD (mm)	Tritium activity ($\mu\text{Ci/g}$)
0.51	0.25	3.84
1.02	1.02	0.24
1.02	2.03	0.21
1.52	3.30	0.21
1.52	9.4	0.22
1.52	15.5	0.22
1.52	21.6	0.23
1.52	24.6	0.23
1.57	35.5	0.26
1.59	37.1	0.47

^aRadial width of sample.

were operated for much different times, the levels are very similar at this element location.

The tritium activity levels measured in graphite that surrounded the purge gas entry tube and in the graphite of the porous plug of element F03-01 are given in Table 5.46. These data were obtained by cutting the top reflector assembly into axial sections and drilling out the inner surface of the purge tube from its original diameter of 0.64 cm (1/4 in.) to 0.79 cm (5/16 in.).

The porous plug was also axially sectioned, and core-drilled samples were acquired from each section. We note by comparison with the sleeve specimens of Table 5.2 that the tritium level in the graphite surrounding

Table 5.46. Axial distributions of tritium in the graphite surrounding the purge gas entry hole and in the porous plug of element F03-01 (corrected to October 31, 1974)

Location ^a (cm)	Sample weight ^b (g)	Section length ^b (cm)	Total activity (μ Ci)	Tritium activity (μ Ci/g)
<u>Samples from purge hole^c</u>				
4.1	2.99	8.1	2.57	0.86
12.4	3.12	8.5	3.12	1.0
20.4	2.77	7.6	3.82	1.38
27.3	1.76	5.2	3.52	2.04
32.4	1.84	5.1	3.83	2.08
37.2	1.52	4.4	4.04	2.66
42.1	1.79	5.4	5.35	2.99
<u>Samples from porous plug</u>				
43.4		1.2		22.73
46.6		1.2		27.88
48.0		1.7		24.22
49.8		1.9		33.7
51.8		2.1		51.9
54.0		2.3		91.3
56.0		1.7		157.3

^aDistance from top of element to center of the section.

^bThe purge hole diameter was 1/4 in., and the radial thickness of the graphite sample was 1/32 in.

^cData were obtained by cutting the top reflector into axial sections and drilling the inner surface of purge tube and portions of the porous plug.

the purge hole is similar to the levels found near the exterior surface of the upper reflector region. However, the concentration of tritium in the porous plug was found to be much higher than that in the adjacent graphite and increased rapidly with proximity to the fuel. The high surface area of the porous plug probably resulted in a greater tritium uptake from the helium than that exhibited by the tube graphite.

Two of the more interesting possible tritium sinks in the Peach Bottom fuel element are the bottom reflector and fission product trap. The bottom reflector, a solid graphite cylindrical body the size of a fuel compact, is immediately below the stack of fuel compacts. Below the bottom reflector is the fission product trap, which consists of several parallel channels filled with coconut shell activated charcoal. (Reference 3 gives a detailed description of the fission product trap geometry.) Purge gas that has swept by the fuel flows past the bottom reflector in four small V-shaped grooves that run axially along the outer surface of the bottom reflector, through a graphite cloth into the fission product trap, and then into coolant cleanup plant. One would expect the tritium content of the bottom reflector and fission product trap to be indicative of the tritium content of the purge gas as it exits the fuel region of the elements. Element E14-01, with its poisoned spine containing natural zirconium boride (a tritium source) was of special interest because of the possibility of tritium release from the spine.

Tritium concentrations were measured in the bottom reflector pieces of elements E14-01 and F03-01 in samples drilled from the upper face (toward the fuel) in the vicinity of one of the V-shaped grooves. The face was sampled in the middle and about halfway between the center and the circumference. Samples were taken from the groove at axial locations near both ends and near the center of the reflector body. The depth of sampling ranged from about 5 to 15 mm. Results of the analysis, given in Table 5.47, indicate that the tritium distributions in the bottom reflectors were fairly homogeneous. The ^3H level in the groove of the E14-01 reflector appeared to be slightly lower than that in the face, and the overall level seemed to be slightly lower than that in the reflector of F03-01. These results give no evidence that the poisoned spine of element E14-01 contributed significant amounts of tritium to the purge gas that exited the fuel region of this element.

Table 5.47. Tritium activities in bottom reflectors of fuel elements E14-01 and F03-01 (corrected to October 31, 1974)

Element	Tritium activity ($\mu\text{Ci/g}$)		
	Samples from groove	Samples from face	Mean ^a
E14-01	13.7 \pm 2.2	24.8 \pm 1.5	18.2 \pm 1.7
F03-01	27.9 \pm 2.4	25.2 \pm 2.6	21.9 \pm 0.5
			Overall 20.0

^aUncertainty values are standard deviations on the mean calculated by: sample standard deviation/ \sqrt{N} .

Tables 5.48 to 5.51 and Fig. 5.6 give the axial distributions of tritium found in the fission product traps of elements E11-07, F03-01, E01-01, and F05-05. Since it is known that charcoal has at least the possibility of significantly higher lithium levels than graphite (because of its lower firing temperature), lithium levels in the charcoal trap were measured to determine if the observed tritium concentration resulted from deposition from the purge flow or from ⁶Li. As indicated in Table 3.4, the lithium concentration in the trap charcoal was only 15 ppb, which is far too low to account for the observed tritium concentrations. Therefore, if equilibrium sorption data were known for HT on charcoal at the temperature of the trap, the profiles could be interpreted in terms of the tritium concentration in the purge gas. An estimate is so made in Sect. 6.3.1.

5.4 Concentrations in the Fuel

Tritium concentrations were measured in bulk fuel samples taken from two elements and in individual particle pairs obtained from four compacts in element E11-07. Table 5.52 compares the bulk fuel data with tritium activities estimated from the ternary fission source. The estimates were based on an assumed tritium yield of 1.0×10^{-4} . Previously measured^{3,4} inventories of ¹³⁷Cs and ⁹⁵Zr, appropriately corrected for differences in half-life, were employed as a measure of the number of fissions experienced

Table 5.48. Axial distribution of tritium in fission
product trap of element E11-07
(corrected to September 14, 1973)

Axial location of sample ^a (cm)	Weight of charcoal (g)	Specific activity of ³ H (μ Ci)	Total activity in sample (μ Ci)
1.3	7.16	333	2380
4.8	17.3	292	5050
10.8	20.8	250	5200
17.0	20.1	310	6230
25.2	32.9	243	8000
Total ^b	98.3		2.68E4

^aDistance from trap entrance to sample midpoint.

^bTotal mass of charcoal in trap and total tritium activity in trap.

Table 5.49. Axial distribution of tritium in fission product trap of element F03-01 (corrected to October 31, 1974)

Sample location ^a (cm)	Sample weight (g)	Specific activity of ³ H (μ Ci/g)	Total activity in sample (μ Ci)
1.3	0.45	396	178
3.8	2.59	473	1230
6.4	7.10	472	3350
9.9	9.65	425	4110
11.4	6.74	371	2500
14.0	8.88	369	3280
16.5	9.40	365	3430
19.1	9.75	355	3460
21.6	7.26	336	2440
24.1	3.58	346	1239
26.7	8.89	327	2910
29.2	<u>4.90</u>	313	<u>1540</u>
Total ^b	79.2		2.55E4

^aDistance from trap entrance to sample midpoint.

^bTotal mass of charcoal in trap and total activity in trap.

Table 5.50. Axial distribution of tritium in fission
product trap of element E01-01
(corrected to October 31, 1974)

Sample location ^a (cm)	Sample weight (g)	Specific activity of tritium ($\mu\text{Ci/g}$)	Total activity in sample (μCi)
1.3	3.62	428	1.55E3
3.8	6.32	396	2.50E3
6.4	9.50	383	3.64E3
9.9	10.84	471	5.11E3
11.4	10.70	385	4.12E3
14.0	9.38	402	3.77E3
16.5	9.88	435	4.30E3
19.1	10.09	451	4.55E3
21.6	9.97	353	3.52E3
24.1	8.82	453	3.99E3
26.7	9.08	449	4.08E3
29.2	<u>3.89</u>	398	<u>1.55E3</u>
Total ^b	102.1		4.27E4

^aDistance from trap entrance to sample midpoint.

^bTotal mass of charcoal in trap and total activity in trap.

Table 5.51. Axial distribution of tritium in fission
product trap of element F05-05
(corrected to October 31, 1974)

Sample location ^a (cm)	Sample weight (g)	Specific activity of tritium ($\mu\text{Ci/g}$)	Total activity in sample (μCi)
1.3	9.44	552	5.21E3
3.8	5.71	499	2.85E3
6.4	5.99	459	2.75E3
9.9	6.08	430	2.61E3
11.4	9.18	424	3.89E3
14.0	7.41	406	3.01E3
16.5	9.92	397	3.94E3
19.1	10.18	407	4.14E3
21.6	9.82	402	3.95E3
24.1	7.64	375	2.87E3
26.7	9.21	350	3.22E3
29.2	<u>4.51</u>	310	<u>1.40E3</u>
Total ^b	96.08		3.98E4

^aDistance from trap entrance to sample midpoint.

^bTotal mass of charcoal in trap and total activity in trap.

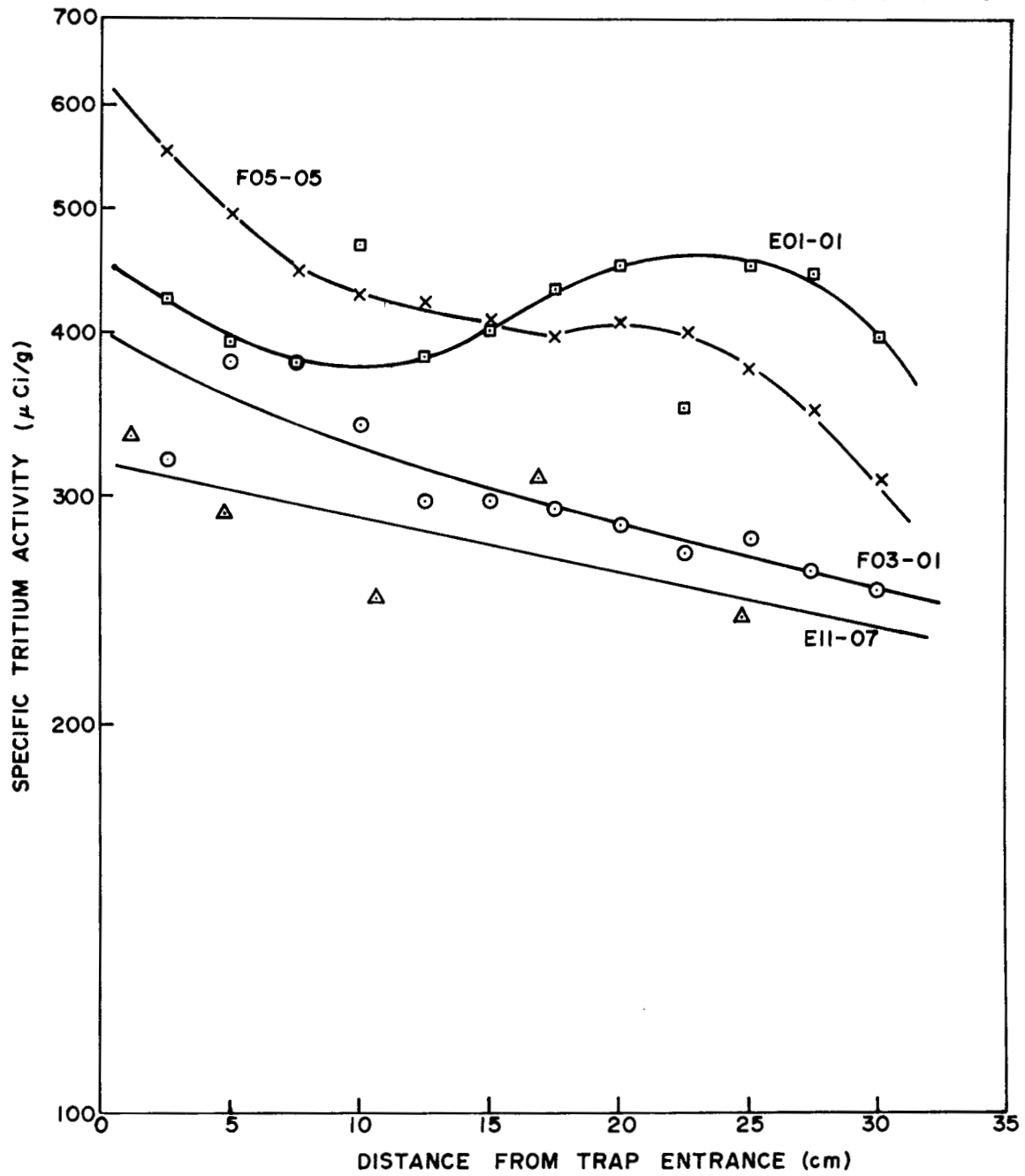


Fig. 5.6. Axial distribution of tritium found in fission product trap of Peach Bottom HTGR fuel elements.

Table 5.52. Tritium activities in Peach Bottom HTGR fuel
(corrected to October 31, 1974)

Element	Compact	Sample	Activity (Ci/g)		Tritium released (%)	Operating temperature of compact ^b (°C)		Thermal-neutron fluence ^c (neutrons/cm ² x 10 ⁻²¹)
			Measured	Estimated ^a		Average	Maximum	
E14-01	2	1	117	93	-26	625	671	1.74
	14	1	168	190	11	1065	1165	4.86
	23	1	115	166	31	1025	1170	4.11
F03-01	2	1	124					
		2	116					
		Mean	120	86	-39	600	693	1.48
	9	1	86					
		2	81					
		Mean	83	140	41	920	1079	3.63
16	1	17.9						
	2	19.3						
	Mean	18.6	161	88	1050	1285	4.24	

^aBased on a yield of 1.0×10^{-4} .

^bFrom ref. 37.

^cFrom ref. 42.

in each fuel compact. The table also gives the estimated average and maximum temperatures experienced by the fuel compact, taken from ref. 37, and the thermal-neutron fluence at the location, obtained from ref. 42. Large uncertainties exist in the estimated fuel compact temperature; however, the general axial trends are certainly valid.

The bulk fuel samples were analyzed for tritium by procedures similar to those described in Sect. 5.1 for graphite samples. The specimens weighed from 3 to 6 g and contained from 2000 to 5000 fuel particles.

The results in Table 5.52 clearly show that most of the fuel compacts measured experienced significant tritium loss. The greatest loss was exhibited by compact 16 of element F03-01, where a measured specific activity of only 19 $\mu\text{Ci/g}$ was determined, compared with 161 $\mu\text{Ci/g}$ estimated from ternary fission. In contrast, the measured activity levels in compact 2 of elements E14-01 and F03-01, both cool locations near the coolant entry point, had measured activity levels actually in excess of the calculated value.

Since Gainey¹⁶ reports published tritium fission yields ranging from 0.8×10^{-4} to 1.3×10^{-4} , at least a part of the apparent tritium excess at the cool location (compact 2) may be due to an underestimation of the tritium source. However, it appears more likely that the major part of the 26 and 39% excess was due to deposition of tritium at this location from the purge gas, since compact location 2 is near the downstream end of the purge flow path through the fuel element.

Owing to the few data points and the uncertainty regarding actual fuel temperatures, it is not possible to distinguish between the effects of high temperature or neutron fluence as the principal cause for tritium leakage from the fuel compacts. However, compacts exposed to both high temperature and high fluence clearly lost a significant portion of the tritium born within the fuel kernels.

These observations appear to be consistent with the experiments reported in ref. 27 (and abstracted by Gainey¹⁶), which indicated that UC_2 Biso kernels retained >70% of the tritium at 750°C but only 23% at 1275°C. Somewhat higher retentions were observed with $(\text{Th,U})\text{C}_2$ compared with UC_2

kernels for equal exposure conditions. Reported measurements on core 1 element D13-05 showed that only about 25% of the tritium was released from the fuel despite almost complete particle coating failure.

Table 5.53 lists tritium activities measured on individual particle pairs obtained from four deconsolidated compacts from element E11-07. Comparison with ^{106}Ru activity, which is thought to be immobile with time in the fuel particle, shows that the highest relative tritium activity is in the samples from compact 2. Progressively lower tritium levels were observed in particles taken from compacts 13, 24, and 20, in the order of increasing compact temperature.

Table 5.53. Tritium activities in samples of fuel particle pairs recovered from the fuel of element E11-07

Compact	Sample	Tritium activity (μCi)	Activity ratio ($^3\text{H}/^{106}\text{Ru}$)
2	1	0.067	3.4E-3
	2	0.048	2.3E-3
	3	0.122	5.7E-3
13	1	0.069	1.8E-3
	2	0.185	2.5E-3
	3	0.062	1.9E-3
20	1	<1.4E-3	<3.4E-5
	2	<6.6E-4	<2.5E-5
	3	<7.0E-4	<1.6E-5
24	1	0.037	5.9E-4
	2	0.047	1.1E-3
	3	0.067	1.1E-3

5.5 Distribution in Radial Reflector Element A18-08

The active core of the Peach Bottom HTGR was surrounded by three radial rows (rows 18 to 20) of solid graphite elements termed "the removable reflector elements." In addition to their role as neutron reflectors, these

elements served to prevent radial flow of the coolant from the core by virtue of their hexagonal cross section and tightly packed arrangement. The distance across flats of the reflector element approximately equaled the fuel element diameter (8.9 cm), and the total lengths were equal. Other descriptive data regarding the removable reflector elements are given in Table 5.54.

Table 5.54. Descriptive data for removable reflector elements

Number of elements	341
Cross-sectional area, cm ²	70.39
Length, cm	3657.7
Density, ^a g/cm ³	1.59
Mass per element, g	4.05E4
Total mass, g	1.38E7

^aMeasured on specimen from element A18-08.

To evaluate the role played by the reflectors as sources and sinks of tritium, one of the reflectors, designated A18-08, was dissected and analyzed for tritium and lithium. Results for lithium impurities were reported in Sect. 3.3. Since reflector A18-08 was in the inner row of reflectors, two of its six faces were adjacent to the two active fuel elements A17-07 and A17-08.

The removable reflector element was dissected by cutting cross-sectional wafers of about 4 mm thicknesses at 1-ft (30.5-cm) intervals along the element, beginning 1 ft from the bottom of the core. Wafers are referred to by numbers 1 through 11 from bottom to top to identify their axial location. The radial distributions of tritium within the reflector were determined in the five wafers numbered 2, 4, 6, 8, and 11.

Figure 5.7 is a schematic representation of the sampling locations and results. The numbers in the hexagonal cross sections denote the observed tritium concentrations corrected to October 31, 1974. These data

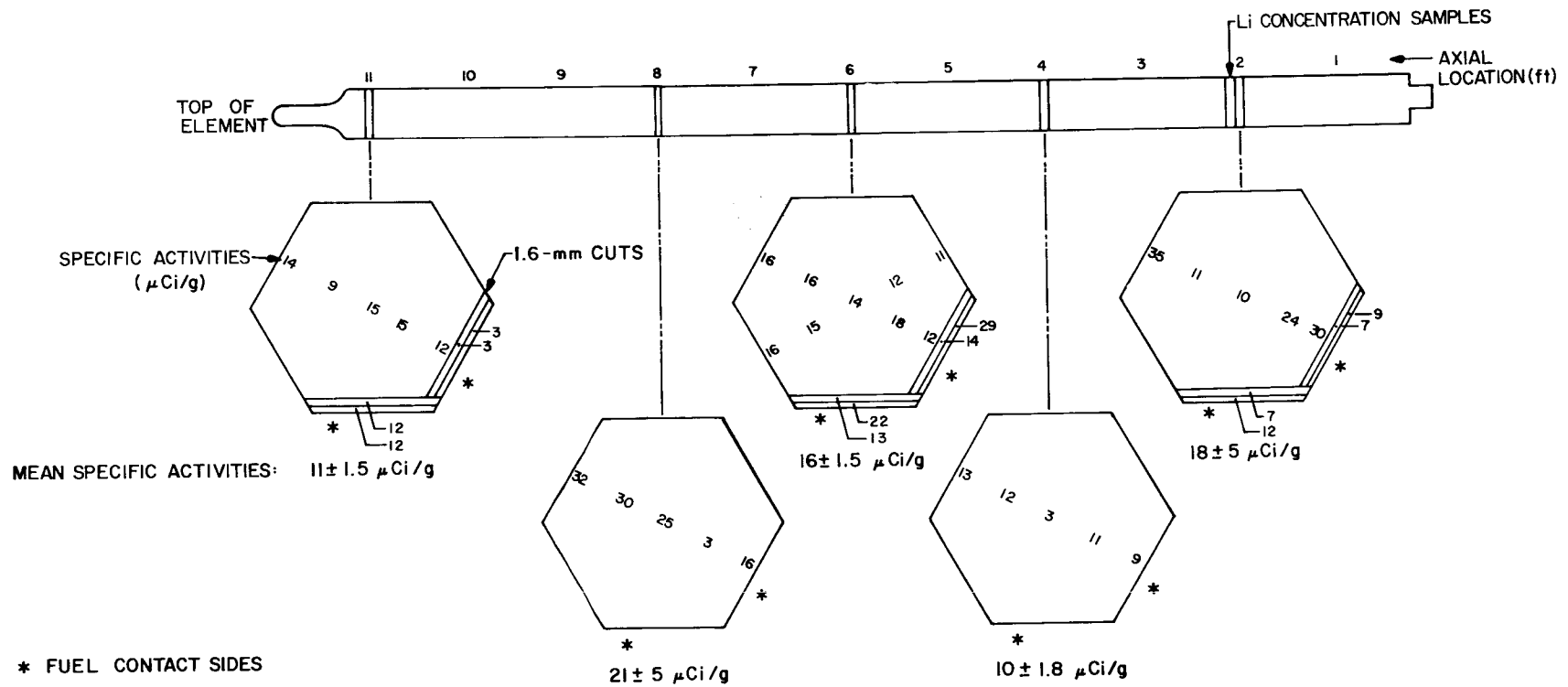


Fig. 5.7. Schematic representation of sampling points at which tritium was measured in removable radial reflector element A18-08. (Numbers denote tritium specific activity on Oct. 31, 1974.)

appear on the drawings at locations that roughly correspond to the sampling locations. Most of the sampling was done by drilling through the wafers with a 3/8-in. drill and collecting the dust that was generated; each sample weighed about 0.1 g. The samples taken near the exterior were within about 6 to 8 mm of the edges. Generally, samples were acquired at five equally spaced locations across the wafers, starting at an edge that had been adjacent to a fuel element. Note that a cross-shaped sampling pattern was used on wafer 6. In addition to specimens obtained by drilling, two samples were obtained from wafers 2, 6, and 11 by shaving off 2 to 3 mm of graphite from the edges adjacent to the fuel.

There is considerable scatter in the measured tritium concentrations in Fig. 5.7, but a broad maximum appears to exist in the top third section of the element. No trend is readily apparent in the radial distribution of tritium within the reflector element. The average concentrations at each of the axial locations and an average for the element are summarized in Table 5.55. Figure 5.5 is a plot of the axial distribution of tritium in the reflector in relation to similar plots obtained for fuel element sleeves and spines. The level of tritium in the reflector lies between the levels observed for the sleeves and spines.

Table 5.55. Axial distribution of tritium in Peach Bottom reflector element A18-08

Distance from bottom of element (m)	Number of samples measured	Mean tritium concentration ($\mu\text{Ci/g}$)
0.71	9	18 ± 15
1.2	5	9.5 ± 4.0
1.8	13	15.7 ± 5.0
2.4	5	21.2 ± 12
3.3	9	10.4 ± 21.8
		15.0 ± 9.3

Source level estimates in Sects. 6.1.2 and 6.1.3 indicate that approximately 4 $\mu\text{Ci/g}$ of tritium may result from births in place due to ^6Li and ^3He . Since the observed levels range from 3 to 50 $\mu\text{Ci/g}$, with averages at each axial location from 10 to 21 $\mu\text{Ci/g}$, it is clear that the reflector was a sink for tritium born elsewhere.

6. ESTIMATED SOURCE LEVELS, INVENTORIES, AND LOSSES

6.1 Source Estimation

Tritium source levels in the reactor from ternary fission and neutron reactions with ^6Li , ^{10}B , and ^3He are estimated here using modified versions of methods described by Gainey.¹⁶ These methods, in turn, were abstracted from procedures described by Compere,²⁷ Forsyth,²³ and internal GAC memoranda.

6.1.1 Production of tritium in fuel

If one assumes an average yield Y of tritium atoms per fission, the tritium production rate from fission may be expressed as

$$\frac{dN_T}{dt} = KYP(t) - \lambda N_T(t), \quad (6.1)$$

where

$N_T(t)$ = atoms of tritium at time t ,

K = fission rate per thermal megawatt (3.121×10^{16} fissions/sec·MW),

$P(t)$ = power at time t (MW),

λ = decay constant (1.793×10^{-9} sec⁻¹),

Y = average yield per fission (1×10^{-4}).

Rather than numerically integrate Eq. (6.1) through the complex power history $P(t)$ experienced by core 2, no significant error is introduced by employing an average power \bar{P} assumed constant over the life of the core estimated from

$$\bar{P} = P_{\text{rated}} (\text{EFPD}/t_f), \quad (6.2)$$

where

$$\begin{aligned} P_{\text{rated}} &= \text{rated power [115 MW(t)]}, \\ \text{EFPD} &= \text{equivalent full-power days at EOL (897 days)}, \\ t_f &= \text{duration of core 2 operation (1550 days)}. \end{aligned}$$

From the above, $\bar{P} = 66.6 \text{ MW(t)}$ and Eq. (6.1) is solved for constant power to yield

$$N_T(t_f) = K \bar{P} Y \left(\frac{1 - \exp(-\lambda t_f)}{\lambda} \right). \quad (6.3)$$

Employing values given above in Eq. (6.3) yields a value of 1210 Ci of tritium produced by ternary fissions over the life of the core and present at EOL.

6.1.2 Production from ^3He in the coolant

As noted in Sect. 2.1, tritium is produced from ^3He via an (n,p) reaction with thermal neutrons. Compere et al.²⁷ report the effective cross section for this reaction as 2280 barns, averaged over the thermal energy range of 0 to 2.4 eV. The level of ^3He contamination in commercially available helium has been shown to vary with the source. In general, helium derived from natural-gas wells contains approximately 0.2 ppm ^3He , whereas ^3He levels in atmospheric helium are about ten times higher. Determinations of helium at Peach Bottom indicated a ^3He level of 0.16 ppm; ⁴³ hence, this level will be assumed in the source estimates below.

The total moles of ^3He in the primary system, N_3 , is governed by the relation

$$\frac{dN_3}{dt} = -\sigma_3 N_3 (\alpha_1 \bar{\phi}_{\text{th},1} + \alpha_2 \bar{\phi}_{\text{th},2}) + Q_2 ([^3\text{He}]_1 - [^3\text{He}]), \quad (6.4)$$

where

$$\begin{aligned} \sigma_3 &= \text{effective cross section for } ^3\text{He}(n,p)\text{T (2880 barns)}; \\ \alpha_1 &= \text{fraction of } N_3 \text{ in the coolant holes, sleeve, removable radial reflectors, and purge flow passages}; \\ \alpha_2 &= \text{fraction of } N_3 \text{ in the axial and permanent radial reflector}; \end{aligned}$$

$$\begin{aligned}
\bar{\phi}_{th} &= \text{thermal flux in core and in removable radial reflector;} \\
\bar{\phi}_{th,2} &= \text{thermal flux in axial and permanent radial reflectors;} \\
Q_2 &= \text{helium makeup (and leakage) rate (cm}^3\text{/sec);} \\
[{}^3\text{He}]_i &= \text{{}^3He concentration in makeup helium (moles/cm}^3\text{);} \\
[{}^3\text{He}] &= \text{{}^3He concentration in primary systems (moles/cm}^3\text{)}.
\end{aligned}$$

Equation (6.4) presumes that the average thermal flux in the active core and the removable radial reflector is approximately equal ($\bar{\phi}_{th}$). Similarly, the average thermal flux in the axial blanket and permanent radial reflector zones is assumed to be equal to $\bar{\phi}_{th,2}$.

The values for N_3 and the ${}^3\text{He}$ concentration are related by

$$[{}^3\text{He}] = N_3/V, \quad (6.5)$$

where V is the volume of the primary system that is readily accessible to ${}^3\text{He}$. This includes the coolant passages between the fuel elements (V_1), and the piping, plenums, and steam-generator tubing forming the ex-core primary system volume (V_2). In addition, following Compere et al.,²⁷ we assume that the connected porosity in portions of the graphite core components are readily accessible to ${}^3\text{He}$ permeation. Thus, the connected pores in the sleeve (V_3), removable radial reflector (V_4), axial reflector (V_5), permanent radial reflector (V_6), and purge flow volume within the fuel elements (V_7) are assumed to be readily accessible to ${}^3\text{He}$ and are therefore included in V . However, the interior portions of the fuel element (i.e., the fuel compact and spine) are assumed to be shielded from ${}^3\text{He}$ replenishment. Thus the effective helium volume of the primary system includes

$$V = V_1 + V_2 + V_3 + V_4 + V_5 + V_6, \quad (6.6)$$

where

$$\begin{aligned}
V_1 &= \text{volume of coolant passages in core,} \\
V_2 &= \text{ex-core primary system volume,} \\
V_3 &= \text{connected porosity in sleeve graphite,} \\
V_4 &= \text{connected porosity in removable radial reflector,} \\
V_5 &= \text{connected porosity in axial reflector,} \\
V_6 &= \text{connected porosity in permanent radial reflector.}
\end{aligned}$$

Thus

$$\alpha_1 = \frac{V_1 + V_3 + V_4 + V_7}{V} ,$$

and

$$\alpha_2 = \frac{V_5 + V_6}{V} . \quad (6.7)$$

Numerical values for the parameters in Eqs. (6.5) to (6.7) are summarized in Table 6.1. Although σ_3 is quite large (2280 barns), the ^3He burnup rate is relatively slow because most of the helium is outside the core ($\alpha_1 = 0.0185$ and $\alpha_2 = 0.0140$). On the other hand, the helium loss of 7 lb_m/day due to leakage and makeup is relatively rapid and dominates the ^3He decay constant implied in Eq. (6.5). Owing to the rapid makeup rate, the effective decay time of ^3He in the primary system was approximately 87 days and hence the equilibrium value for N_3 may be employed without significant loss of accuracy. Since the equilibrium is due overwhelmingly to the large value for Q_2 in Eq. (6.4), N_3 is given as approximately

$$N_3(\infty) = V[{}^3\text{He}]_i , \quad (6.8)$$

that is, the ^3He concentration in the Peach Bottom primary circuit was very nearly equal to that in the helium makeup.

Following Compere et al.,²⁷ we will assume that tritium atoms born in the graphite pores will remain chemisorbed there; hence it is necessary to distinguish between the coolant space and graphite void source locations. The quantity of tritium in the coolant space (including the purge flow gaps), N_{T1} , follows the relation

$$\frac{dN_{T1}}{dt} = \frac{V_1 + V_7}{V} \bar{\phi}_{th} \sigma_3 N_3 - Q[T] - \lambda_T N_{T1} , \quad (6.9)$$

where the ratio $(V_1 + V_7)/V$ represents the fraction of N_3 that exists in the coolant and purge flow passages of the core. The total moles of tritium circulating in the reactor with the coolant, N_{T1} , is related to the concentration $[T]$ (moles/cm³) by

$$N_{T1} = [T](V_1 + V_2 + V_7) . \quad (6.10)$$

Table 6.1. Parameters used for estimating tritium production from ^3He

Parameter	Symbol	Value
^3He concentration in makeup helium, ^a moles/cm ³	$[^3\text{He}]_i$	5.78×10^{-11}
Flow to chemical cleanup system plus 10% of purge flow, cm ³ /sec	Q_1	2.40×10^4
Leakage flow rate from primary system, ^b cm ³ /sec	Q_2	25.5
Sum of $Q_1 + Q_2$, cm ³ /sec	Q	2.40×10^4
Volume of coolant passages in core, cm ³	V_1	1.77×10^6
Ex-core loop volume, cm ³ /sec	V_2	1.88×10^8
Volume of connected pores, cm ³		
In sleeve graphite	V_3	3.44×10^5
In removable radial reflector	V_4	8.46×10^5
In axial reflector	V_5	3.92×10^5
In permanent radial reflector	V_6	2.32×10^6
Purge flow passages, cm ³	V_7	6.32×10^5
Sum V_1 through V_7 , ^c cm ³	V	1.94×10^8
Average thermal flux, neutrons/cm ² ·sec		
In core	$\bar{\phi}_{th}$	2.82×10^{13}
In removable radial reflector, core 2	$\bar{\phi}_{th}$	2.82×10^{13}
In removable radial reflector, core 1	$\bar{\phi}_{th,1}$	2.57×10^{13}
In axial reflector	$\bar{\phi}_{th,2}$	1.41×10^{13}
In permanent radial reflector	$\bar{\phi}_{th,3}$	1.41×10^{13}
Duration, sec		
Core 2	t_f	1.339×10^8
Core 1	t_f	7.36×10^7
Tritium decay constant, 1/sec	λ_T	1.793×10^{-9}
Effective cross section for $^3\text{He}(n,p)\text{T}$, barns	σ_3	2880

^aBased on 0.16 ppm ^3He in helium.

^bBased on 7 lb_m/day helium loss reported in ref. 8.

^cTotal volume of primary system accessible to ^3He .

Since in this case, $V_1 + V_2 + V_7$ is very nearly the total primary system volume, Eq. (6.10) is very nearly $N_{T1} + [T]V$.

The helium loss flow rate Q in Eq. (6.9), which is effective in removing tritium from the primary system, is the sum of the chemical cleanup system flow Q_1 , the helium leakage (hence makeup) flow rate Q_2 , and some portion of the purge flow to the fission product cleanup system. As discussed in Sect. 2.4, operational evidence indicated that the liquid-nitrogen-cooled trap, through which about 10% of the purge flow passed, effectively removed tritium; that is, more than 99% of the observed gaseous tritium activity in the stack monitor was correlated with the measured tritium inventory in the holdup vessel that received the regeneration gases from this bed.

Thus, we will assume that Q is properly the sum of Q_1 , Q_2 , and 10% of the total fuel element purge flow rate of 454 g/hr. Concurrently, we will assume that the tritium content of the remainder of the purge flow (90%) was unaffected by passage through the water- and Freon-cooled delay beds. The 36-kg/hr (80-lb_m/hr) flow from the compressor seals to the Freon-cooled delay bed in the fission product trapping system, shown in Fig. 2.2, is not considered a leakage flow for tritium since its source is the purified helium system rather than the primary loop coolant.

The appropriate value for Q in Eq. (6.9) is the indicated sum, averaged for all time, including shutdown times. Since the reactor operated 1018 days of the total duration of 1550 days, the average leakage flow is less than the nominal value by the factor 1018/1550. The volume flow is computed based on an average primary loop temperature of 809 K and a pressure of 23 atm.

As for ${}^3\text{He}$, the value of N_{T1} should come rapidly to equilibrium and allow algebraic solution for N_{T1} from Eqs. (6.9) and (6.10). The result is

$$N_{T1} = \frac{(V_1 + V_7)\bar{\phi}_{th}\sigma_3 N_3}{Q + \lambda_T V}, \quad (6.11)$$

where the value for N_3 is obtained from Eq. (6.8).

In contrast, tritium atoms born in sleeve graphite from ${}^3\text{He}$ (N_{T2}) build up with time according to

$$\frac{dN_{T2}}{dt} = \frac{V_3}{V} \bar{\phi}_{th} \sigma_3 N_3 - \lambda_T N_{T2} . \quad (6.12)$$

Similarly, for the removable radial reflector,

$$\frac{dN_{T3}}{dt} = \frac{V_4}{V} \bar{\phi}_{th,1} \sigma_3 N_3 - \lambda_T N_{T3} , \quad (6.13)$$

where $\bar{\phi}_{th,1}$ is the average thermal flux in the reflector. Solutions for N_{T2} and N_{T3} at EOL (t_f) are thus

$$N_{T2}(t_f) = \frac{V_3}{V} \bar{\phi}_{th} \sigma_3 N_3 \left[\frac{1 - \exp(-\lambda_T t_f)}{\lambda_T} \right] \quad (6.14)$$

and

$$N_{T3}(t_f) = \frac{V_4}{V} \bar{\phi}_{th,1} \sigma_3 N_3 \left[\frac{1 - \exp(-\lambda_T t_f)}{\lambda_T} \right] . \quad (6.15)$$

Equations for tritium buildup from ${}^3\text{He}$ in the permanent radial reflector (N_{T4}) and in the axial reflector (N_{T5}) are identical in form with Eqs. (6.14) and (6.15), except that the appropriate value for the interconnected pore volume is substituted for V_3 or V_4 and the appropriate value for the average thermal flux is used.

Note that since the removable radial reflector was not replaced before the operation of core 2, part of its tritium inventory deposited by ${}^3\text{He}$ reactions resulted from core 1 operation. The estimate of this portion of the tritium source was made using Eq. (6.15) with appropriate time and flux parameters for core 1. Core 1 operated 451 EFPDs between June 1, 1967, and October 3, 1969, when the reactor was shut down for refueling. The tritium deposited at the shutdown date of core 1 was corrected for decay to the end of core 2 operation (decay time = 1.60×10^8 sec). Since the core actually operated 852 days, the estimated time-average thermal flux for core 1 was obtained by multiplying the thermal flux for core 2 by the ratio $(451/852)/(898/1550) = 0.91$. The numerator of this ratio is the fractional time that core 1 operated at full power, and the denominator is

the corresponding fraction for core 2. The average thermal flux of core 1 was thus taken to be about 9% lower than that of core 2.

Table 6.1 summarizes the parameters required for estimating tritium production from ^3He in the coolant. The values for the volumes of connected pores in the graphite components were estimated from the mass of the components given in Table 1.2 and the reported graphite densities. The densities of the sleeve and spine graphite according to the FHSR were 1.90 and 1.85 g/cm³, respectively. The replaceable radial reflectors had a measured density of 1.59 g/cm³, a value which was assumed for the permanent radial reflector as well. The connected porosity in the graphite was assumed to be half the total porosity computed from the stated bulk densities. The leakage flow rate (and hence the makeup flow) was taken as 25.5 cm³/sec, which is equivalent to the 7 lb_m/day reported in ref. 8 and confirmed by personal communication with Philadelphia Electric Company personnel.

The value for V , the total primary loop volume accessible to ^3He , and values for V_1 through V_6 were found in the FHSR. A total primary loop volume (evidently including the core plus reflectors) of 8200 ft³ is given in the FHSR. (The dimensions of the core and reflectors are shown in Fig. 1.4.)

To determine $\bar{\phi}_{\text{th}}$, the axial-averaged thermal fluxes at element locations E06-01, F03-01, E11-07, and E14-01 were averaged over time. Values for the thermal flux at these core locations are listed in a number of correspondence documents supplied by GAC during the course of the Peach Bottom Surveillance Program.⁴² Location E06-01 was occupied by FTE-18 from full-power day 384 to EOL; axially averaged fluxes are recorded for this location and time in ref. 22. It should be noted that fluxes for location E11-07 were available only for the first 700 days of full-power operation. Numerically time-averaging the thermal flux at the indicated element locations in the core yielded a value of 2.82×10^{13} neutrons/cm²·sec for $\bar{\phi}_{\text{th}}$.

Here again, $\bar{\phi}_{\text{th}}$ is the thermal flux, defined in Peach Bottom neutronics calculations as the 0- to 2.38-eV energy group, averaged over the entire

time span of core 2 operation, including shutdown periods. The motivation for averaging the flux in this fashion is to simplify the estimate for radioactive decay, which occurs whether the reactor is operating or shut down.

The values of the average thermal flux in the various reflector zones relative to $\bar{\phi}_{th}$ in the core are only educated guesses at best. The inner radial reflector region experiences some localized flux elevation due to thermalization of faster groups prior to decline because of leakage; hence $\bar{\phi}_{th,1}$ is assumed to be approximately equal to $\bar{\phi}_{th}$. Values for $\bar{\phi}_{th,2}$ and $\bar{\phi}_{th,3}$ were taken simply as half the average core thermal flux.

The total moles of ^3He in the primary system, computed using Eq. (6.8) and parameters in Table 6.1, are given in Table 6.2 along with the resulting amounts of tritium in the various primary system regions at EOL, computed from Eqs. (6.10), (6.14), and (6.15). We note that the major portion of the tritium in the primary system at EOL due to ^3He resides in the graphite; the inventory in the circulating flow is evidently kept low by the purification flow Q_1 , which includes the baffle purge flow plus the portion of the fuel element purge that passes through the liquid-nitrogen trap.

Table 6.2. Total ^3He and tritium in the primary system at EOL due to ^3He content in the helium supply

Quantity	Symbol	Value (moles)
Total ^3He in primary system	N_3	1.11×10^{-2}
Total ^3He at EOL due to ^3He		
In circulating coolant	N_{T1}	1.25×10^{-7}
In sleeve graphite	$N_{T2}(t_f)$	1.88×10^{-4}
In removable radial reflector		
Core 2	$N_{T3}(t_f)$	4.63×10^{-4}
Core 1		1.14×10^{-4}
Cores 1 and 2		6.47×10^{-4}
In permanent radial reflector	$N_{T4}(t_f)$	5.31×10^{-4}
In axial reflector	$N_{T5}(t_f)$	1.07×10^{-4}
Deposited in chemical cleanup system	$N_{T6}(t_f)$	1.14×10^{-4}

The estimated inventory of tritium circulating in the primary coolant resulting from ${}^3\text{He}$, 9.19×10^{-8} mole (corresponding to $1.35 \times 10^{-5} \mu\text{Ci}/\text{cm}^3$), represents approximately 67% of the "typical" circulating concentration reported by ref. 8 and listed in Table 4.1.

Table 6.3 lists the average tritium levels in the core graphites due to ${}^3\text{He}$ in total curies and on a per-gram-of-graphite basis. A total tritium level in the graphite core components due to ${}^3\text{He}$ is estimated to be 42.9 Ci, 25.4 Ci of which resulted from births in the removable reflector during core 1. Average specific inventories due to production from ${}^3\text{He}$ are estimated to range from 0.4 to 1.5 $\mu\text{Ci}/\text{g}$.

Table 6.3. Total and average specific tritium inventories in graphite core components at EOL due to ${}^3\text{He}$

	Activity	
	Total (Ci)	Specific ($\mu\text{Ci}/\text{g}$)
Sleeve	5.4	0.63
Removable radial reflector, Core 2	13.5	1.5
Core 1	5.4	0.58
Total	<u>18.9</u>	<u>2.0</u>
Permanent radial reflector	15.5	1.1
Axial reflector	<u>3.1</u>	0.4
Total	42.9	

The amount of tritium formed from ${}^3\text{He}$ in the circulating coolant and removed to the chemical cleanup system during core 2 operation may be estimated by

$$N_{T6}(t_f) = Q_{Cs} \frac{N_{T1}}{V} \left[\frac{1 - \exp(-\lambda_T t_f)}{\lambda_T} \right], \quad (6.16)$$

where N_{T6} is the moles of tritium deposited by EOL corrected for decay and Q_{Cs} , the flow to the chemical cleanup system, equals two-thirds of Q_1 , the total effective tritium purification flow. Substituting values given in

Tables 6.1 and 6.2 into Eq. (6.16) yields a value of 4.47×10^{-4} mole of tritium (13.1 Ci) deposited in the chemical cleanup system due to formation from ^3He in the coolant. (In Sect. 6.3.2, the total quantity of tritium removed by the chemical purification system is estimated as 68 Ci.)

6.1.3 Production from lithium in graphite

The rate of production of tritium from the ^6Li contained in graphite is described by

$$\frac{dN_T}{dt} = \phi_{\text{th}}(t) \sigma_6 N_6(t) - \lambda_T N_T(t), \quad (6.17)$$

where

$N_T(t)$ = atoms of tritium at time t ,

$\phi_{\text{th}}(t)$ = thermal flux at time t ,

σ_6 = effective thermal cross section for $^6\text{Li}(n,\alpha)\text{T}$ (408 barns),

$N_6(t)$ = atoms of ^6Li at time t .

The depletion of ^6Li is given by

$$\frac{dN_6}{dt} = -\phi_{\text{th}}(t) \sigma_6 N_6(t). \quad (6.18)$$

If a constant average value for $\bar{\phi}_{\text{th}}(t)$ is assumed, Eqs. (6.17) and (6.18) may readily be solved to yield

$$N_T(t_f) = \left(\frac{\bar{\phi}_{\text{th}} \sigma_6 N_6(0)}{\lambda_T - \bar{\phi}_{\text{th}} \sigma_6} \right) \left[e^{-\bar{\phi}_{\text{th}} \sigma_6 t_f} - e^{-\lambda_T t_f} \right], \quad (6.19)$$

where t_f is again the duration of core 2 operation including shutdown periods ($t_f = 1.34 \times 10^8$ sec, or 1550 days) and $\bar{\phi}_{\text{th}}$ is the thermal flux averaged over this period of time. Neutronics calculations performed at GAC employed four neutron energy groups with thermal ranges extending from 0 to 2.38 eV. Compere et al.²⁴ determined that σ_6 averaged over this energy range takes a value of 408 barns.

As noted in Sect. 3.3, lithium levels in graphite are expected to be so low that determination of an appropriate average concentration for a large graphite mass would be difficult from both analytical chemistry and

sampling procedure considerations. The nine ^7Li concentration determinations reported in Sect. 3.3 for sleeve graphite material ranged from an upper limit of 3 ppb to 15 ppb. Averaging these nine values, including the three upper-limit values, yields a ^7Li concentration of 7.0 ppb, which we will assume to be representative of the sleeve graphite.

The three lithium concentrations given in Sect. 3.3 for spine graphite are all upper-limit values of 1.0 ppb, and we assume here that this value is the appropriate average for spine graphite for the sake of carrying through the estimate. We should recall that this is an upper-limit value and also that the ^7Li value of 7.0 ppb in the sleeve included some upper-limit values. Hence the estimates of tritium production from lithium in the graphite presented below are probably higher than actually occurred.

Equation (6.19) may be applied to the sleeve, spine, replaceable and permanent radial reflectors, axial reflector zones, and matrix graphite, where the appropriate values for $\bar{\phi}_{\text{th}}$ and $N_6(0)$ for each case are assumed in turn. These values are summarized in Table 6.4. The listed value of 10 ppb for matrix graphite is based on one determination using an archive fuel compact. The sample was acquired by drilling the compact; hence, fuel and pyrocarbon material was included in the sample, although the major portion was matrix graphite. The reported value of 10 ppb, determined by isotope dilution mass spectrometry, is 50 times lower than the "most-probable" value for matrix graphite given by Gainey.¹⁶ Since matrix graphite is fired at 1800°C compared with about 2800°C for other graphites, there is at least a tendency for high lithium levels in matrix material since lithium halides, present in all graphite starting materials, are less likely to be completely driven off. However, this appeared not to be the case for the Peach Bottom fuel matrix material, which exhibited initial lithium levels comparable to those of other graphite components.

Values for the average thermal flux are the same as assumed in the previous section for the estimation of $^3\text{He}(n,p)\text{T}$ reaction rates in each zone. The initial moles of ^6Li were computed from the estimated graphite masses in each zone given in Table 1.2 and the measured lithium concentrations.

Table 6.4. Quantities of lithium in graphite core components

Component	Lithium concentration (ppb)	Average thermal flux ^a	Initial amount of ⁶ Li (moles)
Sleeve	7 ^b	1	6.99 x 10 ⁻⁴
Spine	1 ^c	1	5.17 x 10 ⁻⁵
Replaceable radial reflector	7 ^d	1	7.56 x 10 ⁻⁴
Permanent radial reflector	7 ^e	0.5	1.12 x 10 ⁻³
Axial reflector	7 ^e	0.5	6.74 x 10 ⁻⁴
Matrix	10 ^f	1	7.76 x 10 ⁻⁴

^aRelative to 2.82×10^{13} neutrons/cm².sec.

^bAverage of nine determinations.

^cUpper-limit value.

^dAverage of seven determinations.

^eAssumed.

^fMeasured value on one archive compact; Gainey¹⁶ recommends a "most-probable" value of 500 ppb for matrix graphite.

Again note that the radial reflectors were not replaced at the end of core 1 operation. Hence, for these components, Eq. (6.19) was applied sequentially, first with core 1 parameters of flux and time as given in Table 6.1 and then with core 2 parameters.

Table 6.5 gives the results obtained using Eq. (6.19) with the initial lithium levels in Table 6.4. The tritium levels that result at EOL from ⁶Li contamination in the graphite correspond to about 80% of the initial quantity of ⁶Li. The specific concentrations are based on graphite masses presented in Table 1.2. The specific activities are space-average values, and local concentrations will vary approximately with the thermal flux distribution.

Table 6.5. Tritium levels at EOL due to lithium contamination in graphite

Graphite component	Activity	
	Total (Ci)	Specific ($\mu\text{Ci/g}$)
Sleeve	14.0	1.6
Spine	1.0	0.23
Replaceable radial reflector	16.4	1.8
Permanent radial reflector	18.8	1.4
Axial reflector	<u>9.2</u>	1.1
Total graphite	59.4	
Fuel matrix due to ^6Li	13.1	2.3
Fuel matrix due to ternary fission in tramp fuel	<u>2.2</u>	0.38
Total matrix	15.3	

As shown in Table 6.5, approximately 59.4 Ci of tritium appeared in the graphite components of the core (excluding the matrix) at EOL due to lithium contamination. Specific inventories averaged $\sim 1.5 \mu\text{Ci/g}$ in graphite components other than the spine.

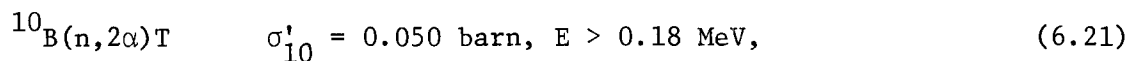
Tritium was produced in matrix graphite from both lithium contamination and from ternary fissions due to tramp fuel. Approximately 13.1 Ci was produced in matrix material due to lithium contamination, based on the measured initial level of 10 ppb lithium. Again we note that matrix graphite has at least the possibility of a significantly higher initial lithium level which, however, was not observed in Peach Bottom archive compact material.

Tritium produced in the matrix from ternary fission of tramp fuel may be estimated fairly accurately. Wichner and Botts,⁷ in the course of particle failure fraction studies, found that approximately 0.18% of

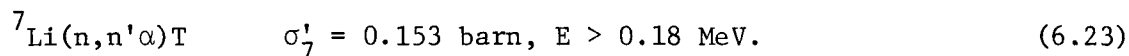
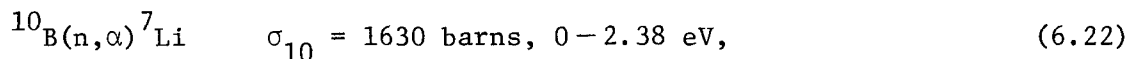
the uranium in the core existed as tramp fuel (i.e., as contamination in the matrix). Since an estimated 1211 Ci of tritium was produced by ternary fission in the fuel (Sect. 6.1.1), 0.18% of this amount (2.2 Ci) should have appeared in the matrix due to ternary fission of tramp fuel.

6.1.4 Production from ^{10}B in control rods and poisoned spines

As noted in Sect. 2.1, tritium is produced from ^{10}B either directly via



or via the chain



The Peach Bottom core contained 1.10 kg of natural boron as a burnable poison within the graphite spines of 60 of the 804 fuel elements. The boron, as ZrB_2 , was sintered with graphite and pressed into pellets 2.20 cm in diameter and 5.13 cm long. Each of the three spine pieces of the 60 poisoned spine elements was hollow and contained 14 ZrB_2 pellets. Reference 3, a postirradiation examination report on such a poisoned fuel element, gives precise dimensions of the poisoned spine.

Tritium produced from boron in the poisoned fuel elements was well shielded from the primary circuit coolant. The concentration profiles presented in Sect. 5.1 indicate that only a small portion of the total production penetrated the spine; furthermore, the portion that did penetrate was probably carried with the purge gas flow to the fission product trap or the external trapping system. In contrast, the boron in the control rods was cooled by direct contact with the primary coolant, and hence the tritium produced at least had a ready path for entering the primary circuit.

An estimate of the amount of tritium formed within the poisoned spines may be gained from approximate depletion equations based on the

above neutron reactions. However, the tritium formed in the control rods must be estimated differently because the control rod positions varied with time.

The depletion of ^{10}B in the poisoned fuel elements may be approximated by

$$\frac{dN_{10}}{dt} = -(\beta\bar{\phi}_{\text{th}}\sigma_{10} + \bar{\phi}_f\sigma'_{10}) N_{10}(t), \quad (6.24)$$

where

$$\begin{aligned} \beta &= \text{self-shielding factor;} \\ \bar{\phi}_{\text{th}} &= \text{average flux in 0- to 2.38-eV range;} \\ \bar{\phi}_f &= \text{average flux in excess of 0.18 MeV;} \\ \sigma_{10}, \sigma'_{10} &= \text{cross sections for reactions (6.21) and (6.22),} \\ &\quad \text{respectively;} \\ N_{10} &= \text{moles of } ^{10}\text{B}. \end{aligned}$$

The buildup of ^7Li and tritium is governed by

$$\frac{dN_7}{dt} = \beta\bar{\phi}_{\text{th}}\sigma_{10}N_{10}(t) - \bar{\phi}_f\sigma'_7N_7(t) \quad (6.25)$$

and

$$\frac{dN_T}{dt} = \bar{\phi}_f\sigma'_{10}N_{10}(t) + \bar{\phi}_f\sigma'_7N_7(t) - \lambda_T N_T(t), \quad (6.26)$$

where σ'_7 is the cross section for reaction (6.23) and N_7 and N_T are moles of ^7Li and tritium, respectively.

Equations (6.24) to (6.26) may be solved to yield

$$\begin{aligned} \frac{N_T(t)_f}{N_{10}(0)} &= \frac{ba}{(b-a)(\lambda_T - a)} \left(e^{-at_f} - e^{-\lambda_T t_f} \right) - \frac{ba}{(b-a)(\lambda_T - b)} \left(e^{-bt_f} - e^{-\lambda_T t_f} \right) \\ &\quad + \frac{c}{(\lambda_T - a)} \left(e^{-at_f} - e^{-\lambda_T t_f} \right), \end{aligned} \quad (6.27)$$

where $a = \beta\bar{\phi}_{\text{th}}\sigma_{10}$, $b = \bar{\phi}_f\sigma'_7$, and $c = \bar{\phi}_f\sigma$.

The above solution presumes that the depletion of ^{10}B by thermal neutrons greatly exceeds that by fast neutrons (i.e., $a \gg c$). This reasonable assumption is readily verified. The sum of the first two terms in Eq. (6.27) represents the tritium yield from ^7Li , and the third represents direct production from $^{10}\text{B}(n,2\alpha)\text{T}$.

We will assume a value of 0.0141 for the self-shielding factor β , as determined in ref. 43 for a control rod in a large HTGR core. Application of this value as the depletion factor for the boronated spine in Peach Bottom fuel elements represents quite a crude approximation. Properly, β and the flux depression due to the boron spine can be accurately determined only by multigroup neutronics computer codes.

The values used to estimate the tritium production from ^{10}B in the fuel element spines by Eq. (6.27) are listed in Table 6.6. (The average thermal flux was determined in Sect. 6.1.3.) The same sources and method were used to determine $\bar{\phi}_f$, the average flux above 0.18 MeV. Cross sections for reactions (6.21), (6.22), and (6.23) are given in Table 2.2. The value of $N_{10}(0)$, the initial amount of ^{10}B in moles, was determined using the stated mass of 1.1 kg natural boron with a 19.8% abundance for ^{10}B .

The numerical results in Table 6.6 indicate that about 85.7 Ci of tritium was produced by the ^{10}B within the poisoned fuel element spines. The major share (88%) was due to the direct fast reaction $^{10}\text{B}(n,2\alpha)\text{T}$ and the balance to $^{10}\text{B}(n,\alpha)^7\text{Li}(n,n'\alpha)\text{T}$. Evidence presented in Sect. 5.1 indicates that virtually all the tritium from this source remained within the poisoned spines isolated from the primary circuit.

Tritium formed from the boron in the control rods cannot be estimated in the above fashion because the quantity in the active core varies with time. In addition, the mass of boron in the control rods is not specified in the FHSR and can be surmised only from the amount of excess reactivity they control. Therefore, the following procedure was used for estimating the amount of tritium produced in the control rods based on reported values of the excess reactivity of the core and average thermal power.

Table II-10 of the FHSR¹⁸ lists an initial value of 1.06 for k_{eff} of the hot unrodded core 1 with equilibrium level of poison and an EOL

Table 6.6. Estimation of tritium produced from ^{10}B in poisoned spines using Eq. (6.27)

Self-shielding factor, β	0.0141
Average thermal flux, $\bar{\phi}_{\text{th}}$	2.82×10^{13}
Average fast flux, $\bar{\phi}_{\text{f}}$	2.26×10^{13}
Cross sections, barns	
σ_{10}	1630
σ'_{10}	0.050
σ'_7	0.153
Total reactor life, t_{f} , sec	1.339×10^8
Tritium decay constant, λ_{T} , sec^{-1}	1.793×10^{-9}
Constants defined for Eq. (6.27), sec^{-1}	
$a = \beta \bar{\phi}_{\text{th}} \sigma_{10}$	6.48×10^{-10}
$b = \bar{\phi} \sigma'_7$	3.46×10^{-12}
$c = \bar{\phi}_{\text{f}} \sigma'_{10}$	1.13×10^{-12}
Initial ^{10}B , $N_{10}(0)$, moles	20.15
Amount of ^3H at EOL due to ^{10}B , moles	
Directly from $^{10}\text{B}(n, 2\alpha)\text{T}$	2.58×10^{-3}
Indirectly through ^7Li	3.6×10^{-4}
Total tritium, moles	2.94×10^{-3}
Tritium activity at EOL, Ci	85.7

value for core 1 under the same conditions of 1.01; hence, the average hot, unrodded k_{eff} for core 1 was approximately 1.035. The equivalent values for core 2 are not explicitly given in the revised version of the FHSR,¹⁹ but data in ref. 19 clearly indicate that k_{eff} values were lower. For example, the unrodded, clean, k_{eff} for core 2 at 1200 K is given as 1.106, compared with 1.119 for core 1 under the same conditions. In addition, it is known that core 2 at EOL had essentially no excess reactivity at the operating temperature but was kept operating by reducing the average temperature below the design value to effect an increase in k_{eff} . Thus k_{eff} at core 2 EOL was essentially 1.00. Therefore, we estimate the hot, unrodded k_{eff} for core 2 with equilibrium poison inventory to be the average of 1.05 (~ 0.01 lower than the initial core 1 value) and 1.00 (i.e., 1.025). Thus at average insertion, neutron absorptions in the control rods diminished the thermal utilization factor by 2.5%; that is,

$$\text{Absorptions in the control rods} = 0.025 \times \text{absorptions in the unrodded core} \quad (6.28)$$

The absorption rate (sec^{-1}) in the unrodded core may be obtained from the average value of the thermal utilization factor f and the average power level \bar{P} [MW(t)] as follows:

$$\begin{aligned} \text{Absorption rate in unrodded core} &= \frac{\text{absorptions in fuel}}{f} \\ &= \frac{\text{fission rate}}{f} \left(\frac{\sigma_a}{\sigma_f} \right)_{\text{fuel}} = 3.1 \times 10^{16} \frac{\bar{P}}{f} \left(\frac{\sigma_a}{\sigma_f} \right)_{\text{fuel}} \end{aligned} \quad (6.29)$$

Substituting the appropriate Peach Bottom values into Eqs. (6.28) and (6.29) (see Table 6.7) yields a neutron absorption rate for the control rods of 1.31×10^{-7} (mole/sec) averaged over the total 1550 days of core 2 operation. The value employed for f is the average of the beginning and EOL values given in Table II-10 and II-14, respectively, of the FHSR.¹⁸

The neutron absorption rate in ^{10}B estimated above is predominately due to the principal absorber reaction $^{10}\text{B}(n,\alpha)^7\text{Li}$. The rate of the fast-neutron reaction forming tritium directly from $^{10}\text{B}(n,2\alpha)\text{T}$ may be estimated by the ratio

Table 6.7. Determination of tritium formed due to ^{10}B in the control rods

Average power over 1550 days, \bar{P} , MW(t)	66.6
Average thermal utilization factor, f	0.774
Average hot unrodded excess reactivity, $1 - k_{\text{eff}}$	0.025
Fuel (^{235}U) cross sections, barns	
σ_a	683
σ_f	577
Unrodded-core neutron absorption rate, moles/sec	5.34×10^{-6}
Average absorption rate in control rods, moles/sec	1.31×10^{-7}
Tritium produced at EOL, moles (Ci)	0.027 (790)

$$\text{Rate of tritium production} = \frac{\sigma'_{10}\bar{\phi}_f}{\beta\sigma_{10}\bar{\phi}_{\text{th}}} \times 1.31 \times 10^{-7} . \quad (6.30)$$

Therefore, the balance equation for tritium formation in the control rods may be written as

$$\frac{dN_T}{dt} = \left[\left(\frac{\sigma_{10}\bar{\phi}_f}{\beta\sigma_{10}\bar{\phi}_{\text{th}}} \right) 1.31 \times 10^{-7} + \sigma'_{7}\bar{\phi}_f N_7(t) \right] - \lambda_T N_T(t) . \quad (6.31)$$

Solution of this equation may be simplified by noting that production from ^7Li , from the second term in brackets, is small compared with the direct production from $^{10}\text{B}(n,2\alpha)\text{T}$. Therefore, a sufficiently accurate solution of Eq. (6.31) may be written as

$$N_T(t_f) = \frac{\sigma'_{10}\bar{\phi}_f}{\beta\sigma_{10}\bar{\phi}_{\text{th}}} \times 1.31 \times 10^{-7} \left[\frac{1 - \exp(-\lambda_T t_f)}{\lambda_T} \right] . \quad (6.32)$$

As noted in Table 6.7, substitution of appropriate values into Eq. (6.32) yields a value of 0.027 mole of tritium (790 Ci) at EOL due to absorptions in the control rod.

6.1.5 Summary of tritium sources

The tritium source information developed in Sects. 6.1.1 through 6.1.4 and presented in Tables 6.1 through 6.7 is summarized in Table 7.1 and in the associated discussion in Sects. 7.1 and 7.2.

6.2 Estimated Tritium Inventories in Core 2 Components Based on Measured Concentrations

6.2.1 Fuel inventory

The tritium inventory in the fuel compacts of the Peach Bottom HTGR core was estimated from the measured concentrations given in Sect. 5.3 and listed in Table 5.52. It should be emphasized that tritium was determined in only three fuel bodies from each of two elements. Because of this paucity of data and the complexity of the formation and release, the inventory of tritium in the fuel can be estimated in only a very crude manner.

The axial distributions of tritium found in the fuel of elements E14-01 and F03-01 in Table 5.52 are plotted in Fig. 6.1 along with the estimated thermal-neutron fluence experienced by element F03-01. The neutron fluences³⁸ are somewhat different in magnitude for the two elements, but the shapes of the distributions are similar. Since the tritium activity formed in the fuel bodies is proportional to the neutron flux, the observed activity decrease in the fuel of F03-01 as the fluence increases toward the element midplane indicates that much of the tritium produced in F03-01 was released from the fuel. This is in accord with the observations relative to Table 5.52 in which the measured tritium concentrations are compared with levels predicted from the fission source. We note there that the measured levels were significantly lower than predicted at the hot locations for both elements. On the other hand, the reverse is true for compact location 2 (near the coolant inlet or purge gas outlet), indicative of tritium depositing at this location.

Tritium behavior in the fuel may be better understood by examining the curves shown in Fig. 6.2, which shows the activity ratio ${}^3\text{H}/{}^{95}\text{Zr}$ and the estimated maximum temperatures experienced by the fuel of the two

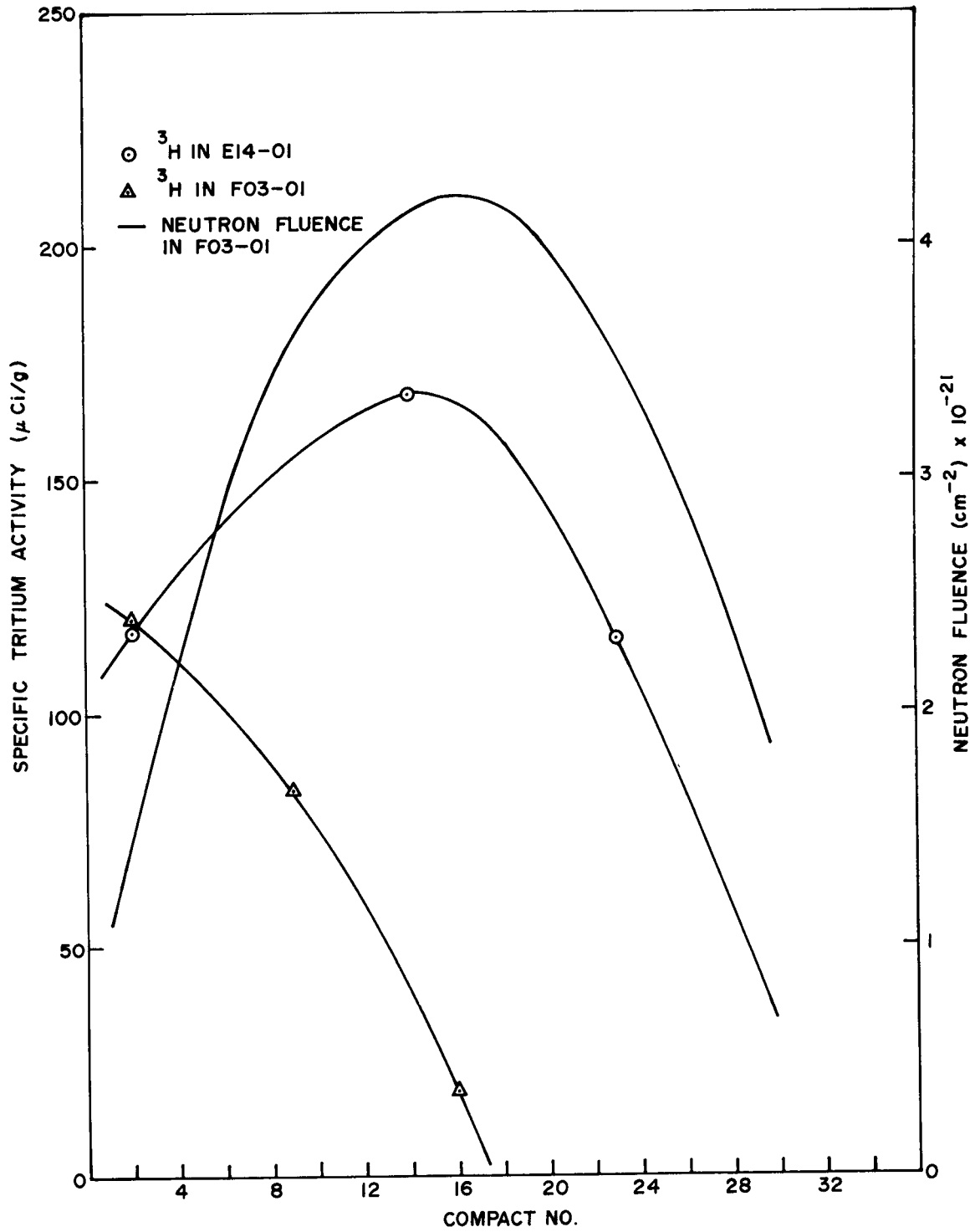


Fig. 6.1. Axial distributions of tritium in fuel elements E14-01 and F03-01.

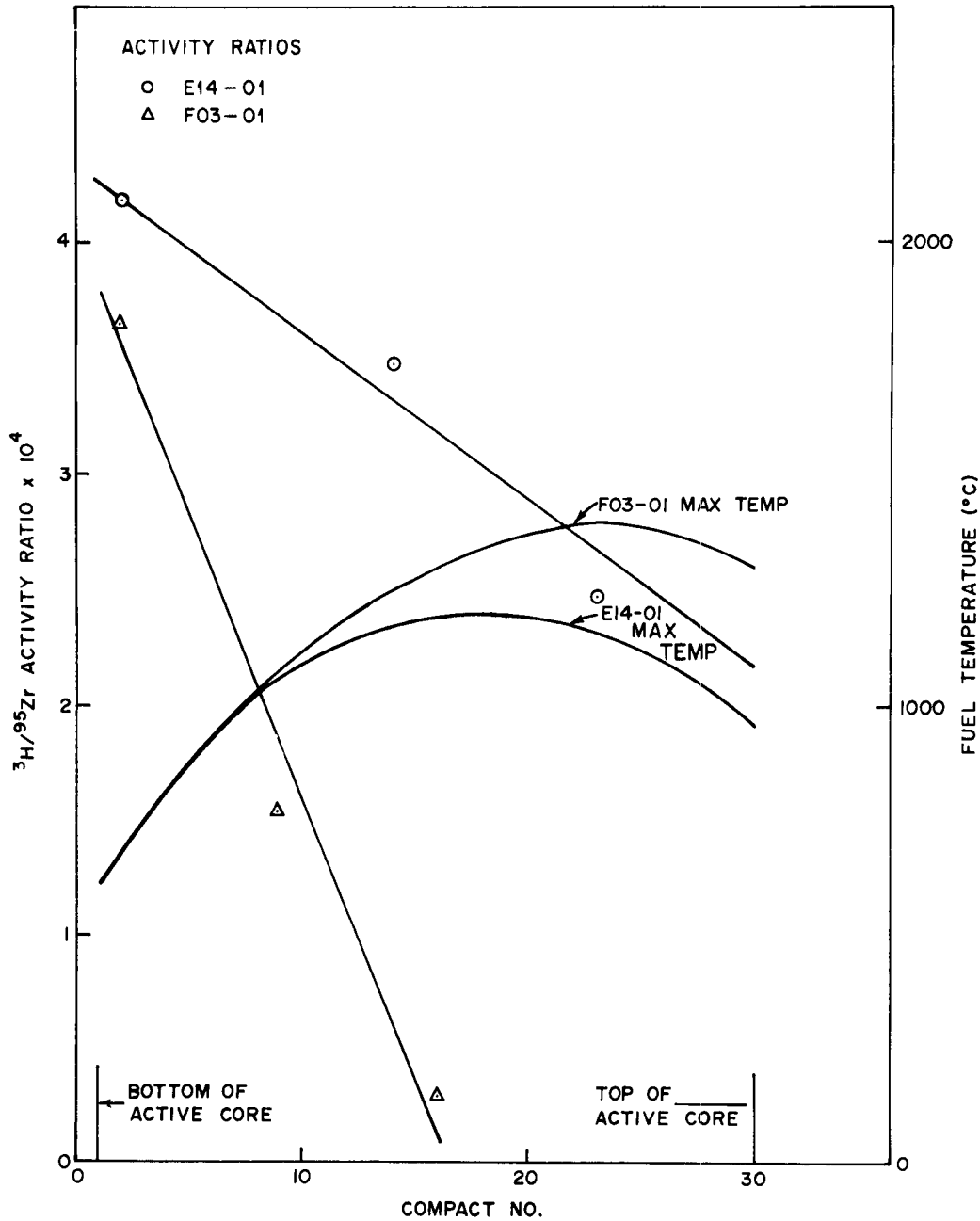


Fig. 6.2. Axial distributions of the activity ratio ${}^3\text{H}/{}^{95}\text{Zr}$ and operating temperatures of the fuel compacts in elements E14-01 and F03-01.

elements. The measured ^{95}Zr activities were taken from refs. 3 and 4, and the temperatures were obtained from ref. 38. Because zirconium is not released from the fuel at these operating temperatures, the axial distribution of the ^{95}Zr activity closely follows the neutron fluence.^{3,4} If tritium in the fuel were produced only by fission and none were released, the $^3\text{H}/^{95}\text{Zr}$ activity ratio would depend principally on the relative fission yields of ^3H and ^{95}Zr and the distribution of the ratio would be nearly uniform. If a portion of the ^3H in the fuel were produced from ^6Li impurity in the matrix and it too were not released, the distribution of the ratio would tend to be similar to the neutron fluence and be peaked in the center of the element to an extent that depends on the ^6Li concentration. Since the observed activity ratio decreased with increasing neutron fluence, it seems evident that tritium was released from the fuel by both elements, but to a much larger extent from F03-01.

The apparent large differences in the tritium lost from the fuel of the two elements is not consistent with the estimated average operating temperatures reported in ref. 37. For example, the estimated time-averaged operating temperature of element F03-01 is given to be lower than that of E14-01 from the bottom of the fuel element (compact 1) up to about compact 21. Nevertheless, the high tritium loss fraction experienced in the central portion of F03-01 is evidence that F03-01 temperatures significantly exceeded those for E14-01. Cesium and other fission product distributions observed in refs. 3 and 4 substantiate this observation.

The total inventories of tritium in the fuel of elements E14-01 and F03-01 in Table 6.8 were obtained by graphically integrating the axial distributions in Fig. 6.1. An average specific activity of 130 $\mu\text{Ci/g}$ was obtained graphically for element E14-01, which indicates a total tritium inventory of 1.2 Ci. Assuming this level to be typical for the 60 similar elements with poisoned spines leads to a total tritium inventory of 78 Ci for these elements.

The total tritium inventory of element F03-01 was obtained by assuming that the specific inventory in fuel compacts above No. 16 was equal to the level determined for compact 16. This leads to an estimated inventory of 0.52 Ci for element F03-01. Again, assuming that the remaining

Table 6.8. Tritium in the fuel of elements
E14-01 and F03-01^a

Source	Activity (Ci)
Element E14-01	1.31
Element F03-01	0.52
60 elements like E14-01	78
744 elements like F03-01	387
Total (est.)	465

^aBased on data in Fig. 6.1 and estimated inventories in the fuel of the whole core.

744 fuel elements have equal tritium contents leads to a total inventory of 387 Ci for these remaining elements. Thus, the total tritium inventory in fuel of 465 Ci is roughly estimated.

It is interesting to compare these measured estimates with the predicted fission source levels given in Sect. 6.1.1 and summarized in Table 6.8. The ternary fission source predicts 1210 Ci of tritium in the fuel, compared with the ~465 Ci based on measurements in elements E14-01 and F03-01. This indicates that about 62% of the tritium born in the fuel (and not decayed by EOL) left the fuel during reactor operation.

On the other hand, the tritium level observed in element E14-01 is approximately the anticipated level based on the estimated tritium source in the fuel. That is, dividing the total estimated fuel source of 1210 Ci by the number of fuel elements (804) yields a predicted tritium inventory of 1.5 Ci for elements that retained tritium. This is only about 13% higher than the estimated inventory in element E14-01 based on the measured concentrations in the fuel.

6.2.2 Sleeve and spine inventories

The tritium inventories in the sleeves and spines of the Peach Bottom HTGR fuel elements were derived by graphically integrating the axial

distribution data given in Table 5.42. The concentrations of tritium in the sleeve and spine end sections (i.e., from the ends to the locations nearest the ends at which measurements were made) were considered to be uniform and equal to the values observed nearest the ends. The weights of graphite per unit length of sleeve (44.5 g/cm) and spine (25.2 g/cm) listed in ref. 1 were used to convert concentrations to inventories.

The tritium levels in the sleeve and spine based on measured concentrations (Table 6.9) significantly exceed predicted levels due to formation from ${}^6\text{Li}$ and ${}^3\text{He}$ (Tables 6.3 and 6.5). Table 6.9 gives 258 Ci for the sleeves of all fuel elements based on the measured concentrations, compared with 19 Ci predicted in Sects. 6.1.2 and 6.1.3. Thus, approximately 239 Ci of tritium migrated into the sleeve. The table gives 18.5 Ci for the spine based on measured concentrations, compared with a predicted level of 1.0 Ci due to formation from ${}^6\text{Li}$. (The spine was assumed to have been shielded from ${}^3\text{He}$.)

Table 6.9. Tritium inventories in the sleeves and spines of the Peach Bottom HTGR fuel elements

Element	${}^3\text{H}$ inventory (Ci)	
	Sleeve	Spine
E11-07	0.200 ^a	0.018
E14-01	0.346	0.034
F03-01	0.363	0.022
E01-01	0.400	0.014
F05-05	0.295	0.027
Mean	0.321 ± 0.035^b	0.023 ± 0.003^b
Total for core ^c	258 ± 28^b	18.5 ± 2.4^b

^aElement E11-07 was taken out of service on Sept. 14, 1973, and the inventory is computed for that date. Results for other elements pertain to Oct. 31, 1974.

^bUncertainty values are standard deviations on the means.

^cMean values for single elements multiplied by 804.

6.2.3 Removable radial reflector inventory

Tritium measurements on element A18-08 (one of 341 hexagonal removable reflector elements) indicated that the overall distribution of tritium throughout the element was relatively uniform although large local variations existed. The mean concentration of tritium determined from 41 analyses was $15 \mu\text{Ci/g}$ with a sample standard deviation of $9 \mu\text{Ci/g}$. The standard deviation on the mean was thus $9/\sqrt{41}$ ($1.4 \mu\text{Ci/g}$), while the 95% confidence interval for the mean was estimated as $15 \pm 2.8 \mu\text{Ci/g}$. The lower bound of the 95% confidence interval ($12.2 \mu\text{Ci/g}$) is several times larger than the specific activity of $2.3 \mu\text{Ci/g}$ predicted in Sect. 6.1.3 for the tritium produced from ${}^6\text{Li}$ impurity in the reflector graphite.

From the above data and the mass per reflector element, we compute the tritium inventory for the reflector element as $0.61 \pm 0.11 \text{ Ci}$ (Table 6.10). The uncertainty value in the table corresponds to the 95% confidence limits computed for the specific activity of element A18-08. The total inventory of tritium in the removable radial reflector (208 Ci) is estimated by scaling the 0.61-Ci inventory to 341 removable reflector elements. This substantially exceeds (by about 173 Ci) the tritium source in the reflector due to births from ${}^3\text{He}$ and ${}^6\text{Li}$ listed in Tables 6.3 and 6.5. Therefore, the reflector graphite was a repository for tritium born elsewhere in the core.

Table 6.10. Tritium inventory in removable radial reflector elements

Specific activity in A18-08, $\mu\text{Ci/g}$	15 ± 2.8
Total activity in A18-08, Ci	0.61 ± 0.11
Activity scaled to 341 elements, Ci	208 ± 39

6.2.4 Inventories in the upper and lower axial reflector regions of the driver fuel elements

Estimates of tritium inventories for those parts of the fuel elements that lie above and below the fueled region are given in Table 6.11. These

Table 6.11. Tritium inventory of parts of the fuel element that lie above and below fuel region

	Specific activity ($\mu\text{Ci/g}$)	Mass of part per element (g)	Inventory (Ci)	
			Per element	Total of core
Top reflector, bulk graphite	0.3	5200	1.5E-3	1.2
Porous plug	74 ^a	175	1.29E-2	10.4
Region enclosed by sleeve below fuel				
Bottom reflector	20.0 ^b	523	0.01	8.4
Fission product trap	325.0 ^c	100	0.0325 \pm 0.0035	26.1 \pm 2.8
Sleeve	0.3 ^d	2800	8E-4	0.7
Bottom connector	0.3 ^e	2200	6.5E-4	0.5
Total			5.8E-2	46.0

^a Average value computed from data in Table 5.46 and plug dimensions.

^b Result from sleeve portion of Table 5.37.

^c Average value computed from data of Tables 5.47 through 5.50.

^d Value assumed to be the same as observed in bottom connector.

^e Average value calculated from data of Table 5.45.

include the top reflector assembly, the bottom connector, the bottom reflector, the fission product trap, and the part of the sleeve that lies below the fueled region joining to the bottom connector. The top reflector assembly was subdivided into a bulk graphite portion and the porous plug through which the purge gas entered the element. Since specific activity of tritium in the top reflector bulk graphite was measured only in element E06-01 (irradiated 384 EFPDs), tritium activity in the upper reflector was taken to be the same as that measured in the bottom connector of element F03-01 as given in Table 5.45. All the estimated inventories listed in Table 6.11 were derived from data given in Sect. 5; the exact sources of the data are indicated in the table footnotes.

6.2.5 Summary of inventories derived from observed specific activities

The tritium inventories in the Peach Bottom HTGR fuel elements and radial reflector elements that were derived in Sects. 6.2.1 through 6.2.4 are summarized in Table 6.12 along with values normalized to the total core. For a comparison of these inventories with estimated sources and leakage flows, see Tables 7.1 through 7.3 and the associated discussion in Sect. 7.1.

Table 6.12. Summary of tritium inventories in the Peach Bottom HTGR core derived from observed activities

Component	Activity (Ci)	
	Average per element	Total in core
Fuel element		
Top reflector region ^a	0.0144	11.6
Sleeve	0.321 ± 0.035	258 ± 28
Spine	0.023 ± 0.035	18.5 ± 2.4
Fuel	0.578	465
Bottom reflector region ^b	0.0444	35.7
	Subtotal	789
Removable radial reflector	0.61	208
	Total	997

^aIncludes top reflector assembly and porous plug.

^bIncludes bottom reflector, fission trap, and sleeve.

6.3 Estimated Tritium Losses from the Primary System

6.3.1 Transport to the fission product trapping system

The ex-core fission product trapping system received about 454 kg/hr of the helium that swept the interior of each fuel element (0.56 kg/hr per element). As noted in Sect. 2.2, the fuel element purge flow passed through a charcoal filter located at the cool end of each fuel element prior to leaving the core and passing on to the fission product trapping system.

The special tritium survey conducted at the Peach Bottom reactor⁸ in 1971 reported that a "typical" tritium concentration in the purge gas downstream from the charcoal traps contained in the fuel elements was $5 \times 10^{-5} \mu\text{Ci}/\text{cm}^3$ (see Table 4.1). If one assumes this concentration to be effective for the entire 1018 operating days of core 2 and the purge flow conditions of temperature and pressure to be approximately those of the adjacent primary coolant, about 310 Ci of tritium (as HT principally) left the core for the fission product trapping system. We should note that this amounts to about 25% of the estimated source due to fissions in the fuel (see Table 7.1). In addition, details regarding the nature and times of this experimental determination are lacking in ref. 8; we have not determined precisely what is meant by "typical" in the description of the measured concentration. As shown in Fig. 4.1, the tritium concentration of the primary coolant fluctuated by about a factor of 100 during 1971 due to frequent shutdowns and startups; thus the measured concentration of $5 \times 10^{-5} \mu\text{Ci}/\text{cm}^3$ may not be typical for the life of core 2. However, in the HT levels in helium for 1974 (Fig. 4.3), there appeared to be no general increasing trend in tritium level in the primary coolant with time such as was observed for cesium; that is, there appeared to be no "breakthrough" phenomenon for tritium.

An alternative estimate of the quantity of tritium that passed into the ex-core trapping system may be gained from the axial profiles of tritium in the fuel element charcoal traps, provided the equilibrium adsorption characteristics of the charcoal are known. Unfortunately, as shown in Table 3.1, we have located data for adsorption on charcoal only

for the temperature range -183 to 0°C . These data are plotted in Fig. 6.3 as circular points in terms of curies adsorbed per gram of charcoal per unit concentration ($\mu\text{mole}/\text{cm}^3$) in the gas phase. It is assumed that tritium adsorbs as HT in carrying out the unit conversion that was originally given in terms of volume of H_2 adsorbed per unit H_2 pressure. The triangular point in Fig. 6.3, taken from Fischer's data³⁵ summarized in Table 3.1, represents the equilibrium loading on slightly oxidized matrix graphite at 900°C . Partly oxidized matrix graphite perhaps resembles charcoal in HT sorption characteristics; if not, it is the closest we have come to HT sorption data on charcoal above 0°C .

The dashed connection in Fig. 6.3 represents possible adsorption behavior between the available data at 0 and 900°C , and the vertical arrows indicate inlet and outlet temperatures of the fuel element charcoal traps. At the trap exit, Fig. 6.3 shows an equilibrium charcoal loading of 0.15 Ci/g per $\mu\text{mole}/\text{cm}^3$ of HT in the gas phase.

The actual gas-phase concentrations in the charcoal traps may be estimated by analyzing the axial tritium profiles shown in Fig. 5.6. The simplest procedure, and probably all that is warranted in the absence of adequate sorption data, is to assume that the gas leaving the bed is in equilibrium with respect to HT sorption. Therefore, since an average tritium loading of 325 $\mu\text{Ci}/\text{g}$ near the bed exit is displayed in Fig. 5.6 for the three EOL elements (E01-01, F05-05, and F03-01), the resulting gas-phase concentration at the trap exit of 325×10^{-6} (Ci/g)/ 0.15 (Ci/g per $\mu\text{mole}/\text{cm}^3$) = 2.2×10^{-3} $\mu\text{mole}/\text{cm}^3$ is indicated. Conversion to curies per unit volume yields 6.3×10^{-5} $\mu\text{Ci}/\text{cm}^3$, which compares very well with the 5×10^{-5} $\mu\text{Ci}/\text{cm}^3$ value reported as typical in the special tritium survey.⁸

We therefore conclude that the data from the tritium site survey⁸ and the concentration of tritium in the charcoal traps in the vicinity of the exit both indicate that about 310 Ci of tritium as HT passed into the ex-core fission product trapping system during the life of core 2.

As noted earlier, the ultimate fate of this tritium is not known with certainty because the sorption characteristics of the Freon- and

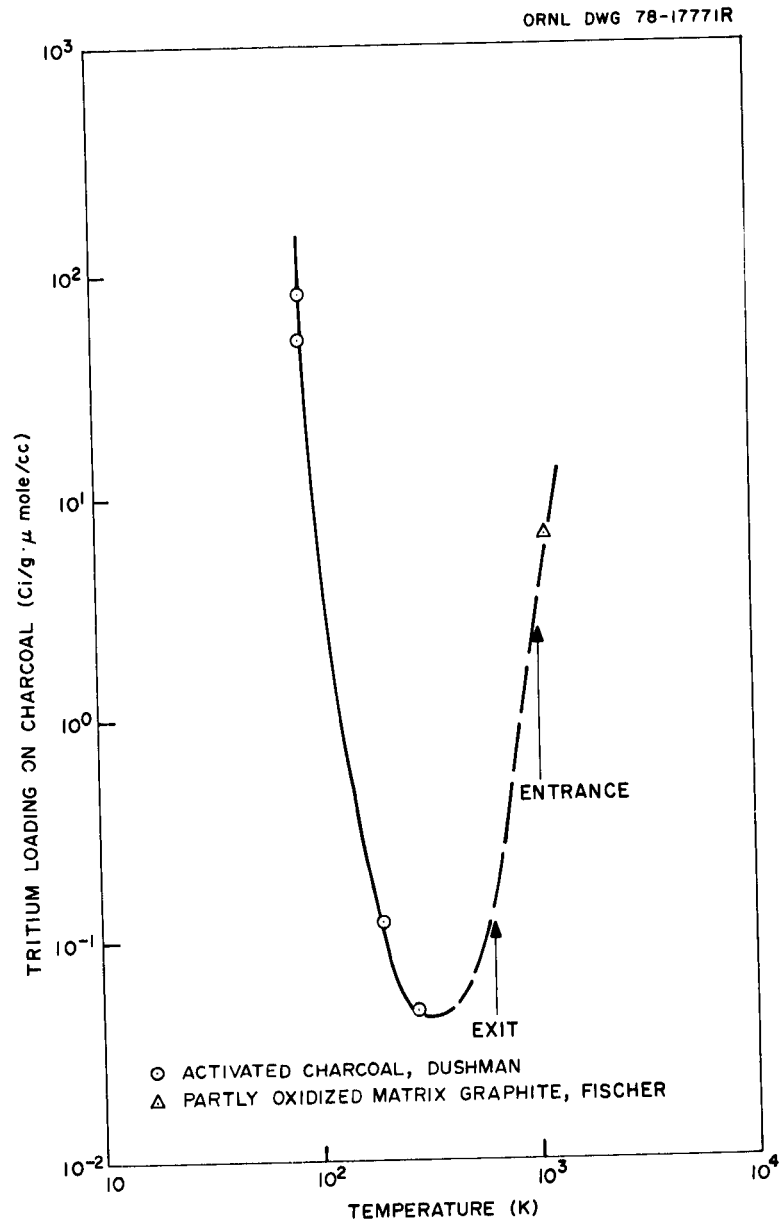


Fig. 6.3. Equilibrium loading of HT on charcoal per unit concentration in gas. (The arrows mark the average temperatures of the entrance and exit of the fuel element fission product trap.)

water-cooled delay beds in the trapping system are not known. We have assumed in this study that these beds do not permanently retain tritium but that the 10% of the purge gas flow that passes through the liquid-nitrogen-cooled delay bed does represent a permanent tritium sink. Therefore, 10% of 310 Ci (or 31 Ci) of tritium was retained in the liquid-nitrogen-cooled traps for ultimate discharge with the gaseous waste flow via the stack following bed regeneration. The remaining tritium activity, about 279 Ci, passed through the trapping system to join the helium coolant.

6.3.2 Transport to the chemical cleanup system (and disposal as solid waste)

As noted in Sect. 2.2, about 91 kg/hr (200 lb_m/hr) of helium was drawn from the primary coolant passing through the steam generator and sent to the chemical cleanup system. Since the oxidizer unit in the system converted HT to HTO, which was separated in a molecular-sieve dehydrator and drawn off to the waste disposal drain tank (WDDT), the chemical cleanup plant flow represented a true sink for tritium in the reactor.

The WDDT (Sect. 2.3) was installed after the reactor was in operation to collect liquid wastes from the chemical cleanup plant. The liquids collected included the condensate from the oxidizer and dehydrator units and solutions from the caustic scrubber that were used to regenerate the oxidizer. The chemical cleanup plant served mainly to remove hydrogen (H₂ and HT) from the helium, and levels of tritium in the WDDT liquids often reached several hundred microcuries per cubic centimeter, as evidenced from the activity measured in 1974 and reported in Table 4.1. The liquids collected by the WDDT were not transferred to the liquid waste monitor tanks but instead were solidified by adsorption on a claylike material and shipped offsite for disposal. This procedure was adopted⁴⁴ because the liquids collected in the WDDT were highly alkaline from the solutions resulting from the caustic scrubber and therefore posed a corrosion problem to the liquid waste disposal system. No account of the total tritium activity collected by the WDDT has been found. However, the total tritium discharged from the WDDT can be estimated from the

estimated flow to the chemical cleanup system from the steam generator and the average tritium concentration in the primary coolant reported in ref. 8.

The problem of selecting an appropriate average tritium concentration in the primary coolant is discussed in Sect. 6.3.3, which is devoted to estimation of the permeation rate through the steam-generator tubing. In view of the data scatter at most times, an average concentration is selected from a period of steady readings which existed in the first half of 1974, when a steady level of about $4.3 \times 10^{-5} \mu\text{Ci}/\text{cm}^3$ was observed in the primary coolant. Assuming that this concentration ($4.3 \times 10^{-5} \mu\text{Ci}/\text{cm}^3$) existed in the flow to the chemical cleanup system for 1018 operating days yields a loss of 68 Ci of tritium from the primary system by this means.

6.3.3 Leakage through the steam-generator tubing

According to Strehlow and Savage,²⁹ the permeation rate of tritium through a metallic barrier may be expressed as

$$J = K' \left(P_1^{1/2} - P_2^{1/2} \right), \quad (6.33)$$

where K' is the permeation coefficient, which depends on temperature, type of material, and its surface condition, while P_1 and P_2 are the tritium partial pressures on either side of the barrier. In the present case, the low tritium partial pressure side is the steam side of the steam-generator tube where the preponderance of $\text{H}_2\text{O}(\text{g})$ drives the exchange reaction $\text{H}_2\text{O} + \text{HT} \rightleftharpoons \text{HTO} + \text{H}_2$ to the right. Thus overwhelmingly, tritium activity on the steam side exists as HTO, which has an extremely low solubility in steel compared with HT, and the downsteam partial pressure P_2 in Eq. (6.33) is effectively zero for the present case.

In order to more conveniently make use of tritium concentrations that are usually reported in microcuries per cubic centimeter, we will approximate Eq. (6.33) with

$$J = K[\text{T}]_{\text{He}}^{1/2}, \quad (6.34)$$

where the mass flux J is expressed in units of microcuries per cm^2 per hour and $[\text{T}]_{\text{He}}$, the tritium concentration on the helium side, is

given in microcuries per cubic centimeter. Use of $[T]_{\text{He}}$ as the driving force for tritium permeation instead of the theoretically correct tritium partial pressure is a convenient approximation that is adopted with some caution, as explained below.

First, the temperature dependency is incorrect; that is, for a given value of $[T]_{\text{He}}$, the tritium partial pressure, which is the true driving force, varies directly with the temperature. Hence, Eq. (6.34) is strictly valid over a limited temperature range. However, the far greater temperature dependency of an empirically determined permeation coefficient tends to dwarf the incorrect temperature dependency implicit in using $[T]_{\text{He}}$.

Second, one must be assured of the dominant molecular form of the tritium activity. In the present case, the Peach Bottom coolant was strongly reducing, with the exchange reaction $1/2\text{H}_2 + 1/2\text{T}_2 \rightleftharpoons \text{HT}$ driven to the right; the tritium activity existed overwhelmingly as HT. The permeation experiments of Yang et al.³⁰ on the Peach Bottom steam-generator tubing were performed in a similar reducing atmosphere of helium. Since the predominant form of tritium was also HT in these experiments, their measured permeation rates may be applied directly to Peach Bottom reactor conditions.

Values for the permeation coefficient K may be calculated from measurements reported by Yang et al.³⁰ on samples of economizer, evaporator, and superheater tubing taken from the Peach Bottom reactor at EOL. They report the following measured permeation rates on as-received samples of tubing for the economizer, evaporator, and superheater, respectively:

$$J_{\text{econ}} = 7.78 \times 10^{-3} \exp(-4500/T), \quad (6.35)$$

$$J_{\text{evap}} = 0.697 \exp(-6830/T), \quad (6.36)$$

$$J_{\text{spr}} = 0.172 \exp(-6440/T), \quad (6.37)$$

where the fluxes are in microcuries per square centimeter per hour. The measurements were performed by applying a tritium concentration of $6 \times 10^{-4} \text{ Ci/cm}^3$ to the helium side of tubing while sweeping the downstream side rapidly enough to make the backpressure P_2 effectively zero. Applying these conditions to Eq. (6.34) yields the following permeation

coefficients in units of $(\mu\text{Ci}/\text{cm})^{1/2}/\text{hr}$:

$$K_{\text{econ}} = 0.318 \exp(-4500/T), \quad (6.38)$$

$$K_{\text{evap}} = 28.5 \exp(-6830/T), \quad (6.39)$$

$$K_{\text{spr}} = 7.02 \exp(-6440/T). \quad (6.40)$$

The tritium concentration on the helium side of the Peach Bottom steam-generator tubing was measured frequently during the course of operation. Unfortunately, as shown in Figs. 4.1 to 4.3, the measurements were evidently affected by numerous operating variables and hence were often erratic. In addition, measurements for all of 1972 are not reported due to instrumentation malfunction. Under these circumstances, it seems best to employ the average tritium concentrations reported over the five-month period of steady operation from Jan. 5, 1974, to May 30, 1974, to compute a typical permeation rate. During this period (Fig. 4.3), the tritium concentration in the primary coolant varied smoothly with time between approximately 7×10^{-5} and $3 \times 10^{-5} \mu\text{Ci}/\text{cm}^3$ for an estimated time-averaged level of $4.3 \times 10^{-5} \mu\text{Ci}/\text{cm}^3$.

The total permeation rate for each section of steam-generator tubing may be estimated by integrating Eq. (6.34) over the length of the section. For example, for the economizer,

$$R_{\text{econ}} = \int_0^{A_{\text{econ}}} a e^{-b/T} [T]_{\text{He}}^{1/2} dA'_{\text{econ}}, \quad (6.41)$$

where R_{econ} is given in microcuries per hour, $a e^{-b/T}$ is the permeation coefficient given by Eq. (6.38), and A_{econ} is the surface area of the economizer.

In order to numerically integrate Eq. (6.41), we will assume that the average metal temperature $T(\text{K})$ varies linearly along the length of the economizer. The economizer, evaporator, and superheater areas and the inlet and outlet temperatures of each section are recorded in Table 1.1, taken from Yang et al.³⁰

The results of numerical integration of Eq. (6.41) for each section of heat exchanger tube, along with the principal input information used to make the estimates, are given in Table 6.13. Note that a total permeation rate of 45.9 $\mu\text{Ci/hr}$ for two steam generators is estimated based on the data obtained for the operating period January 5 to May 30, 1974. The major portion of this permeation took place through the superheater tubing because of its higher temperature and despite the fact that the evaporator section had about twice the surface area. If one assumes 45.9 $\mu\text{Ci/hr}$ as the effective permeation over the full 1018 hr of core 2 operation, an estimated 1.1 Ci of tritium leaked through the steam-generator tubing.

Table 6.13. Tritium permeation through the Peach Bottom HTGR steam-generator tubes

Parameter	Symbol	Value
Helium-side tritium concentration, ^a $\mu\text{Ci/cm}^3$	$[\text{T}]_{\text{He}}$	4.3×10^{-5}
Permeation coefficients, $(\mu\text{Ci/cm})^{1/2}/\text{hr}$		
Economizer		Eq. (6.38)
Evaporator		Eq. (6.39)
Superheater		Eq. (6.40)
Temperature ranges and surface areas		Table 1.1
Estimated tritium permeation rates, $\mu\text{Ci/hr}$		
Economizer	R^{econ}	1.4
Evaporator	R^{evap}	11.2
Superheater	R^{spr}	<u>33.3</u>
Total		45.9
Total tritium permeation during core 2, ^b Ci		1.1
Total tritium permeation estimated by Yang, ³⁰ Ci		5.1

^a Average for operating period January 5 to May 30, 1974.

^b Based on estimated rates being effective for 1018 days of core 2 operation.

As noted in Table 6.13, Yang's³⁰ estimate of the total permeation through the steam-generator tubes is about four times higher than the present estimate. This is approximately as it should be since Yang's result was based on tritium permeation rates observed using a higher tritium concentration in the helium than occurred during the selected operating period (6.0×10^{-4} vs 4.3×10^{-5} $\mu\text{Ci}/\text{cm}^3$).

6.3.4 Loss due to containment leakage

As noted in Sect. 2.4, tests¹⁰ conducted in 1972 indicated an average leakage rate of 0.1%/day from the approximately $2.04 \times 10^4 \text{ m}^3$ ($720,000 \text{ ft}^3$) of nitrogen in the containment vessel. The special tritium survey,⁸ the results of which are summarized in Table 4.1, showed a typical tritium concentration of $5 \times 10^{-7} \mu\text{Ci}/\text{cm}^3$ in the containment atmosphere (at least during the period in 1971 when the measurements were obtained). If this concentration was typical for the 1018 days of core 2 operation, tritium loss due to containment leakage is estimated to be $2.04 \times 10^{10} \text{ cm}^3 \times 0.001 \text{ day}^{-1} \times 1018 \text{ days} \times 5 \times 10^{-13} \text{ Ci}/\text{cm}^3 = 0.010 \text{ Ci}$.

6.3.5 Discharge with gaseous waste flow

As noted in Sect. 2, Peach Bottom operations reports⁹⁻¹⁴ show that the only significant gaseous tritium discharge occurred during regeneration of the liquid-nitrogen-cooled charcoal delay beds in the fission product cleanup plant. These beds were periodically regenerated by allowing them to warm up and expel the adsorbed gases, principally ⁸⁵Kr, N₂, H₂, and HT. These gases were piped into a gaseous activity holdup tank. After a sample was taken and the levels of the radionuclides were measured, the gas was slowly released through the stack. The activity of tritium discharged in this manner was abstracted from refs. 9 to 14 and is given on an annual basis in Table 4.2. Except for 1970 and the first half of 1971, when tritium measurements were not made, the tabulated values indicate that approximately 31 Ci of tritium was so released. This value compares well with the estimated amount of tritium that was transported to the liquid-nitrogen-cooled trap via the purge gas flow (see Sect. 6.3.1).

An additional small amount of tritium was discharged through the stack as the result of the eight containment deinerting* procedures that took place during core 2 operation. The discharge from these procedures is estimated to be $8 \times 2.04 \times 10^{10} \text{ cm}^3 \times 5 \times 10^{-7} \text{ } \mu\text{Ci}/\text{cm}^3 \times 10^{-6} \text{ cm}^3/\mu\text{Ci} = 0.08 \text{ Ci}$.

An additional source for tritium activity in the containment atmosphere was helium leakage from the primary system. As noted in Sect. 6.1.2, operations personnel indicated that the primary system leakage rate was 3.2 kg/day (7 lb_m/day), or a volumetric loss of $1.8 \times 10^6 \text{ cm}^3/\text{day}$ based on average primary system conditions. The resulting tritium activity in the containment is given by

$$A_c = \frac{A_p Q_p}{Q_c} \left[1 - \exp\left(-\frac{Q_c t}{V}\right) \right], \quad (6.42)$$

where

A_p = concentration of tritium in the primary coolant
($2 \times 10^{-5} \text{ } \mu\text{Ci}/\text{cm}^3$ in Table 4.1),

Q_p = rate of release of primary coolant into containment
($1.75 \times 10^6 \text{ cm}^3/\text{day}$),

Q_c = rate of release of containment atmosphere
($2.04 \times 10^{10} \text{ cm}^3 \cdot \frac{10^{-3}}{\text{day}} = 2.04 \times 10^7 \text{ cm}^3/\text{day}$),

V = volume of containment ($2.04 \times 10^{10} \text{ cm}^3$),

t = elapsed time between deinerting operations, days
(approximately $1018 \text{ days}/8 = 127 \text{ days}$).

This results in a containment activity of $2.1 \times 10^{-7} \text{ } \mu\text{Ci}/\text{cm}^3$ near the end of the 127 days, which is approximately 40% of the value observed in 1971 during the special tritium survey.⁸

6.3.6 Discharge with liquid wastes

The various classes of liquids composing the liquid wastes and the wastes system are discussed in Sect. 2.3. Specifically excluded are the

* During a reactor shutdown when maintenance work is required, the entire containment nitrogen atmosphere must be replaced by air.

flows to the WDDT, which were kept separate from the liquid waste system (Sect. 6.3.5).

As noted in Table 4.2, routine operational monitoring indicated that 9.4 Ci of tritium was collected in liquid waste monitor tanks during core 2 operation. After dilution, the tritium was discharged to Conowingo pond.

6.3.7 Summary of leakage rates

Estimates for tritium flows from the primary system, developed in Sects. 6.3.1 to 6.3.4, are summarized in Table 7.3. The associated discussion in Sect. 7.1 compares these estimates with source and inventory estimates.

7. CONCLUSIONS AND RECOMMENDATIONS

7.1 Conclusions

The tritium source estimates developed in Sects. 6.1.1 through 6.1.4 are summarized in Table 7.1. As anticipated, the largest source resulted from ternary fission; however, the magnitude of the source due to neutron reactions with ^{10}B in the control rods was not expected in view of the results from previous tritium source estimates in large HTGRs. Table 7.1 shows estimated tritium sources of 1212 Ci from ternary fission, 42.9 Ci from ^3He impurity in the coolant, 72.5 Ci from lithium impurity in graphite, and 876 Ci from neutron reactions with ^{10}B , for a total of 2200 Ci formed in four years of reactor life and undecayed at EOL.

Estimates of tritium production due to ^3He contaminant in the coolant (Sect. 6.1.2) were based on helium makeup rates (3.2 kg fresh helium per day) and an abundance of ^3H in the helium supply (0.18 ppm) determined onsite by reactor operations personnel. It was assumed that half the measured porosity of the sleeve and reflector graphites was open porosity and hence accessible to helium permeation. The specific activities reported in Table 7.1 would result if the tritium born in the graphite remained in place.

Table 7.1. Summary of tritium sources (referred to time at EOL)

	Amount of ^3H at EOL	
	Total (Ci)	Specific ($\mu\text{Ci/g}$)
Ternary fission		
In fuel particles	1210	
In tramp fuel	<u>2.2</u>	
Subtotal	1212	
Due to $^3\text{He}(n,p)\text{T}$ in graphite		
Sleeve	5.4	0.63
Removable radial reflector	18.9	2.0
Permanent radial reflector	15.5	1.1
Axial reflector	<u>3.1</u>	0.4
Subtotal	42.9	
Due to $^6\text{Li}(n,\alpha)\text{T}$ in graphite		
Sleeve	14.0	1.6
Spine	1.0	0.23
Removable radial reflector	16.4	1.8
Permanent radial reflector	18.8	1.4
Axial reflector	9.2	1.1
Fuel matrix	<u>13.1</u>	2.3
Subtotal	72.5	
Due to ^{10}B reactions		
In poisoned spines	85.7	
In control rods	<u>790</u>	
Subtotal	876	
Total	2200	

The tritium due to lithium in the core graphite was based on measured contaminant levels in the sleeve, spine, reflectors, and matrix graphites. Measured lithium levels (Table 6.4) ranged from 1 ppb in the spine graphite to a high of 10 ppb in the fuel matrix material. Matrix graphites could have significantly higher lithium levels because of their lower firing temperature (1800 vs 2800°C) relative to other graphites. Other reported lithium levels in matrix graphite are 50 times higher than those observed

here. If this higher level had existed at Peach Bottom, the resulting tritium source would have been equal to about half the fission source.

The tritium source due to ^{10}B reactions in the poisoned spines of fuel elements (60 elements out of 804) was estimated to be 85.7 Ci by a method employed in other studies. However, this method is inappropriate for estimating the source due to ^{10}B contained in the control rods because of their variable axial locations, and a more appropriate method was devised (see Sect. 6.1.4) based on the average value of the hot, unrodded core k_{eff} with equilibrium poison reported in the FHSR. The neutron absorption rate, and hence the tritium production rate in the control rods, was estimated from this value for k_{eff} . As shown in Table 7.1, the result yields an unexpectedly large tritium source in the control rods. Tritium concentrations measured in element E14-01 (a poisoned spine element), however, indicate that the tritium born within the zirconium boride did not migrate from the spine. It is believed, however with no direct evidence, that neither did the large quantities of tritium born in the boron carbide of the control rods migrate from the control rods, despite intimate contact with the primary coolant.

Measured levels of tritium found in the graphite portions (sleeve, spine, porous plug, purge hole, and upper and lower reflectors) of six fuel elements are presented in Sects. 5.1 through 5.3. These data were developed in the course of the Peach Bottom Surveillance Program and were summarized from previously published reports. The data are far more extensive than needed for the immediate purposes of this report; for example, extensive radial profile information is given which could, with appropriate analysis, contribute to an understanding of tritium diffusion in graphite. In addition, data on tritium levels measured in the fuel element porous plug and purge hole may be interpreted in terms of tritium concentrations in the coolant, provided equilibrium sorption data are developed for these materials. Sections 5.1 through 5.3 provide a convenient summary for future use of all tritium-related data from the published series of fuel element examinations.

Measured tritium concentrations in three fuel compacts taken from each of two fuel elements are reported in Sect. 5.4. The results, summarized in Table 5.52 and plotted in Figs. 6.1 and 5.2, clearly show that hot elements like F03-01 lost significant portions of tritium. An estimate based on three measurements in element F03-01 indicates that about two-thirds of the tritium was lost from the fuel. On the other hand, a cooler element, like E14-01, retained the major portion of its fission-source tritium within the fuel compact.

Tritium concentration measurements in Sect. 5 are interpreted in terms of corewide tritium inventories in Sect. 6.2. A comparison of Table 7.2, which summarizes these results, with Table 7.1 shows that about 45% of the total estimated tritium source (2200 Ci) is accounted for by measured concentrations in core components (997 Ci). A very rough estimate, based on only six measurements, indicates a tritium inventory in the fuel compacts of 465 Ci, compared with an estimated fission source in the fuel of 1210 Ci. Therefore, corewide, approximately 62% of the tritium born in the fuel escaped. Much of this tritium appeared to have deposited on nearby sleeve graphite material, as indicated by the high inventory estimate for sleeve material. Of the estimated 258 Ci of tritium residing in the sleeve, only about 19.4 Ci (Table 7.1) is thought to have been born there due to ^3He and ^6Li reactions.

Table 7.2. Estimated tritium activities in the core based on measured concentrations (referred to time at EOL)

Component	Inventory (Ci)
Fuel elements	
Top reflector region	11.6
Sleeve	258 ± 28
Spine	18.5 ± 2.4
Fuel compacts	465
Bottom reflector region	9.2
Fission product trap	<u>26.1 ± 2.8</u>
Subtotal	789
Removable radial reflector	<u>208</u>
Total	997

The removable radial reflector was found to be a significant repository of tritium in the core. About 21% of the core tritium inventory was found there, second in magnitude only to the fuel and sleeve.

Tritium leakage estimates developed in Sect. 6.3 are summarized in Table 7.3. The leakage to the ex-core fission product trapping system via the fuel element purge flow, which first passed through a charcoal trap in each element, was estimated as 310 Ci. Early (1971) surveillance concentration measurements of the purge gas as well as analyses of charcoal trap tritium levels lead to this approximate value. However, both of these estimates are highly conjectural despite the agreement. The surveillance concentration was measured during a period of large tritium level variations in the primary system, and the estimate based on observed charcoal trap concentrations employed a widely extrapolated equilibrium sorption value.

Table 7.3. Tritium losses from the primary system during core 2 operation

Loss mechanism	Value (Ci)
Leakage to the ex-core fission product trapping system	(310) ^a
Return to primary coolant	(279) ^a
Trapped on liquid-nitrogen-cooled delay bed and vented to containment on bed regeneration	31
Discharge with off-gas through the stack ^b	31.4
Leakage to the chemical cleanup system via the steam-generator purge ^c	68
Discharge in liquid waste flow ^b	9.4
Leakage through the steam-generator tubing	1.1
Leakage from the containment vessel	0.01

^aDoes not represent leakage from the primary system.

^bBased on concentration measurements in waste flows.

^cOxidized to HTO, adsorbed on clay, and disposed of as solid waste.

Operations personnel have indicated that more than 99% of the tritium released via the stack was from the gaseous waste holdup vessel that received the regeneration off-gas from the liquid-nitrogen-cooled delay beds. Therefore, we have concluded that only the portion of the 310 Ci entering the delay bed system that passed through the liquid-nitrogen traps (10% of the total flow) was retained and degassed during bed regeneration and sent to the holdup tanks for discharge via the stack. The remainder of the tritium in the purge flow (90% of the total) either passed through the water- and Freon-cooled beds and returned to the primary coolant or was permanently retained in these charcoal beds. The latter is less likely but is still possible in view of the large mass of graphite in these delay beds. At any rate, it is certain that only an insignificantly small quantity of tritium desorbed from the water- and Freon-cooled beds (to the containment volume and ultimately to the stack) compared with that desorbed from the liquid-nitrogen trap.

The tritium leakage to the chemical cleanup system via the purge flow from the heat exchanger baffle is estimated (Sect. 6.3.2) to have been 68 Ci during the operation of core 2. This tritium was oxidized to HTO, separated from the helium by molecular sieves, adsorbed on solids, and shipped offsite as solid waste.

Relatively small amounts of tritium were lost by permeation through the steam-generator tubing or by leakage of nitrogen through the containment vessel. A total permeation of 1.1 Ci through the steam-generator tubing for four years of operation is estimated in Sect. 6.3.3. This is about a factor of 4 less than a previous estimate³⁰ employing an atypically high helium-side tritium concentration.

The magnitudes of several tritium transport paths were not evaluated due to the lack of sufficient information. For example, tritium egress from the secondary coolant with the condensate purge or blowdown flow was not evaluated because no information was available on the flow rates; similarly, the tritium transport rate from the WDDT to the containment via vents on this drain tank was not estimated.

Table 7.4 summarizes the tritium mass balance in the reactor for the four years of core 2 operation. Tritium from ^{10}B sources is excluded since it evidently stayed in place. The table notes a total movable tritium source of 1325 Ci (excluding ^{10}B sources), compared with 997 Ci measured inventory and 108 Ci leakage. Thus the total inventory plus leakage (1107 Ci) is about 218 Ci less than the estimated source. Table 7.2 does not include the tritium inventory in the permanent radial reflector or in the ex-core charcoal traps at EOL; these repositories were not sampled. Undoubtedly, some of the estimated 218 Ci excess (sources over inventory plus leakage) may be accounted for as residing in these two unsampled locations. We therefore conclude that, despite certain gaps in the analyses (some of which are discussed in Sect. 7.2), a reasonably complete picture of tritium sources and the ultimate fate of tritium formed in the Peach Bottom HTGR has been developed.

Table 7.4. Summary of tritium balance

	Value (Ci)
Source ^a	
Ternary fission	1210
^3He	42
^6Li	<u>73</u>
	1325
Inventory at EOL ^b	
Fuel compacts	465
Fuel element graphite	324
Replaceable radial reflector	<u>208</u>
	997
Leakage	
Liquid waste	9.4
Gaseous discharge through stack	31.0
Solid waste	68.0
Containment leakage	<u>0.01</u>
	108.4

^a Excluding ^{10}B sources.

^b Excluding control rods, poisoned spines, ex-core charcoal beds, and permanent reflector graphite.

7.2 Recommendations

Equilibrium sorption data of HT on charcoal and graphite are needed to develop improved estimates of tritium transport in the following areas:

1. Sorption data are needed on fission product charcoal in the 350 to 500°C temperature range to allow interpretation of the axial concentration profiles in the traps in terms of tritium concentrations in the purge gas. It is quite important that this estimate be improved in view of the significant tritium loss exhibited by the fuel particles, much of which entered the purge gas.

2. Sorption data of HT on core and reflector graphite material are needed for an improved understanding of how the core acts as a sink for graphite, whether or not its efficiency for tritium absorption diminishes with operating life, and to what extent tritium desorbs under normal or off-normal shutdown conditions.

3. Sorption data on the charcoal in the ex-core fission product traps are needed to determine the degree of tritium holdup in the water- and Freon-cooled delay beds, to determine the amount of tritium desorbed during bed regeneration, and to estimate the amount permanently retained in the bed.

Our estimate of tritium release from fuel particles is based on too few data to yield a good indication of whole-core release. Further work on tritium modeling of the Peach Bottom HTGR would require additional analyses of tritium concentrations in fuel samples.

Further study of the fate of the tritium born in the control rods is warranted in view of the large source due to ^{10}B reactions. This study should include diffusion and sorption measurements of HT on boron carbide at control rod temperatures and an estimation of the degree of pickup in helium flow using simulated control rod geometry.

8. REFERENCES

1. F. F. Dyer, R. P. Wichner, W. J. Martin, L. L. Fairchild, R. J. Kedl, and H. J. de Nordwall, Postirradiation Examination of Peach Bottom HTGR Fuel Element EO6-01, ORNL-5126 (March 1976).

2. R. P. Wichner, F. F. Dyer, W. J. Martin, and L. C. Bate, Distribution of Fission Products in Peach Bottom HTGR Fuel Element E11-07, ORNL-5214 (April 1977).
3. R. P. Wichner, F. F. Dyer, and W. J. Martin, Distribution of Fission Products in Peach Bottom HTGR Fuel Element E14-01, ORNL/TM-5730 (August 1977).
4. F. F. Dyer, R. P. Wichner, W. J. Martin, and L. L. Fairchild, Distribution of Fission Products in Peach Bottom HTGR Fuel Element F03-01, ORNL/TM-5996 (June 1978).
5. R. P. Wichner, F. F. Dyer, W. J. Martin, and L. L. Fairchild, Distribution of Fission Products in Peach Bottom HTGR Fuel Element E01-01, ORNL/TM-6353 (August 1978).
6. R. P. Wichner, F. F. Dyer, W. J. Martin, and L. L. Fairchild, Distribution of Fission Products in Peach Bottom HTGR Fuel Element F05-05, ORNL/TM-6455 (January 1979).
7. R. P. Wichner and J. L. Botts, "Fuel Particle Failure Fractions in Peach Bottom HTGR Fuel Elements," Trans. ANS 28, 689-91 (1978).
8. W. J. Scheffel, N. L. Baldwin, and R. W. Tomlin, Operating History for the Peach Bottom HTGR, GA-A13907 (1976).
9. Philadelphia Electric Company Semi-Annual Operations Report No. 65, July 1, 1971, through December 31, 1971, submitted to the USAEC.
10. Philadelphia Electric Company Semi-Annual Operations Report No. 66, January 1, 1972, through June 30, 1972, submitted to the USAEC.
11. Philadelphia Electric Company Semi-Annual Operations Report No. 67, July 1, 1972, through December 31, 1972, submitted to the USAEC.
12. Philadelphia Electric Company Semi-Annual Operations Report No. 68, January 1, 1973, through June 30, 1973, submitted to the USAEC.
13. Philadelphia Electric Company Semi-Annual Operations Report No. 69, July 1, 1973, through December 31, 1973, submitted to the USAEC.
14. Philadelphia Electric Company Semi-Annual Operations Report No. 70, January 1, 1974, through June 30, 1974, submitted to the USAEC.

15. "Radioactive Material in Light-Water-Cooled Nuclear Power Reactor Effluents," Federal Register 40(87) (1975).
16. B. W. Gainey, A Review of Tritium Behavior in HTGR Systems, GA-A13461 (1976).
17. "Environmental Radiation Production Standards for Nuclear Power Operation," 40 CFR 190, Federal Register 42(9) (1977).
18. Peach Bottom Atomic Power Station, Final Hazards Summary Report, NP-9115, Part C, Vol. 2 (March 1964).
19. Proposed Facility Change and Technical Specifications Change No. 13 to the Final Hazards Summary Report (January 1970).
20. R. F. Turner, R. D. Burnette, and W. J. Scheffel, HTGR Fuel Performance in the Peach Bottom Reactor, G-GA-A12675 (1973).
21. R. D. Burnette et al., Chemical Impurities in the Helium Coolant at the Peach Bottom HTGR, G-GA-A10809.
22. C. F. Wallroth et al., Postirradiation Examination of Peach Bottom FTE-18, GA-A(13699) (June 1976).
23. C. F. Wallroth et al., Postirradiation Examination of Peach Bottom FTE-4, GA-A13452 (July 1977).
24. C. F. Wallroth et al., Postirradiation Examination of Peach Bottom FTE-6, GA-A13943 (September 1977).
25. N. Forsyth, Tritium Production, Migration and Removal in the Dragon Reactor Between Core 5 Charge III and Core I Charge IV, D.P. Report 799 (1972).
26. N. Forsyth, Tritium Generation, Retention, Distribution and Environmental Release in a 1500 MW(t) HTR, D.P. Report 905 (1974).
27. E. L. Compere, S. H. Freid, and C. W. Nestor, Distribution and Release of Tritium in HTGR's as a Function of Design, Operational and Material Parameters, ORNL-TM-4304 (1974).
28. H. D. Rohrig, P. G. Fischer, and R. Hecker, "Tritium Balance in HTGR's," J. Am. Ceram. Soc. 59, 316-20 (1976).

29. R. A. Strehlow and H. C. Savage, "The Permeation of Hydrogen Isotopes through Structural Metals at Low Pressures and through Metals with Oxide Film Barriers," *Nucl. Technol.* 22, 127-37 (1974).
30. L. Yang, W. A. Baugh, and N. L. Baldwin, Study of Tritium Permeation through Peach Bottom Steam Generator Tubes, GA-A14376 (1977).
31. HTGR Base Program Quarterly Progress Report for the Period Ending August 31, 1972, GA-A12222 (September 1972).
32. K. H. Walter and G. Lange, "Liberation of Tritium from Coated Fuel Particles," p. 311 in Reaktortagung, Proceedings of the Reactor Conference, Hamburg, 1972 (G-GA-tr-12247).
33. K. H. Walter, K. H. Kienberger, and G. Lange, *J. Nucl. Mater.* 48, 287-92 (1973).
34. R. A. Causey, Tritium Diffusion and Deuterions Solubility in Silicon Carbide and Pyrolytic Carbon, North Carolina State Ph.D. Thesis (1977).
35. P. G. Fischer, Behavior of Tritium in Reactor Graphites, KFA-Jülich Rept., JUL-1238-RG (1975); available as translation LLL 02144.
36. GAC Project Staff, Metallurgical Examination of Primary Circuit Components from the Peach Bottom HTGR, GA-A14506 (1978).
37. Internal GAC correspondence, J. J. Sauerwein to C. F. Wallroth, "Temperature, Fluence, and Fuel Performance Data for Peach Bottom Fuel Elements E01-01, F03-01, F05-05, E06-01, E11-07, and E14-01," May 9, 1978.
38. P. G. Fischer et al., "On the Behavior of Tritium in Reactor Graphites," *J. Nucl. Mater.* 64, 281-88 (1977).
39. B. M. W. Trapnell, Chemisorption, Chap. 3, Academic Press, New York, 1955.
40. J. P. Redmond and P. L. Walker, *J. Phys. Chem.* 64, 1093 (1960).
41. S. Dushman, Vacuum Technique, 2d ed., Chap. 7, Wiley, New York, 1962.
42. Internal GAC correspondence, Frances McCord to C. F. Wallroth, June 27, 1975 (E06-01), July 25, 1975 (E11-07), Aug. 8, 1975 (E14-01), Aug. 8, 1975 (F03-01).

43. Internal GAC memorandum, M. J. Haire and D. R. Lofing, to D. W. McEachren, Nov. 28, 1973.
44. N. Gazda, Philadelphia Electric Co., private communication, Nov. 2, 1978.

INTERNAL DISTRIBUTION

- | | | | |
|--------|-------------------|--------|-------------------------------|
| 1. | W. D. Burch | 29. | M. F. Osborne |
| 2. | E. L. Compere | 30. | G. W. Parker |
| 3. | D. A. Costanzo | 31. | J. W. Snider |
| 4. | W. R. Davis, Jr. | 32. | M. G. Stewart |
| 5-10. | F. F. Dyer | 33. | R. M. Westfall |
| 11. | G. L. Haag | 34-43. | R. P. Wichner |
| 12. | D. W. Holladay | 44. | L. J. Colby, Jr. (consultant) |
| 13. | F. J. Homan | 45. | G. R. Choppin (consultant) |
| 14-21. | P. R. Kasten | 46. | E. L. Gaden, Jr. (consultant) |
| 22. | W. J. Lackey | 47. | L. E. Swabb, Jr. (consultant) |
| 23. | T. B. Lindemer | 48. | K. D. Timmerhaus (consultant) |
| 24. | E. L. Long, Jr. | 49-50. | Central Research Library |
| 25. | R. A. Lorenz | 51. | ORNL-Y-12 Technical Library |
| 26. | A. P. Malinauskas | | Document Reference Section |
| 27. | F. R. Mynatt | 52-56. | Laboratory Records |
| 28. | R. E. Norman | 57. | Laboratory Records, ORNL-RC |
| | | 58. | ORNL Patent Section |

EXTERNAL DISTRIBUTION

59. Office of Assistant Manager, Energy Research and Development, DOE-ORO, P.O. Box E, Oak Ridge, TN 37830
60. Director, Nuclear Research and Development Division, DOE-ORO, P.O. Box E, Oak Ridge, TN 37830
- 61-62. Director, Division of Reactor Research and Technology, DOE, Washington, DC 20545
- 63-238. Given distribution as shown in TID-4500 under Gas-Cooled Reactor Technology category